

Systematics of the post-spinel transition in Fe-bearing compositions

Dissertation

zur Erlangung des Doktorgrades

der Naturwissenschaften

vorgelegt beim Fachbereich Geowissenschaften/Geographie

der Goethe Universität Frankfurt

in Frankfurt am Main

von

Klaus Schollenbruch

aus Kaufbeuren

Frankfurt (2010)

(D 30)

vom Fachbereich Geowissenschaften/Geographie der Goethe Universität als
Dissertation angenommen

Dekan: Prof. Dr. Robert Pütz

Gutachter: Prof. Dr. Alan Woodland
Prof. Dr. Falko Langenhorst

Datum der Disputation: 17. 12. 2010

Table of Contents

1. INTRODUCTION.....	5
1.1. OCCURRENCE OF SPINELS	5
1.2. CRYSTAL STRUCTURE OF SPINELS	6
1.3. USE OF SOME FE-BEARING SPINELS	8
1.4. POST-SPINEL STRUCTURES.....	10
1.5. GOAL OF THIS STUDY	12
1.6. REFERENCES	12
2. THE STABILITY OF HERCYNITE AT HIGH PRESSURES AND TEMPERATURES	20
2.1. INTRODUCTION.....	20
2.2. EXPERIMENTAL METHODS	21
2.3. RESULTS AND DISCUSSION.....	25
2.3.1. Hercynite breakdown.....	25
2.3.2. A high pressure FeAl ₂ O ₄ polymorph	30
2.5. ACKNOWLEDGEMENTS	31
2.6. REFERENCES	31
3. DETECTING THE SPINEL – POST-SPINEL TRANSITION IN FE₃O₄ BY IN SITU ELECTRICAL RESISTIVITY MEASUREMENTS.....	35
3.1. INTRODUCTION.....	35
3.2. EXPERIMENTAL	35
3.3. RESULTS AND DISCUSSION	37
3.3.1. The measurements	37
3.3.2. TEM investigations.....	39
3.3.3. The phase boundary.....	40
3.4. REFERENCES	41
4. IN SITU DETERMINATION OF THE SPINEL – POST-SPINEL TRANSITION IN FE₃O₄ AT HIGH TEMPERATURE AND PRESSURE BY SYNCHROTRON X-RAY DIFFRACTION.....	44
4.1. INTRODUCTION.....	44
4.2. EXPERIMENTAL METHODS	45
4.3. RESULTS AND DISCUSSION.....	47
4.3.1. In situ observations.....	47
4.3.2. Post-experiment analysis	51
4.3.3. Additional phases	52
4.3.4. The h-Fe ₃ O ₄ phase	52
4.3.5. TEM observations.....	54
4.3.6. The transition.....	55
4.3.7. The phase boundary.....	57
4.4. IMPLICATIONS	59
4.5. ACKNOWLEDGEMENTS	60
4.6. REFERENCES	61
5. PHASE TRANSFORMATIONS OF FE₃O₄-FE₂SIO₄ SOLID SOLUTIONS AND FE₃O₄-FECr₂O₄ SOLID SOLUTIONS AT HIGH TEMPERATURE AND PRESSURE	65
5.1. INTRODUCTION.....	65
5.2. EXPERIMENTAL	66
5.2. RESULTS.....	68
5.2.1. Fe ₃ O ₄ – Fe ₂ SiO ₄	68
5.2.1.1. X-ray diffraction	68
5.2.1.2. EMPA	70
5.2.2. Fe ₃ O ₄ – FeCr ₂ O ₄	71
5.2.2.1. X-ray diffraction.....	72
5.2.2.2. EMPA	73
5.2.3. Further characterisation of run-products.....	74
5.2.3.1. Raman spectroscopy – preliminary measurements.....	75
5.2.3.2. Raman measurements on experimental products	76
5.2.3.3. TEM.....	78
5.3. DISCUSSION.....	78

5.3.1. Mt-Fay solid solutions	78
5.3.2. Mt-Chr solid solutions	80
5.4. FURTHER WORK.....	82
5.5. REFERENCES	82
6.A SUMMARY AND OUTLOOK	86
6.1.A HERCYNITE	86
6.2.A MAGNETITE	87
6.2.1.a Resistivity measurements.....	87
6.2.2.a Synchrotron measurements	88
6.3.A SPINEL SOLID SOLUTIONS.....	89
6.4.A REFERENCES	90
6.B ZUSAMMENFASSUNG UND AUSBLICK	93
6.1.B HERCYNIT	93
6.2.B MAGNETIT.....	94
6.2.1.b Widerstandsmessungen.....	94
6.2.2.b Synchrotron-Experimente.....	95
6.3.B MISCHKRISTALLE.....	97
6.4.B REFERENZEN	98
SUPPLEMENTARY MATERIAL	101

1. Introduction

1.1. Occurrence of spinels

Spinel-structured minerals (spinel) are common accessory minerals in most kinds of crustal rocks, where they occur in magmatic, metamorphic and sedimentary rocks. The name of the whole structural group derives from the mineral spinel (MgAl_2O_4), which originates from the Greek word *spinos* for sparkle.

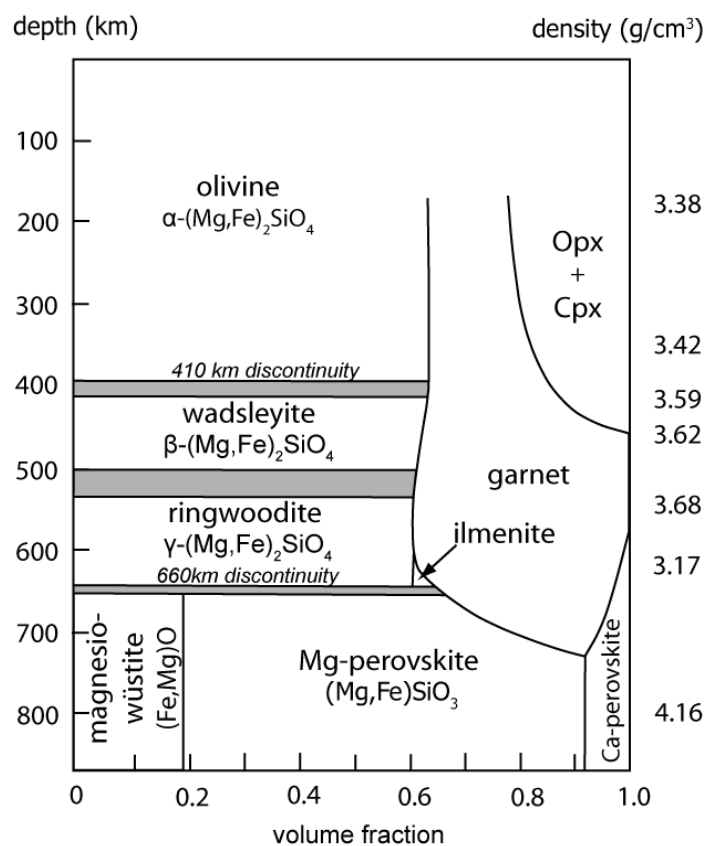


Figure 1.1: Main phase assemblage of a pyrolitic upper mantle (modified from Ringwood, 1991). The densities are given as zero pressure densities.

Of major petrological interest is the spinel structure at high pressure, especially in the upper mantle and in the transition zone of the mantle between 400 km and 650 km. In these regions spinel-type minerals occur with different compositions. In the uppermost mantle, in a depth deeper than 20 km, the assembly plagioclase + olivine + orthopyroxene + clinopyroxene reacts to a spinel-rich peridotite with Mg, Al-rich, and often Si-free spinel solid solutions. The spinel stability lasts down to 60 km, where spinel + orthopyroxene react to garnet + olivine.

The mantle between 400 km and 660 km is characterized by several sudden changes in seismic wave velocities (discontinuities). This region is also described as the transition zone. Several of these discontinuities can be related to phase transformations, expected to occur in a pyrolitic bulk composition. The most important of these discontinuities are the ones at 410 km and 660 km depth (Fig. 1.1). The change in the speed of seismic waves is mainly dependent on density differences between rock forming minerals. The discontinuities in the upper mantle are caused by phase transformations in olivine (e.g., Ringwood 1991). At pressures of ~14 GPa and temperatures of 1600 °C, corresponding to a depth of 410 km, a pyrolitic olivine (Mg_{89}^*) reacts to the first high pressure modification wadsleyite accompanied with a volume loss of 8% (Ringwood 1991). Following a normal geothermal gradient, wadsleyite is stable up to 520 km depth. At higher pressure and temperature (P and T) wadsleyite transforms to the second high pressure modification, the 2% denser ringwoodite with spinel structure. Below 660 km the spinel structure is no longer stable and ringwoodite breaks down to cubic magnesiowüstite and orthorhombic $(\text{Mg,Fe})\text{SiO}_3$ perovskite (Fig. 1.1). As this net transfer reaction is limited to a depth interval of only 4 km (Ito and Takahashi 1989) and as the density jump of 4 % is very high, the change in seismic wave velocities is exceptionally strong. This prominent discontinuity marks the boundary between transition zone and lower mantle.

Apart from seismic data, diamond inclusions are a powerful tool to determine the stability and composition of minerals in the upper region of the mantle. Recent discoveries of diamonds from a depth below 300 km (e.g., Brenker et al. 2005) provide information about deeper regions of the upper mantle. Inclusions of these diamonds demonstrate the existence of areas in the earth's mantle, where Si-free oxides are stable. In diamonds analysed by Stachel et al. (1998) almost pure magnetite and chromite were found. These discoveries have not only implications for the formation of diamonds, but also for the existence of Si-free spinels in the upper mantle.

1.2. Crystal structure of spinels

One of the reasons for the widespread occurrence of spinels is the result of the large number of cations the spinel structure can accommodate. Minerals of the spinel group have the general formula AB_2O_4 . The cubic, face centred spinel structure with the space group $\text{Fd}3\text{m}$ is derived from the cubic closed packing of oxygen, with the A and B cations

distributed on one eighth of the octahedral sites and half of the tetrahedral sites lying between the oxygens (Sickafus et al. 1999). The face-centred structure leads to an enlargement of the unit cell in comparison to the cubic closed packing by $2 \times 2 \times 2$. As a consequence, the unit cell contains 32 oxygens (Fig. 1.2) and has a formula of $A_8B_{16}O_{32}$.

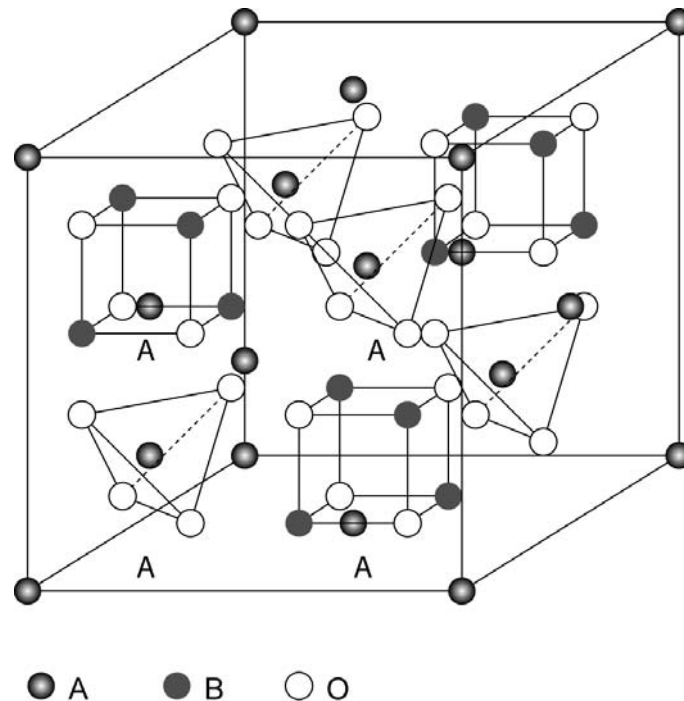


Figure 1.2: The spinel structure AB_2O_4 (modified from Putnis 1992). The distribution of the cations can be described as small cubes and tetrahedrons. The arrangement of the AO_4 -structure and the B_4O_4 cubes puts the B atoms on octahedral sites. The complete structure includes A-atoms at the corners and face-centres of a large cube. Only three B_4O_4 cubes are shown.

Basically, spinels are divided into two groups (Verwey and Heilmann 1947): In *normal* spinels with all cations on the A-site having tetrahedral coordination and all 16 cations on the B-site being octahedrally coordinated and on the other hand in *inverse* spinels, which share 8 tetrahedral sites and 8 octahedral sites on the B site while the A site is completely octahedral. Apart from these two endmembers intermediate spinels, which are a combination of *normal* and *inverse* spinels are very common in nature (Putnis 1992). The spinel structure has the ability to adopt cations that are different in charge and size (O'Neill and Navrotsky 1984). In $MgAl_2O_4$ for example, the usually larger Mg-cation occupies the smaller tetrahedral site, whereas the smaller Al-cation (radius: 0.53 \AA) occupies the larger octahedral site. Thus, the radius of Mg^{2+} changes from typical 0.71 \AA to 0.58 \AA (O'Neill and Navrotsky 1983). In this case the cubic closed packing of the oxygens is not ideal, leading to a slight distortion of the tetrahedrons and octahedrons.

As two different coordinated lattice sites are available, the incorporation of a large number of different cations is possible. In *normal* spinels the A site is occupied by divalent cations like Mg, Fe²⁺, Mg, Co, Ni, Zn, or Mn. The B-site is assigned by trivalent cations like Fe³⁺, Al, Cr, Mn³⁺, or V³⁺ (O'Neill and Navrotsky 1983). There is a complete miscibility between the divalent cations and a limited miscibility between the trivalent cations. In *inverse* spinels the tetrahedral site is occupied by trivalent cations and the octahedral sites are randomly filled with 50 % divalent and 50 % trivalent cations. Intermediate or partly *inverse* spinels are also likely. Apart from these so called 2-3 spinels (referring to the charge of the cations on the A- and B-site) it is also possible to incorporate quadrivalent cations in the spinel structure on the A-site. A prominent example of these 2-4 spinels is ringwoodite with Si⁴⁺ on the tetrahedral site and Fe²⁺ on the octahedral site. Solid solutions between 2-3 spinels and 2-4 spinels are possible, but only by the coupled substitution of a quadrivalent cation together with a divalent cation and two trivalent cations or vice versa. Additionally, the spinel structure may contain vacancies as regular parts of the body (e.g., Sheldon et al. 1999; Menegazzo et al. 1997). This flexibility of the structure and the variable site occupancies explain the huge number of over one hundred minerals with the spinel structure. Among them are numerous important geological and industrial compounds.

1.3. Use of some Fe-bearing spinels

Magnetite (Fe³⁺(Fe²⁺,Fe³⁺)₂O₄; *inverse* spinel): Ferrimagnetic magnetite has the strongest magnetisation of all natural minerals. These properties have been known to mankind since ancient times. For instance the Chinese invented the magnetic compass around the 2nd century B.C. using the magnetic properties of magnetite (Needham 1962). Being an *inverse* spinel, the Fe²⁺ and Fe³⁺ cations are randomly distributed on the B site. This distribution of Fe²⁺ and Fe³⁺ is responsible for electron hopping and polar conductivity. Below the Verwey temperature of 120 K – 125 K (Verwey et al. 1947), magnetite becomes an insulator. This is based on a structural change (e.g., Hargrove and Kundig 1970) and an ordering of Fe²⁺ and Fe³⁺ (e.g., Goff et al. 2005). Above the Curie temperature of 850 K, magnetite loses its magnetic order and becomes non-magnetic (Samara and Giardini 1969). This attribute is used for the relative aging of the seafloor, as titanomagnetites crystallised from high temperature magma at mid ocean ridges are aligned according to the changing polarity of the earth's

magnetic field (e.g., Aramaki and Akimoto 1957; Mullineaux and Crandell 1962; McElhinny and McFadden 2000).

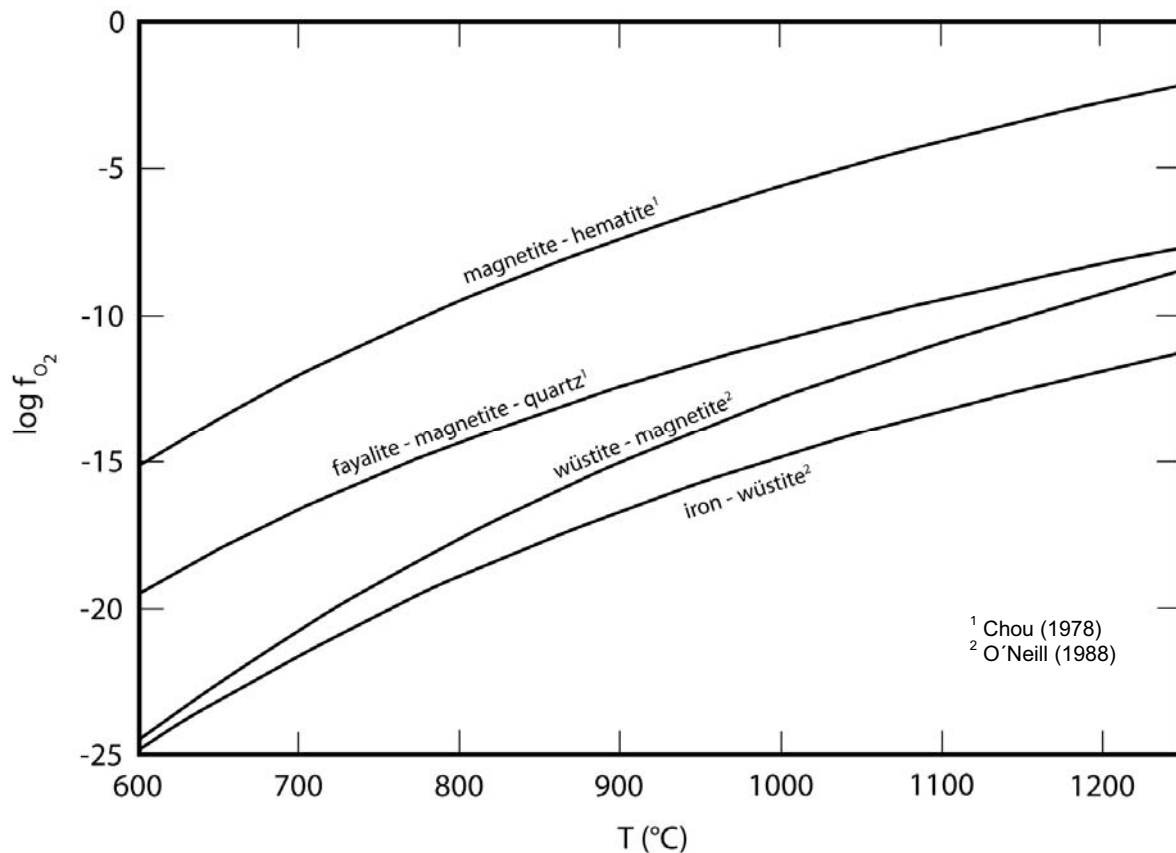


Figure 1.3: Petrological important buffers of Fe-rich minerals.

Spinel with a magnetite compound are very sensitive to changes in oxygen fugacity by the simultaneous incorporation of Fe^{2+} and Fe^{3+} (Fig. 1.3). Especially the join of Fe_3O_4 - Fe_2TiO_4 is one of the most important petrogenetic indicators for $f\text{O}_2$ (e.g., Wood et al. 1991; Woodland et al. 1992).

Due to its physical properties like high temperature stability, magnetism or being a semiconductor, magnetite is used in different branches (e.g., van der Zaag et al. 2000; Cornell and Schwertmann 2003). It is applied as nanoparticles in biomedicine (e.g., Pankhurst et al. 2003; Šafařík and Šafaříková 2002) or in catalysts (e.g., Teja and Koh 2009), has a wide spectrum as a refractory mineral or is used as pigment (e.g., Zuo et al. 1999) or can be applied in magnetic data carriers as well as in water treatment facilities (e.g., Hildebrand et al. 2009).

Chromite ($\text{Fe}^{2+}\text{Cr}_2\text{O}_4$; *normal spinel*): Chromite-rich spinels occur in dunites, mafic rocks (e.g., ophiolites (Rammlmair et al. 1987)) or ultramafic layered intrusions and metamorphic rocks (e.g., Gu and Wills 1988). Chromite is an important petrogenetic

indicator, as equilibration temperatures may be obtained from the Fe-Mg exchange reactions between chromium spinel and coexisting ferromagnesian phases (Sack and Ghiorso 1991). FeCr_2O_4 is the most important natural chromium resource. The two largest deposits of the world, Bushveld complex and the Great Dyke in Zimbabwe, both layered intrusions contain together 95% of the worldwide chromium ore as cumulates (Kogel et al. 2006). Chromium chemicals are used in the steel industry, for leather tanning, as pigments, for the surface treatment of metals and in the refractory industry (Kogel et al. 2006).

Hercynite ($\text{Fe}^{2+}\text{Al}_2\text{O}_4$; *normal* spinel): Hercynite-rich spinels are found in high-grade metamorphosed ferruginous argillaceous sediments. Additionally, they occur in mafic and ultramafic igneous rocks. The thermodynamic properties of FeAl_2O_4 are important in the geothermobarometry of high grade metamorphic rocks in several exchange equilibria (Bohlen et al. 1986; Hensen and Green 1971; Shulters and Bohlen 1989). FeAl_2O_4 is also an important component in some spinels from the mantle (Wood and Virgo 1989; Woodland et al. 1992) In industry, FeAl_2O_4 is used as pigment (e.g., Andreozzi et al. 2004), it occurs in refractory processes (e.g., Zhang et al. 2009) or as a ceramic additive (Udalov et al. 2004). However, its economic importance is significantly lower than for magnetite or chromite. In nature magnetite, chromite and hercynite often occur as components in complex spinels.

1.4. Post-spinel structures

The hP-phase transformations in Fe-bearing spinels are of high relevance, because of the occurrence of their high pressure polymorphs in nature (Chen et al. 2008), their possible existence in the earth's mantle and for the understanding of the system Fe-O. First high pressure experiments on spinel components were conducted by Reid and Ringwood (1969). They detected phase transformations in several spinels at ~12 GPa and 1000 °C to a 10% denser phase with CaMn_2O_4 (CM) structure. The first evidence for an unquenchable high pressure modification of magnetite (h- Fe_3O_4) was detected at room temperature and 25 GPa (Mao et al. 1974). The high pressure phase was indexed to be monoclinic. There is a huge gap in pressure between the reaction magnetite - h- Fe_3O_4 and the back-reaction h- Fe_3O_4 – magnetite. A complete re-transformation occurred close to zero pressure. Subsequent experiments by Huang and Bassett (1986) were conducted at temperatures up to 600 °C to reduce the sluggishness of the reaction. However, the temperatures were still too low to

completely overcome the kinetic barrier and the exact position of the phase transformation could not be determined. Even experiments at 800 °C led to different results concerning the phase boundary (Woodland et al. 2001). It was not even clear, if the slope of the phase boundary is positive or negative. Mössbauer experiments (Pasternak et al. 1994) confirmed the transition at 25 GPa and the sluggishness of the reaction. A missing magnetic ordering was determined in h-Fe₃O₄, which can be ascribed to non-magnetic, metallic properties or a paramagnetic phase. Electrical resistivity measurements resulted in a non-linear change in resistivity (Xu et al. 2004; Morris and Williams 1997). After an increase in resistivity beyond the phase boundary, the resistivity drops at high pressures, which relates to a metallic phase (Dubrovinsky et al. 2003). Precise high-pressure X-ray measurements revealed a volume change of 6.5 % during the transition and a CaMn₂O₄ structure for h-Fe₃O₄ instead of a monoclinic symmetry was proved by Fei et al. (1999). Experiments by Haavik et al. (2000) and Dubrovinsky et al. (2003) proposed the more symmetric CaTi₂O₄ structure for h-Fe₃O₄.

At high pressures chromite shows similar features as magnetite. It also transfers to an orthorhombic phase accompanied by a large volume loss of 10 %. However, in chromite two phase transitions were monitored. First, chromite transforms at ~12 GPa to a phase with CaFe₂O₄ (CF) structure and at ~ 20 GPa it reacts to a high pressure polymorph with CaTi₂O₄ (CT) structure (Chen et al. 2003b). In contrast to Fe₃O₄, both high pressure phases are quenchable and have been found in a meteorite (Chen et al. 2003a, 2008).

Like the already mentioned magnetite and chromite, most spinels transform directly to a high pressure phase with CF, CT or CM structure. More examples for this kind of transformation are Zn₂SnO₄ (Shen et al. 2009), ZnGa₂O₄, ZnAl₂O₄ (López et al. 2009) or ZnFe₂O₄ (Levy et al. 2000). An exception is MgAl₂O₄, which passes through an intermediate step and then transforms to a high pressure polymorph. At pressures above 15 GPa and temperatures at ~ 1000 °C, MgAl₂O₄ decomposes to periclase and corundum (Liu 1975; Ohtani et al. 1975; Akaogi et al. 1999). At 25 GPa and high temperatures MgO + Al₂O₃ reacts to a new orthorhombic phase (ϵ -MgAl₂O₄) with CaFe₂O₄ structure (Irifune et al. 1991; Akaogi et al. 1999). At much higher pressures ϵ -MgAl₂O₄ transforms to a polymorph with CaTi₂O₄ structure (Funamori et al. 1998), which is at least stable up to 117 GPa (Ono et al. 2006). An important difference between the behaviour of h-Fe₃O₄ and h-MgAl₂O₄ is that the high pressure polymorph of MgAl₂O₄ is quenchable, which facilitates the investigation of this phase.

Up to now no systematic research has been done on the high-pressure phase transition of the important endmember spinel hercynite. Ringwood and Reid (1968) report a

decomposition of hercynite at high pressures. However, their results are based on one single experiment performed at 12 GPa and 1000 °C.

1.5. Goal of this study

Based on the existence of nearly pure, Si-free spinels in the upper mantle and the importance of Fe in the mantle, the goal of this study is to gain precise information about the high-P stabilities of Fe-bearing spinels. The position and the slope of the phase boundary of these spinels will be determined. The systematic investigation of the high pressure behaviour of hercynite will be performed by conventional multianvil-quench experiments. Regarding the unquenchable nature of the high-P polymorph of magnetite it is necessary to perform in situ experiments at high P and T. Two independent methods are chosen by using a combination of multianvil experiments with electrical resistivity measurements and in situ synchrotron analysis during multianvil experiments. In subsequent experiments the phase transition of magnetite-Fe₂SiO₄ and magnetite-chromite solid solutions will be analysed, as these compositions are petrological more relevant and Cr and Si may have a stabilising effect on the particular high pressure phase. These experiments will also be performed as multianvil-quench experiments in the hope to produce a stable high pressure modification, which would simplify the analysis.

1.6. References

- Akaogi, M., Hamada, Y., Suzuki, T., Kobayashi, M., and Okada, M. (1999) High pressure transitions in the system MgAl₂O₄-CaAl₂O₄: a new hexagonal aluminous phase with implication for the lower mantle. *Physics of the Earth and Planetary Interiors*, 115(1), pp 67-77.
- Andreozzi, G.B., Baldi, G., Bernardini, G.P., Di Benedetto, F., and Romanelli, M. (2004) ⁵⁷Fe Mössbauer and electronic spectroscopy study on a new synthetic hercynite-based pigment. *Journal of the European Ceramic Society*, 24(5), pp 821-824.

- Aramaki, S., and Akimoto, S. (1957) Temperature estimation of pyroclastic deposits by natural remanent magnetism. *American Journal of Science*, 255(9), pp 619-627.
- Bohlen, S.R., Dollase, W.A., Wall, V.J. (1986) Calibration and applications of spinel equilibria in the system FeO-Al₂O₃-SiO₂. *Journal of Petrology*, 27(5), pp 1143-1156.
- Brenker, F.E., Vincze, L., Vekemans, B., Nasdala, L., Stachel, T., Vollmer, C., Kersten, M., Somogyi, A., Adams, F., Joswig, W., and Harris, J.W. (2005) Detection of a Ca-rich lithology in the Earth's deep (> 300 km) convecting mantle Earth and Planetary Science Letters, 236(3-4), pp 579-587.
- Chen, M., Shu, J.F., and Mao, H.K. (2008) Xieite, a new mineral of high-pressure FeCr₂O₄ polymorph. *Chinese Science Bulletin*, 53(21), pp 3341-3345.
- Chen, M., Shu, J.F., Mao, H.K., Xie, X.D., and Hemley, R.J. (2003a) Natural occurrence and synthesis of two new postspinel polymorphs of chromite. *Proceedings of the National Academy of Sciences of the United States of America*, 100(25), pp 14651-14654.
- Chen, M., Shu, J.F., Xie, X.D., and Mao, H.K. (2003b) Natural CaTi₂O₄-structured FeCr₂O₄ polymorph in the Suizhou meteorite and its significance in mantle mineralogy *Geochimica Et Cosmochimica Acta*, 67(20), pp 3937-3942.
- Chou, I.M. (1978) Calibration of oxygen buffers at elevated P and T using the hydrogen fugacity sensor. *American Mineralogist*, 63, pp 690-703.
- Cornell, R.M., and Schwertmann, U. (2003) *The iron oxides. Structure, properties, reactions occurrences and uses.* Wiley-VCH, Weinheim.
- Dubrovinsky, L.S., Dubrovinskaia, N.A., McCammon, C., Rozenberg, G.K., Ahuja, R., Osorio-Guillen, J.M., Dmitriev, V., Weber, H.P., Le Bihan, T., and Johansson, B. (2003) The structure of the metallic high-pressure Fe₃O₄ polymorph: experimental and theoretical study. *Journal of Physics-Condensed Matter*, 15(45), pp 7697-7706.

- Funamori, H., Jeanloz, R., Hguyen, J.H., Kavner, A., Caldwell, W.A., Fujino, K., Miyajima, N., Shinmei, T., and Tomioka, N. (1998) High-pressure transformations in $MgAl_2O_4$ Journal of Geophysical Research-Solid Earth, 103(B9), pp 20813-20818.
- Goff, R.J., Wright, J.P., Attfield, J.P., and Radaelli, P.G. (2005) Resonant x-ray diffraction study of the charge ordering in magnetite Journal of Physics - Condensed Matter, 17(48), pp 7633-7642.
- Gu, F., and Wills, B.A. (1988) Chromite- mineralogy and processing. Minerals Engineering, 1(13), pp 235-240.
- Haavik, C., Stolen, S., Fjellvag, H., Hanfland, M., and Hausermann, D. (2000) Equation of state of magnetite and its high-pressure modification: Thermodynamics of the Fe-O system at high pressure. American Mineralogist, 85(3-4), pp 514-523.
- Hargrove, R.S., and Kundig, W. (1970) Mössbauer Measurements of magnetite below Verwey transition. Solid State Communications, 8(5), pp 303-308.
- Hensen, B.J. and Green, D.H. (1971) Experimental study of stability of cordierite and garnet in pelitic compositions at high pressures and temperatures. 1. compositions with excess alumino-silicate. Contributions to Mineralogy and Petrology, 33(4), pp 309-330.
- Hildebrand, H., Mackenzie, K., and Kopinke, F.-D. (2009) Highly active Pd-on-magnetite nanocatalysts for aqueous phase hydrodechlorination reactions. Environmental Science & Technology, 43, pp 3254-3259.
- Huang, E., and Bassett, W.A. (1986) Rapid-determination of Fe_3O_4 phase-diagram by synchrotron radiation. Journal of Geophysical Research-Solid Earth and Planets, 91(B5), pp 4697-4703.
- Irifune, T., Fujino, K. and Ohtani, E. (1991) A new high-pressure form of $MgAl_2O_4$. Nature, 349(6308), pp 409-411.

- Ito, E. and Takahashi, E. (1989) Postspinel transformations in the system $Mg_2Si_4-Fe_2SiO_4$ and some geophysical implications. *Journal of Geophysical Research-Solid Earth*, 94(B8), pp 10637-10646.
- Kogel, J.E., Trivedi, N.C., Barker, J.M., and Krukowski, S.T. (2006) *Industrial minerals & rocks - commodities, markets, and uses*, Littleton, Colorado.
- Levy, D., Pavese, A., and Hanfland, M. (2000) Phase transition of synthetic zinc ferrite spinel ($ZnFe_2O_4$) at high pressure, from synchrotron X-ray powder diffraction *Physics and Chemistry of Minerals*, 27(9), pp 638-644.
- Liu, L.G. (1975) Disproportionation of $MgAl_2O_4$ at high pressures and temperatures. *Geophysical Research Letters*, 2(1), pp 9-11.
- López, S., Romero, A.H., Rodríguez-Hernández, P., and Muñoz, A. (2009) First-principles study of the high-pressure phase transition in $ZnAl_2O_4$ and $ZnGa_2O_4$: From cubic spinel to orthorhombic post-spinel structures. *Physical Review B*, 79(21).
- Mao, H.K., Takahashi, T., Bassett, W.A., Kinsland, G.L., and Merrill, L. (1974) Isothermal compression of magnetite to 320 Kbar and pressure-induced phase-transformation. *Journal of Geophysical Research*, 79(8), pp 1165-1170.
- McElhinny, M.W., and McFadden, P.L. (2000) *Paleomagnetism: continents and oceans*. Academic Press, San Diego.
- Menegazzo, G., Carbonin, S., and DellaGiusta, A. (1997) Cation and vacancy distribution in an artificially oxidized natural spinel. *Mineralogical Magazine*, 61(3), pp 411-421.
- Morris, E.R., and Williams, Q. (1997) Electrical resistivity of Fe_3O_4 to 48 GPa: Compression-induced changes in electron hopping at mantle pressures. *Journal of Geophysical Research-Solid Earth*, 102(B8), pp 18139-18148.
- Mullineaux, D.R., and Crandell, D.R. (1962) Recent Lahars from Mount St. Helens, Washington. *Geological Society of American Bulletin*, 73(7), pp 855-870.

- Needham, J. (1962) Astronomy in classical China. *Quarterly Journal of the Royal Astronomical Society*, 3(2), pp 87-91.
- Ohtani, E., Sawamoto, H., Masaki, K., and Kumazawa, M. (1975) Decomposition of spinel MgAl_2O_4 at extremely high-pressure. *Review of Physical Chemistry of Japan*, pp 185-187.
- O'Neill, H.S.C. (1988) Systems Fe-O and Cu-O: Thermodynamic data for the equilibria Fe-"FeO," Fe- Fe_3O_4 , "FeO"- Fe_3O_4 , Fe_3O_4 - Fe_2O_3 , Cu- Cu_2O , and Cu_2O -CuO from emf measurements. *American Mineralogist*, 73, pp 470-486.
- O'Neill, H.S.C. and Navrotsky, A. (1983) Simple spinels: crystallographic parameters, cation radii, lattice energies, and cation distributions. *American Mineralogist*, 68(1-2), pp 181-194.
- O'Neill HStC, Navrotsky A (1984) Cation distributions and thermodynamic properties of binary spinel solid solutions. *American Mineralogist*, 69(7-8), pp 733-753.
- Ono, S., Kikegawa, T., and Ohishi, Y. (2006) The stability and compressibility of MgAl_2O_4 high-pressure polymorphs *Physics and Chemistry of Minerals*, 33(3), pp 200-206.
- Pankhurst, Q.A., Connolly, J., Jones, S.K., and Dobson, J. (2003) Applications of magnetic nanoparticles in biomedicine *Journal of Physics D: Applied Physics*, 36(13), R167-R181.
- Pasternak, M.P., Nasu, S., Wada, K., and Endo, S. (1994) High-pressure phase of magnetite. *Physical Review B*, 50(9), pp 6446-6449.
- Putnis, A. (1992) *Introduction to mineral sciences*. Cambridge University Press, ISBN: 0-521-42947-1.
- Rammelmair, D., Raschka, H., and Steiner, L. (1987) Systematics of chromite occurrences in Central Palawan, Philipines. *Mineralium Deposita*, (22(3), pp 190-197.

- Reid, A.F., and Ringwood, A.E. (1969) Newly observed high pressure transformations in Mn_3O_4 , $CaAl_2O_4$ and $ZrSiO_4$. *Earth and Planetary Science Letters*, 6(3), pp 205-208.
- Ringwood, A.E. (1991) Phase transformations and their bearing on the constitution and dynamics of the mantle. *Geochimica Et Cosmochimica Acta*, 55(8), pp 2083-2110.
- Ringwood, A.E., and Reid, A.F. (1968) High pressure transformations of spinels (I). *Earth and Planetary Science Letters*, 5(4), pp 245-250.
- Sack, R.O., and Ghiorso, M.S. (1991) Chromian spinels as petrogenetic indicators - thermodynamics and petrological applications. *American Mineralogist*, 76(5-6), pp 827-847.
- Šafařík, I., and Šafaříková, M. (2002) Invited review: Magnetic nanoparticles and biosciences. *Monatshefte für Chemie*, 133(6), pp 737-759.
- Samara, G.A. and Giardini, A.A. (1969) Effect of pressure on Néel temperature of magnetite. *Physical Review*, 186(2), pp 577-580.
- Sheldon, R.I., Hartmann, T., Sickafus, K.E., Ibarra, A., Scott, B.L., Argryriou, D.N., Larson, A.C., and Von Dreele, R.B. (1999) Cation disorder and vacancy distribution in nonstoichiometric magnesium aluminate spinel, $MgO \cdot xAl_2O_3$, 82(12), pp 3293-3298.
- Shen, X., Shen, J., You, S.J., Yang, L.X., Tang, L.Y., Li, Y.C., Liu, J., Yang, H., Zhu, K., Liu, Y.L., Zhou, W.Y., Jin, C.Q., Yu, R.C., and Xie, S.S. (2009) Phase transition of Zn_2SnO_4 nanowires under high pressure *Journal of Applied Physics*, 106(11).
- Shulters, J.C. and Bohlen, S.R. (1989) The stability of hercynite and hercynite gahnite spinels in corundum-bearing or quartz-bearing assemblages. *Journal of Petrology*, 30(4), pp 1017-1031.
- Sickafus, K.E., Wills, J.M., and Grimes, N.W. (1999) Structure of Spinel," *Journal of the American Ceramic Society*, 82(12), pp 3279- 3292.

- Stachel, T., Harris, J.W., and Brey, G.P. (1998) Rare and unusual mineral inclusions in diamonds from Mwadui, Tanzania (vol 132, pg 34, 1998). *Contributions to Mineralogy and Petrology*, 132(3), pp 307-307.
- Teja, A.S., and Koh, P.-Y. (2009) Synthesis, properties, and applications of magnetic iron oxide nanoparticles. *Progress in Crystal Growth and Characterization of Materials*, 55(1-2), pp 22-45.
- Udalov, Y.P., Lavrov, B.A., Smirnov, W., Sharov, D.Y., and Sidorov, A.S. (2004) Interaction of molten iron with ceramics based on iron and aluminum oxides. *Glass Physics and Chemistry*, 30(1), pp 90-97.
- van der Zaag, P.J., Bloemen, P.J.H., Gaines, J.M., Wolf, R.M., van der Heijden, P.A.A., van der Veerdonk, R.J.M., and de Jonge, W.J.M. (2000) On the construction of an Fe₃O₄-based all-oxide spin valve *Journal of Magnetism and Magnetic Materials*, 211(1-3), pp 301-308.
- Verwey, E.J., Haayman, P.W., and Romeijn, F.C. (1947) Physical properties and cation arrangement of oxides with spinel structures. II. Electronic conductivity. *Journal of Chemical Physics*, 15(4), pp 181-187.
- Wood, B.J. and Virgo, D. (1989) Upper mantle oxidation state: Ferric iron contents of lherzolite spinels by ⁵⁷Fe Mössbauer-spectroscopy and resultant oxygen fugacities. *Geochimica Et Cosmochimica Acta*, 53(6), pp 1277-1291.
- Wood, B.J., Nell, J., and Woodland, A.B. (1991) Macroscopic and microscopic thermodynamic properties of oxides. *Reviews in Mineralogy*, 25, pp 264-302.
- Woodland, A.B., Angel, R.J., Frost, D.J., and Koch, M. (2001) Determination of the post-spinel phase boundary in magnetite and Si-bearing spinel at high pressures and temperatures. ESRF Report HS1214, European Synchrotron Radiation Facility, Grenoble, France.

Woodland, A.B., Kornprobst, J., and Wood, B.J. (1992) Oxygen thermobarometry of orogenic lherzolite massifs. *Journal of Petrology*, 33(1), pp 203-230.

Xu, W.M., Machavariani, G.Y., Rozenberg, G.K., and Pasternak, M.P. (2004) Mössbauer and resistivity studies of the magnetic and electronic properties of the high-pressure phase of Fe₃O₄. *Physical Review B*, 70(17).

Zhang, J., Xiao, G., Liu, X., Fan, Y., Liu, B., and Zhang, Z. (2009) Preparation of magnesia-hercynite refractories. *Bulletin of the Chinese Ceramic Society*.

Zuo, J., Xu, C.Y., Wang, C.S., and Yushi, Z. (2000) Identification of the pigment in painted pottery from the Xishan site by Raman microscopy. *Journal of Raman Spectroscopy*, 30(12), pp 1053-1055.

2. The stability of hercynite at high pressures and temperatures

K. Schollenbruch¹, A.B. Woodland¹, D.J. Frost²

¹ Institut für Geowissenschaften, Universität Frankfurt, Germany

² Bayerisches Geoinstitut, Universität Bayreuth, 94550 Bayreuth, Germany

Published: *Physics and Chemistry of Minerals* (2010) Vol. 37, pp137-143

2.1. Introduction

Spinel group minerals, with the general formula AB_2O_4 , are ubiquitous in many different rock types in the Earth's crust and mantle. For example, $FeCr_2O_4$, or chromite is associated with oceanic basalts and the occurrence of $MgAl_2O_4$ -rich compositions define the moderate-pressure spinel peridotite facies of the upper mantle. For the most part, naturally occurring minerals with the cubic spinel-type structure are complex solid solutions involving a number of components. Hercynite, $FeAl_2O_4$, is one such component that can be present in significant concentrations in many different geological environments. Its importance in the ceramic and steel industries has led to a large number of studies on the high-temperature stability of hercynite in the Fe-Al-O system (e.g., Richards and White 1954; Atlas and Sumida 1958; Mclean and Ward 1966). Being Fe^{2+} -bearing, hercynite stability is also strongly influenced by the prevailing oxygen fugacity, fO_2 . At ambient pressure and under reducing conditions (~ 2 log units below the Fe-wüstite oxygen buffer equilibrium), hercynite breaks down to a mixture of either corundum and Fe or a defect spinel plus Fe (Woodland and Wood 1990). Above 875°C, $FeAl_2O_4$ forms a complete solid solution with magnetite (Fe_3O_4), stabilising Al-bearing spinel over a range in excess of 8 log units in oxygen fugacity (Turnock and Eugster 1962). This means that at 1 bar pressure, the oxide mixture wüstite + corundum is generally metastable relative to a hercynite-rich spinel. Several mineral equilibria involving hercynite have been investigated at elevated pressure with the aim of calibrating a geobarometer applicable to granulite-facies metamorphic rocks (Bohlen et al. 1986; Shulters and Bohlen 1988).

At high pressures corresponding to those in the deep mantle, many phases with the spinel structure are known to either transform to a denser structure with orthorhombic symmetry or break down into their constituent oxides. For example, magnetite has been found to transform to a phase with a $CaTi_2O_4$ -type structure (Dubrovinsky et al. 2003). Similar post-spinel transformations to either $CaMn_2O_4$ -type or $CaFe_2O_4$ -type structures have been reported at

pressures above 10 GPa for FeCr_2O_4 (Chen et al. 2003), MgFe_2O_4 (Andrault & Bolfan-Casanova 2001; Winell et al. 2006), Mn_3O_4 and CaAl_2O_4 (Ringwood & Reid 1969). Another type of transition behaviour occurs in MgAl_2O_4 where it first decomposes to a mixture of $\text{MgO} + \text{Al}_2\text{O}_3$ at ~ 15 GPa and $1000\text{-}1600^\circ\text{C}$ (Liu 1975), before reforming into a phase with MgAl_2O_4 stoichiometry and a CaFe_2O_4 -type structure at pressures above 25 GPa (Irifune et al. 1991, 2002; Akaogi et al. 1999). Above ~ 40 GPa this phase transforms into another polymorph with the closely related CaTi_2O_4 -type structure (Funamori et al. 1998).

The high-pressure behaviour of hercynite is much less well known. Apparently based upon a single experiment, Ringwood and Reid (1968) reported that hercynite is not stable at 12 GPa and 1000°C , disproportionating into a mixture of corundum and wüstite. However, this breakdown reaction has not been studied in any detail and its position in P-T space remains essentially unconstrained. In addition, it is not known if another phase with FeAl_2O_4 stoichiometry forms at still higher pressures as is observed for MgAl_2O_4 . Therefore, the goals of this study were 1) to investigate the high-pressure stability of hercynite in detail and 2) to test whether a "post-spinel"-type phase with FeAl_2O_4 stoichiometry becomes stable at high pressures and temperatures.

2.2. Experimental methods

The high-pressure experiments were performed at the Bayerisches Geoinstitut in a 500 tonne multi-anvil press. In addition, several experiments at pressures > 15 GPa were performed with a 1000 t multi-anvil press. Hercynite was produced by sintering stoichiometric mixtures of Al_2O_3 and Fe metal in a gas-mixing furnace under controlled $f\text{O}_2$, following the procedure described in Woodland and Wood (1990). The resulting single phase hercynite had a unit-cell parameter, $a_0 = 8.1551(5)\text{\AA}$, which is in excellent agreement with that reported by Hill (1984), but is somewhat larger than values of $8.151\text{-}8.150\text{ \AA}$ reported by Turnock & Eugster (1962) and Larsson et al. (1994). Based on these later studies, we estimate that our hercynite contains ≈ 1 mol % Fe_3O_4 component. Some experiments were performed using a mixture of corundum and wüstite. The corundum was pre-sintered at 1000°C and the wüstite was synthesised by reducing Fe_2O_3 in a gas-mixing furnace at 1100°C and a $\log f\text{O}_2 = -12$.

Experiments in the pressure range 6-9 GPa were performed using an 18mm edge length Cr_2O_3 -doped MgO octahedral pressure assembly in conjunction with tungsten carbide cubes with 11 mm edge length corner truncations (a so called 18/11 assembly). Experiments performed above

15 GPa employed a 10/5 assembly. All assemblies use cylindrical LaCrO_3 heaters. Samples were packed in Ag or Re capsules, which were sealed mechanically. In most experiments, two capsules were used in parallel, one containing hercynite + ~5 wt % Fe metal, and the other containing a stoichiometric mixture of wüstite and corundum \pm 6 wt % Fe. The addition of Fe was intended to help maintain a low f_{O_2} during the experiments and minimise the formation of a magnetite component in the hercynite. The experiments conducted at pressures >15 GPa employed a single capsule containing hercynite. Temperature was monitored by $\text{W}_{75}\text{Re}_{25}/\text{W}_{97}\text{Re}_3$ thermocouples, with emf uncorrected for pressure. The experiments were terminated by turning off the power and were subsequently decompressed. Run times and pressure-temperature conditions are provided in Tab. 2.1.

Table 2.1: experimental results.

exp. ¹ number	pressure (GPa)	temperature (°C)	time (h)	phases produced	unit cell parameter of spinel phase (Å)
V452cw*	7.0	950	3.5	<i>no reaction</i>	-
V452hc	7.0	950	3.5	cor + wü	-
V556cw	7.0	950	3.5	<i>no reaction</i>	-
V429cw*	7.0	1000	4.5	hc	8.2111(1)
V429hc	7.0	1000	4.5	hc + cor	8.1504(1)
V415hc*	7.5	1150	4.5	cor + wü	-
V559cw	7.5	1150	3.5	<i>no reaction</i>	-
V559hc	7.5	1150	3.5	hc + cor	8.1687(16)
V416cw*	7.5	1300	4.5	hc	8.1911(1)
V416hc	7.5	1300	4.5	hc + cor	8.1619(1)
V419cw*	8.0	1450	3.5	hc	8.1836(1)
V419hc	8.0	1450	3.5	cor + wü + hc	8.1701(5)
V557cw	8.0	1450	4.0	hc	8.1703(2)
V454cw*	8.0	1500	1.0	hc	8.1590(2)
V454hc	8.0	1500	1.0	hc + cor	8.1616(1)
V558cw	8.5	1650	4.0	hc	8.1708(1)
V427cw*	8.5	1720	1.2	hc	8.1898(1)
V427hc	8.5	1720	1.2	hc + cor	8.1650(1)
H2648hc*	18	1400	3.0	cor + wü	-
H2704hc*	24	1600	3.5	cor + wü	-

¹ = cw and hc indicate starting materials of corundum + wüstite or hercynite, respectively

* = no metallic iron added

Experiments using the 18/11 assembly were performed using a 500 tonne Walker-type multi-anvil press. The relationship between applied force and sample pressure was found to be slightly more efficient than for an identical assembly in a 1000 tonne split sphere press, as shown in Fig. 2.1. The pressure calibration for this assembly in the 1000 tonne press has been shown to be insensitive to pressure within the uncertainties of the calibration over a broad range of temperature (800-1800°C, see Keppler and Frost 2005). Experiments in the 10/5 assembly employed a 1000 tonne split-sphere multi-anvil, for which the pressure calibration is reported by Keppler and Frost (2005).

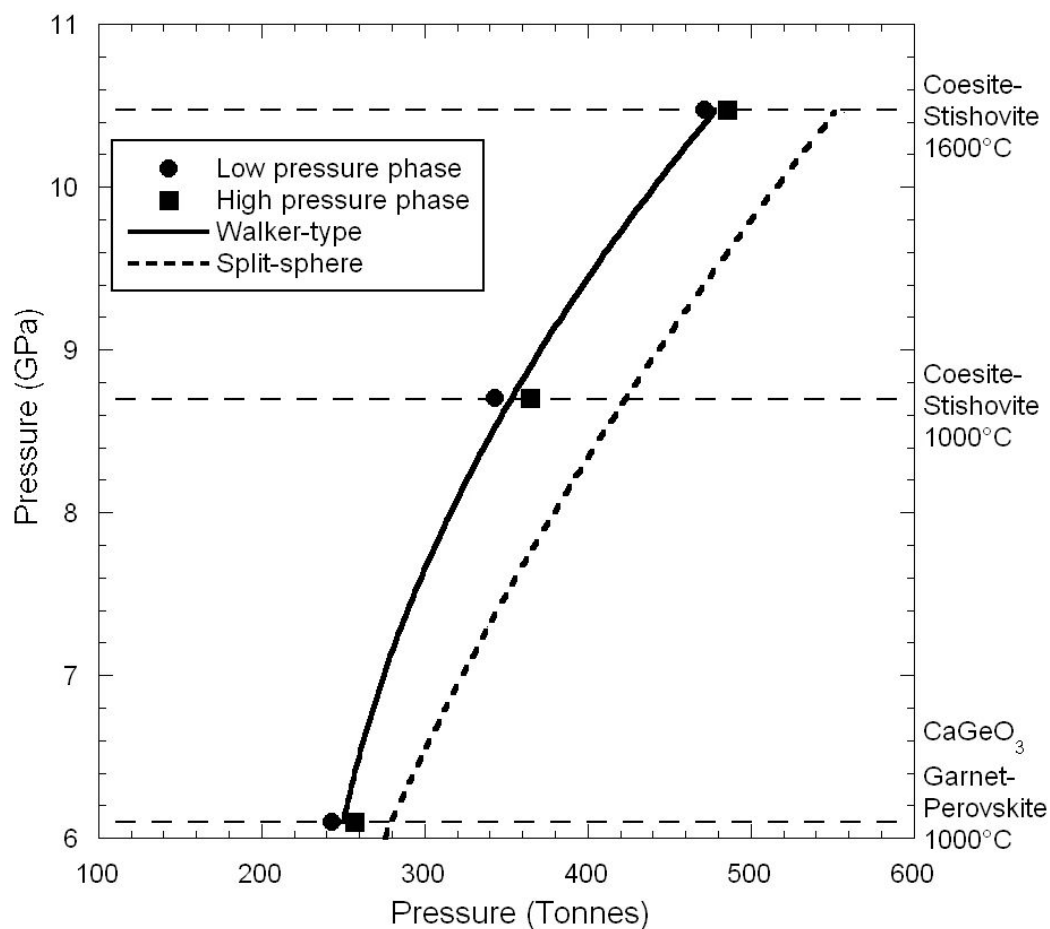


Figure 2.1: Pressure calibration for the Walker-type multi-anvil press at the Bayerisches Geoinstitut. Note that the calibration curve (dashed) for the 1000 t split-sphere multi-anvil press at the same institute (Keppler and Frost 2005) is essentially parallel. See text for further discussion.

The run products were analysed by powder X-ray diffraction using a Philips X'Pert Pro X-ray diffraction system operating in reflection mode, with $\text{CoK}\alpha_1$ ($\lambda = 1.78897 \text{ \AA}$) radiation selected with a focusing monochromator, a symmetrically cut curved Johansson $\text{Ge}_{(111)}$ crystal, and a Philips X'celerator detector. Diffraction patterns were collected between 20° and 120° 2θ

and corundum peaks were used to calibrate each pattern with STOE Win XPOW (version 1.08, Stoe & Cie GmbH) software. Unit-cell parameters of hercynite were determined by LeBail refinement with the GSAS software package (Larson and von Dreele 1988), using the EXPGUI interface of Toby (2001).

Small pieces of selected samples were mounted in epoxy and prepared for investigation with a JEOL SEM JSM-649. This allowed the sample textures to be assessed and to check whether metallic Fe was still present in the sample after the experiment. For example, the formation of hercynite at the expense of corundum and wüstite is clearly observed in experiment V429cw (Fig. 2.2).

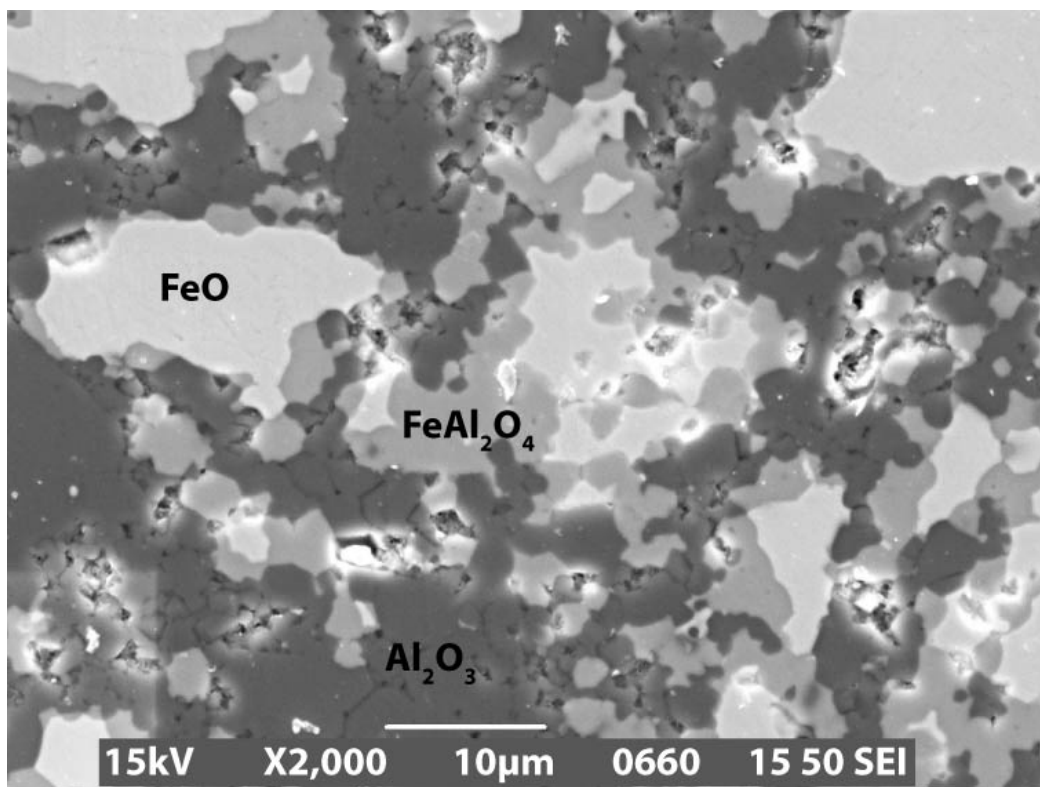


Figure 2.2: Backscattered electron image of sample V429cw (1000° C, 7 GPa) clearly demonstrating the formation of hercynite from corundum and wüstite.

2.3. Results and Discussion

2.3.1. Hercynite breakdown

Analysis of the X-ray powder diffraction patterns unambiguously revealed which phase or phases were stable at the P-T conditions of each experiment. In this case, it was either that hercynite was produced from corundum + wüstite, or that the corundum + wüstite mixture yielded hercynite. Thus, we confirm the observation of Ringwood and Reid (1968) that hercynite breaks down to a mixture of wüstite and corundum at high pressures. However, the breakdown reaction occurs at significantly lower pressure than their single data point at 12 GPa and 1000°C. We have bracketed the reaction to lie between 7 and 8.5 GPa at temperatures of 1000-1650°C (Fig. 2.3).

The position of the hercynite breakdown reaction in P-T space was assessed from a weighted least squares linear regression. For 7.0 and 7.5 GPa, we picked the midpoints defined by our experimental brackets. The method outlined by Powell and Holland (1993) was used to assess appropriate uncertainties in temperature for these two data points (along with an uncertainty of ± 0.5 GPa in pressure. At 8.0 GPa, the hercynite in experiment V419hc clearly yielded the assemblage wüstite + corundum, while in experiment V557cw, the oxide mixture clearly produced hercynite at nominally the same temperature of 1450 °C (Tab. 2.1). As such, we consider the phase boundary to lie at 8.0 GPa and 1450 °C, within the experimental uncertainties of ± 0.5 GPa and ± 30 °C. Only a half bracket is available at 8.5 GPa, where hercynite was produced at 1650 °C from an oxide mixture (Tab. 2.1).

Using the three experimental brackets at 7, 7.5 and 8 GPa and considering uncertainties in both pressure (± 0.5 GPa) and temperature (± 30 -50 K), a least squares regression yields the following relation:

$$2.15(5) \times 10^{-3} T (\text{K}) + 4.29(8) = P (\text{GPa}) \quad (2.1)$$

for the equilibrium:



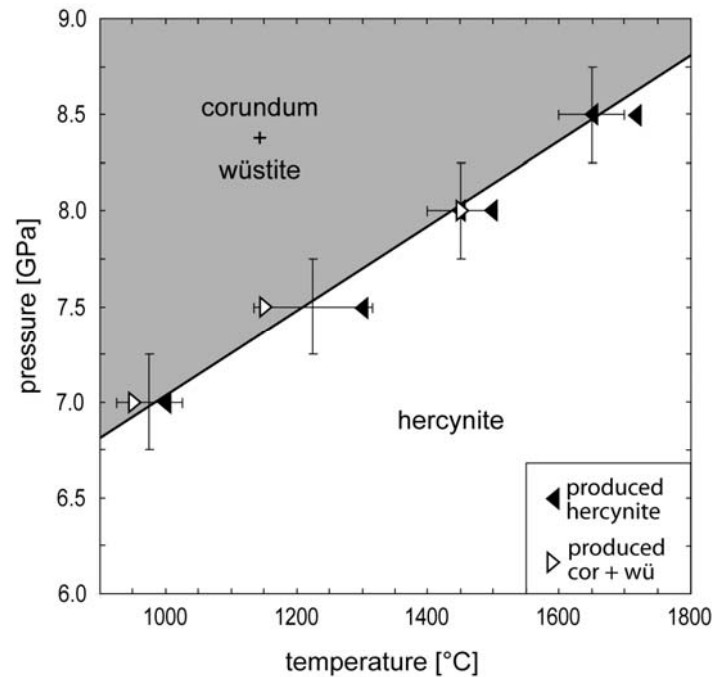


Figure 2.3: Experimental brackets for the breakdown of hercynite. Also shown is the result of a linear regression through these brackets.

The half-bracket from experiment V558cw at 8.5 GPa is just consistent with this boundary (Fig. 2.3).

Inspection of the unit-cell parameter for the hercynite produced in the experiments reveals a progressive shift to larger values with increasing temperature (Tab. 2.1). Such a change in unit-cell parameter is attributable to the incorporation of a small Fe_3O_4 component into the hercynite (i.e. Turnock & Eugster 1962), and is consistent with the additional presence of corundum in these samples. The formation of a magnetite component can be understood in terms of a small degree of oxidation occurring during the experiment, with the extent increasing with increasing temperature. The addition of metallic Fe to the starting materials acted to minimise this effect, but did not completely eliminate it. In fact, metallic Fe was found to only remain in the products of experiments performed at $\leq 1000^\circ\text{C}$. This interpretation is further supported by the fact that the largest cell parameters (and highest magnetite contents) were found in the few experiments where no Fe was added (Tab. 2.1). The formation of the hercynite-magnetite solid solutions also caused some Al to be exsolved, producing corundum as an additional phase. In contrast to the hercynite breakdown reaction (equil. 1), no wüstite is produced during such a process.

The presence of a hercynite-magnetite solid solution in our experiments means that the phase boundary determined above must be shifted relative to its position for the pure endmember

equilibrium (1). We can correct for this by considering the following thermodynamic relation describing the standard free energy change of equilibrium (1) with the standard state defined as the pure phase at the P and T of interest:

$$(\Delta G^\circ)_{P,T} = \Delta H_{1bar,T}^\circ - T\Delta S_{1bar,T}^\circ + \int_{1bar}^P \Delta V^\circ dP = -RT \ln \frac{a_{Al_2O_3}^{hc} a_{FeO}}{a_{FeAl_2O_4}^{hc}} \quad (2.3)$$

Assuming all phases to be pure except the hercynite-magnetite solid solution yields:

$$\Delta H_{1bar,T}^\circ - T\Delta S_{1bar,T}^\circ + \int_{1bar}^P \Delta V^\circ dP = RT \ln a_{FeAl_2O_4}^{hc} \quad (2.4)$$

At constant temperature, the displacement of the equilibrium involving a solid solution relative to the pure endmember equilibrium is related to the activity term:

$$\int_{P_o}^P \Delta V^\circ dP = RT \ln a_{FeAl_2O_4}^{hc} \quad (2.5)$$

where P_o is the actual equilibrium pressure of the endmember equilibrium (1). The relationship between the unit-cell parameter and composition reported by Turnock & Eugster (1962) can be used to estimate the composition of the hercynite-magnetite solid solutions in our experiments (Tab. 2.2). The samples with added metallic Fe were employed here since they should most accurately represent the true extent of the displaced equilibrium due to solid solution in the hercynite. The

activity of hercynite was then computed using the activity-composition model for multi-component spinels from Nell & Wood (1989). To evaluate the magnitude of the displacement in the

Table 2.2: Correction to pressure due to hercynite magnetite solid solution

experimental bracket (P/T)	$X_{FeAl_2O_4}^{Hc}$ ^a	$a_{FeAl_2O_4}^{Hc}$ ^b	P - P ₀ (bar)
7.0 GPa / 985 °C	1	1	0
7.5 GPa / 1227 °C	0.96	0.925	3900
8.0 GPa / 1450 °C	0.93	0.875	7200
8.5 GPa / 1650 °C	0.93	0.874	7900

^a computed from relation given by Turnock & Eugster (1962)

^b computed using activity model of Nell & Wood (1989)

equilibrium pressure (i.e. $P-P_o$), ΔV° was computed for equilibrium (1) at the P and T of each experimental bracket and was assumed to remain constant within the range of P and P_o . For corundum and hercynite, the molar volumes and bulk moduli were taken from Holland & Powell (1998) and two-term thermal expansion coefficients were taken from the tabulation of Fei (1995). Except for the bulk modulus, data for FeO were taken from Haas & Hemingway (1992). In order to maintain the same functional form as for the other phases, the thermal expansion coefficients for FeO were obtained by refitting their molar volumes tabulated as a function of temperature. The bulk modulus was taken from Zhang (2000). The value for the bulk modulus at high temperature for all three phases was taken to be $K_T = K_o (1 - 1.5 \times 10^{-4} (T - 298))$, following the approach used by Holland and Powell (1998). The results are listed in Tab. 2.2. For the experimental bracket at 7.0 GPa and 985°C, the unit-cell parameter indicated that essentially endmember hercynite was present so that no correction was necessary. The other brackets and the half-bracket at 8.5 GPa and 1650°C are systematically shifted to lower pressure by 0.4-0.8 GPa (Fig. 2.4). Making this correction to the experimental brackets yields the following relation for the position of equilibrium (1):

$$6.0(9) \times 10^{-4} T (\text{K}) + 6.2(1) = P (\text{GPa}) \quad (2.6)$$

The corrected position of the experiment at 1650°C (V558cw) lies slightly to the wrong side of this phase boundary, however, considering the uncertainties in the experimental conditions, along with added uncertainties related to the correction procedure, this experiment is reasonably consistent with the other experimental data (Fig. 2.4). Having confirmed that the high-pressure stability of hercynite is limited by its breakdown to constituent oxides (equil. 1), the position of this equilibrium in P-T space can also be computed from available thermodynamic data. We have done this by combining data for hercynite and corundum from Holland & Powell (1990, 1998) with that of FeO from Haas & Hemingway (1992). The heat capacity data for FeO were refit to obtain an expression consistent with the formulation used by Holland and Powell (1998). Two different phase boundaries have been calculated and are plotted in Fig. 2.4. In one case, the data from Holland and Powell (1998) were used. This boundary exhibits a much steeper clapeyron slope compared with the results from this study. In the other instance, all data remained the same except that the standard enthalpy, entropy and heat capacity tabulated for hercynite and corundum in the Holland and Powell (1990) dataset were employed. We opted to keep the more sophisticated formulation for $V_{T,P}$ since our calculations are at pressures

significantly beyond the range intended for application of the Holland and Powell (1990) dataset (i.e. crustal pressures $< \sim 4$ GPa).

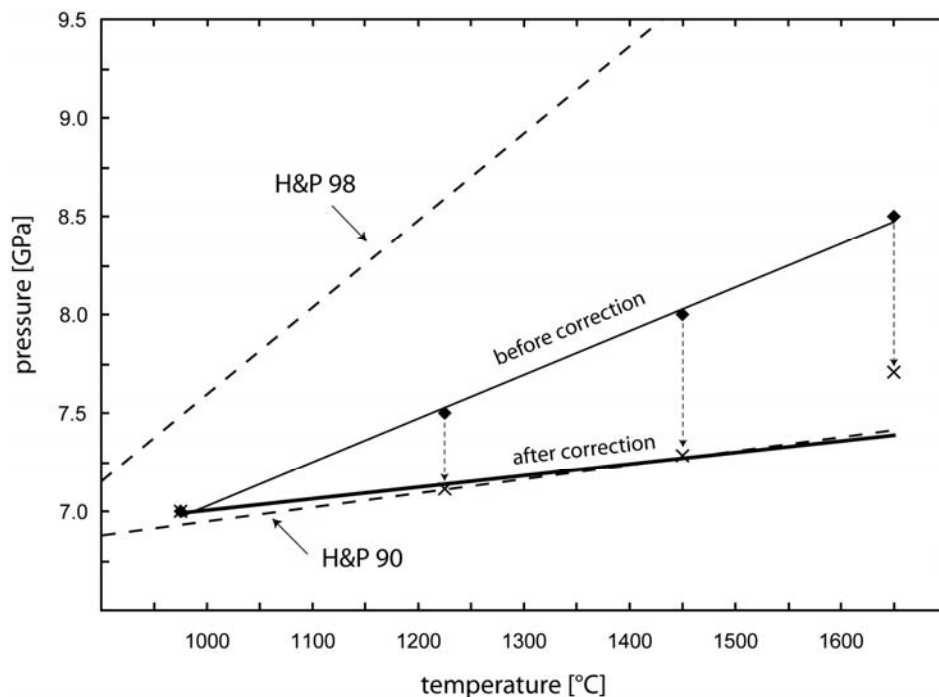


Figure 2.4: Position of the hercynite breakdown reaction (equil. 1) before and after correction for magnetite solid solution in hercynite. Also shown are two calculated phase boundaries primarily based on thermodynamic data from Holland and Powell (1998) (H&P98) and Holland and Powell (1990) (H&P 90), respectively (see text).

The resulting phase boundary is in remarkable agreement with our experimental data after correction for the incorporation of magnetite in the hercynite (Fig. 2.4). The difference in the slopes of the two calculated boundaries is attributable to a significant change in the S°_{298} of hercynite from 116 to 107.5 J mol⁻¹ K⁻¹ between the 1990 and 1998 datasets of Holland and Powell. Concomitant changes in the heat capacity functions of hercynite and corundum between the two datasets clearly have not sufficiently compensated for such a large shift in entropy. Thus, our results are consistent with a larger value for S°_{298} of hercynite than is tabulated in the Holland and Powell (1998) dataset. This supports the results of Klemme & van Miltenburg (2003), who reports a $S^{\circ}_{298} = 113.9$ J mol⁻¹ K⁻¹ for hercynite based upon low temperature calorimetry measurements.

2.3.2. A high pressure FeAl_2O_4 polymorph

The question remains if corundum and wüstite recombine at high pressures to form another phase with FeAl_2O_4 stoichiometry, as is observed in MgAl_2O_4 (Irifune et al. 1991, 2002; Akaogi et al. 1999). It is generally observed that reactions involving Fe^{2+} -bearing oxides and silicates take place at lower pressures compared to the analogous Mg-bearing system. For example, this is the case for $(\text{Mg,Fe})_2\text{SiO}_4$ olivine and $(\text{Mg,Fe})\text{SiO}_3$ pyroxenes (e.g., Ringwood 1975, Woodland & Angel 1997).

If we consider the analogue MgAl_2O_4 system, spinel decomposes to a mixture of $\text{MgO} + \text{Al}_2\text{O}_3$ at ~ 15 GPa and $1200\text{-}1600^\circ\text{C}$ (Liu 1975), which is 7-8 GPa higher than where we observe

the breakdown reaction of FeAl_2O_4 (Fig. 2.5). As the recombination of $\text{MgO} + \text{Al}_2\text{O}_3$ into MgAl_2O_4 with the CaFe_2O_4 -type structure occurs at pressures of $\sim 25\text{-}27$ GPa (Irifune et al. 1991, 2002; Akaogi et al. 1999), we would expect the analogous reaction for FeAl_2O_4 to lie at $\sim 18\text{-}20$ GPa, if such a high-pressure polymorph were stable. As a test, two experiments were performed at 18 and 24 GPa and 1400°C and 1600°C , respectively (Tab. 2.1, Fig. 2.5). In both cases, the hercynite starting

material was found to have broken down to corundum + wüstite. Thus, we conclude that a high-pressure polymorph of FeAl_2O_4 with a CaFe_2O_4 -type or related structure is unlikely. Although

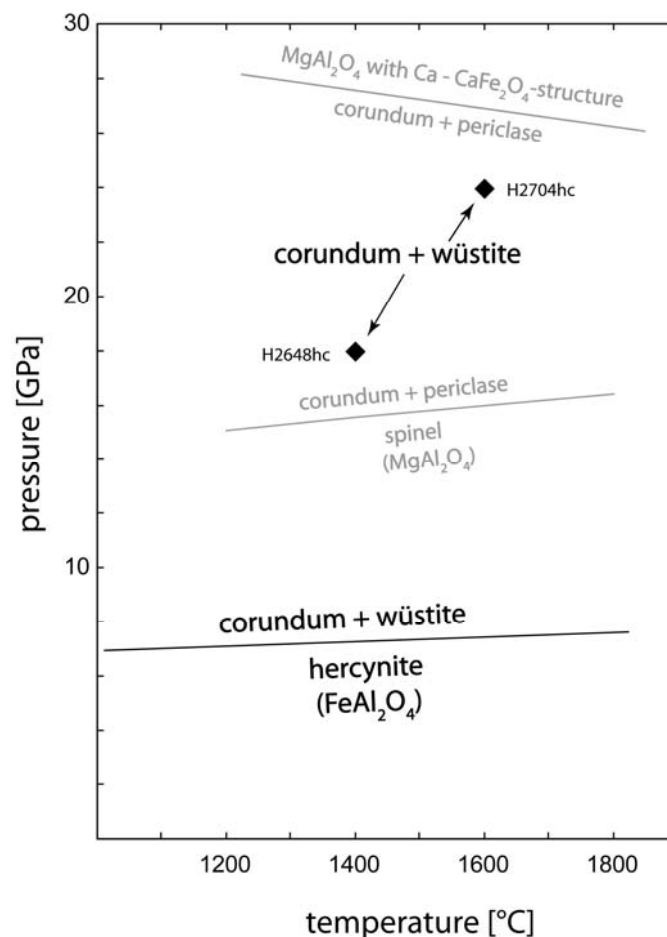


Figure 2.5: Phase stability of hercynite and corundum + wüstite compared with literature data for the analogous MgAl_2O_4 system.

such a polymorph could be stable at pressures > 25 GPa, this would be an exception to the systematic relations between Mg and Fe²⁺-bearing phases described above.

2.5. Acknowledgements

This work was supported by the Deutsche Forschungsgemeinschaft as part of the Schwerpunktprogramm #1236 “Structures and properties of crystals at extreme pressures and temperatures”. T. Boffa Ballaran is thanked for helping with the X-ray diffraction measurements. Reviews by D. Andrault and an anonymous reviewer improved the manuscript and are gratefully acknowledged.

2.6. References

- Akaogi, M., Hamada, Y., Suzuki, T., Kobayashi, M., and Okada, M. (1999) High pressure transitions in the system MgAl₂O₄-CaAl₂O₄: a new hexagonal aluminous phase with implications for the lower mantle. *Physics of the Earth and Planetary Interiors*, (115), pp 67-77.
- Andrault, D. and Bolfan-Casanova, N. (2001) High-pressure phase transformations in the MgFe₂O₄ and Fe₂O₃-MgSiO₃ systems. *Physics and Chemistry of Minerals* (28), pp 211-217.
- Atlas, L.M. and Sumida, W.K. (1958) Solidus, subsolidus, and subdissociation phase equilibria in the system Fe-Al-O. *Journal of the American Ceramic Society* (41), p 140.
- Bohlen, S.R., Dollase, W.A., and Wall, V.J. (1986) Calibration and applications of spinel equilibria in the system FeO-Al₂O₃-SiO₂. *Journal of Petrology* (27), pp 1143-1156.
- Chen, M., Shu, J., Xie, X., and Mao, H. (2003) Natural CaTi₂O₄-structured FeCr₂O₄ polymorph in the Suizhou meteorite and its significance in mantle mineralogy. *Geochimica et Cosmochimica Acta* (67), pp 3937-3942.

- Dubrovinsky, L.S., Dubrovinskaia, N.A., McCammon, C., Rozenberg, G.Kh., Ahuja, R., Osorio-Guillen, J.M., Dmitriev, V., Weber, H.P., Le Bihan, T., and Johansson, B. (2003) The structure of the metallic high pressure Fe_3O_4 polymorph: experimental and theoretical study. *Journal of Physics and Condensed Matter* (15), pp 7697-7706.
- Fei, Y. (1995) Thermal expansion. In: Ahrens TJ (ed) *Mineral Physics & Crystallography - A Handbook of Physical Constants*, 1st edn. American Geophysical Union, Washington DC, pp 29-44.
- Funamori, N., Jeanloz, R., Nguyen, J.H., Kavner, A., Caldwell, W.A., Fujino, K., Miyajima, N., Shinmei, T., and Tomoika, N. (1998) High-pressure transformations in MgAl_2O_4 . *Journal of Geophysical Research* (103), pp 20813-20818.
- Haas, J.L. and Hemingway, B.S. (1992) Recommended standard electrochemical potentials and fugacities of oxygen for the solid buffers and thermodynamic data in the systems iron-silicon-oxygen, nickel-oxygen, and copper-oxygen. U.S. Geological Survey Open-File report 92-267, 733pp.
- Hill, R.J. (1984) X-ray powder diffraction profile refinement of synthetic hercynite. *American Mineralogist* (69), pp 937-942.
- Holland, T.J.B. and Powell, R. (1990) An enlarged and updated internally consistent thermodynamic dataset with uncertainties and correlations: the system $\text{K}_2\text{O}-\text{Na}_2\text{O}-\text{CaO}-\text{MgO}-\text{MnO}-\text{FeO}-\text{Fe}_2\text{O}_3-\text{Al}_2\text{O}_3-\text{TiO}_2-\text{SiO}_2-\text{C}-\text{H}_2-\text{O}_2$. *Journal of Metamorphic Geology* (8), pp 89-124.
- Holland, T.J.B. and Powell, R. (1998) An internally consistent thermodynamic dataset for phases of petrological interest. *Journal of Metamorphic Geology* (16), pp 309-343.
- Irifune, T., Fujino, K., and Ohtani, E. (1991) A new high-pressure form of MgAl_2O_4 . *Nature* (349), pp 409-411.

- Irifune, T., Naka, H., Sanehira, T., Inoue, T., and Funakoshi, K. (2002) In situ X-ray observations of phase transitions in MgAl_2O_4 spinel to 40 GPa using multianvil apparatus with sintered diamond anvils. *Physics and Chemistry of Minerals* (29), pp 645-654.
- Keppler, H. and Frost, D.J. (2005) Introduction to minerals under extreme conditions. In Miletich, R. (ed), *Mineral Behaviour at Extreme Conditions EMU Notes in Mineralogy* 7, Eötvös University Press, Budapest, pp 1-30.
- Klemme, S. and van Miltenburg, J.C. (2003) Thermodynamic properties of hercynite (FeAl_2O_4) based on adiabatic calorimetry at low temperatures. *American Mineralogist* (88), pp 68-72.
- Larsson, L., O'Neill, H.St.C, and Annersten, H. (1994) Crystal chemistry of synthetic hercynite (FeAl_2O_4) from XRD structural refinements and Mössbauer spectroscopy. *European Journal of Mineralogy* (6), pp 39-51.
- Larson, A.C. and von Dreele, R.B. (1988) GSAS manual Los Alamos National Laboratory, report LAUR, pp 86-748.
- Liu, L.-G. (1975) Disproportionation of magnesium aluminium oxide (MgAl_2O_4) spinel at high pressures and temperatures. *Geophysical Research Letters* (2), pp 9-11.
- McLean, A. and Ward, R.G. (1966) Thermodynamics of hercynite formation. *Journal of the Iron and Steel Institute* 204: pp 8-11.
- Nell, J. and Wood, B.J. (1989) Thermodynamic properties in a multicomponent solid solution involving cation disorder: Fe_3O_4 - MgFe_2O_4 - FeAl_2O_4 - MgAl_2O_4 spinels. *American Mineralogist* (74), pp 1000-1015.
- Powell, R. and Holland, T.J.B. (1993) On the formulation of simple mixing models for complex phases. *American Mineralogist* (78), pp 1174-1180.

- Richards, R.G. and White, J. (1954) Phase relationships of iron oxide-containing spinels. Part II. Relationships in the systems Fe-Cr-O, Fe-Mg-O, Fe-Al-Cr-O and Fe-Al-Cr-Mg-O. Transactions of the British Ceramic Society (53), pp 422-459.
- Ringwood, A.E. (1975) Composition and Petrology of the Earth's Mantle. McGraw-Hill, USA 618 pp.
- Ringwood, A.E. and Reid, A.F. (1968) High pressure polymorphs of olivines: The K_2NiF_4 type. Earth and Planetary Science Letters (5), pp 67-70.
- Ringwood, A.E. and Reid, A.F. (1969) High pressure transformations of spinels (I). Earth and Planetary Science Letters (5), pp 245-250.
- Shulters, J.C. and Bohlen, S.R. (1988) The stability of hercynite and hercynite-gahnite in corundum- or quartz-bearing assemblages. Journal of Petrology (30), pp 1017-1031.
- Toby, B.H. (2001) EXPGUI, a graphical user interface for GSAS. Journal of Applied Crystallography (34), pp 79-83.
- Turnock, A.C. and Eugster, H.P. (1962) Fe-Al Oxides: Phase relations below 1000 °C. Journal of Petrology (3), pp 533-565.
- Winell, S., Annersten, H., and Prakapenka, V. (2006) The high-pressure phase transformation and breakdown of $MgFe_2O_4$. American Mineralogist (91), pp 560-567.
- Woodland, A.B. and Angel, R.J. (1997) Reversal of the orthoferrosilite - high-P clinoferrosilite transition, a phase diagram for $FeSiO_3$ and implications for the mineralogy of the Earth's upper mantle. European Journal of Mineralogy (9), pp 245-254.
- Woodland, A.B. and Wood, B.J. (1990) The breakdown of hercynite at low fO_2 . American Mineralogist (75), pp 1342-1348.
- Zhang, J.Z. (2000) Effect of defects on the elastic properties of wüstite. Physical Review Letters (84), pp 507-510.

3. Detecting the Spinel – Post-spinel Transition in Fe₃O₄ by in situ Electrical Resistivity Measurements

Klaus Schollenbruch¹, Alan Woodland¹, Daniel Frost², Falko Langenhorst²

¹, JWG University, Inst. für Geowissenschaften, Frankfurt am Main, Germany

², Bayerisches Geoinstitut, Bayreuth, Germany

Published: High Pressure Research (2009) Vol. 29, No. 4, pp.520-524

3.1. Introduction

Understanding the behaviour of natural iron-bearing systems at high pressures and temperatures relevant to the Earth's mantle requires knowledge of the phase relations in simple systems such as Fe – O. Fe₃O₄ (magnetite) is an important phase which is widespread in rocks and even occurs as inclusions in diamond (Stachel et al. 1998). Magnetite undergoes a first-order phase transformation to a 6.5% denser phase (h-Fe₃O₄) with CaTi₂O₄-structure at ~25-30 GPa and room temperature (Fei et al. 1999; Haavik et al. 2000; Huang and Bassett 1986; Dubrovinsky et al. 2003). However, the position of the phase boundary in P-T space remains poorly constrained because h-Fe₃O₄ is not quenchable and because the phase transformation is very sluggish at low temperatures. To overcome kinetic effects, in situ experiments at high temperature and pressure must be made. Since the electrical conduction of magnetite is controlled by electron hopping between Fe²⁺ and Fe³⁺ on the octahedral sites (e.g., Kündig and Hargrove 1969; Mason and Bowen 1981), structural changes due to a phase transformation should be immediately reflected by a change in resistivity. Here we report the results of high temperature and pressure resistivity measurements performed in a multi-anvil press aimed at detecting the magnetite–h-Fe₃O₄ transition.

3.2. Experimental

Magnetite was synthesized at 1 atm from pure Fe₂O₃ at 1573 K and log *f*_{O₂} = -5.5 to achieve a stoichiometric composition (Diekmann 1982). The X-ray powder diffraction indicated only magnetite reflections, with the unit cell *a*₀ = 8.3966(6) Å, in good agreement

with Haavik et al. (2000). Experiments were performed in a 5000 t multi-anvil press at the Bayerisches Geoinstitut using 18/11 (octahedral edge length/truncation edge length in mm)

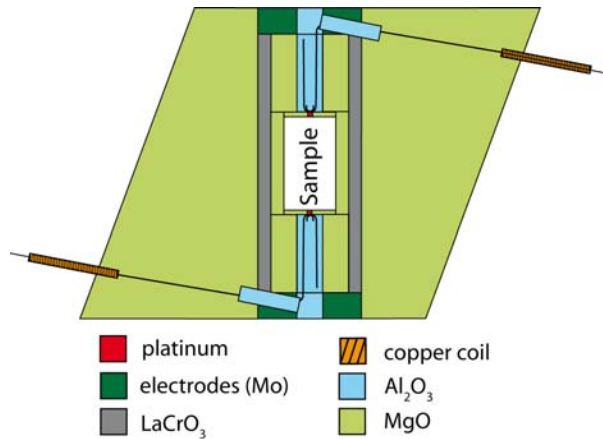


Figure 3.1: Sketch of the pressure cell



Figure 3.2: The pressure cell (with two thermocouples) is surrounded by six (of eight) WC-cubes.

Cr_2O_3 -doped MgO pressure assemblies containing LaCrO_3 heaters (Fig. 3.1). A full description of the pressure calibration is reported by Frost et al. (2004). Temperature was monitored with a $\text{W}_{75}\text{Re}_{25}/\text{W}_{97}\text{Re}_3$ thermocouple (Fig. 3.2). The sample consisted of a pre-pressed cylinder of magnetite produced at 6 GPa and 1200 K for one hour. This treatment minimised compaction during the experiment and allowed us to omit the use of a metal capsule, which might interfere with the electrical measurements. The experiments were carried out by first pressurising to the desired pressure (6, 8, 10 or 12 GPa) and then heating. Such a sequence is necessary to assure the validity of the pressure calibration.

Resistivity measurements employed the four-electrode method (Fig. 3.3), using two thermocouples placed at either end of the sample cylinder. A thin Pt disc separated the sample

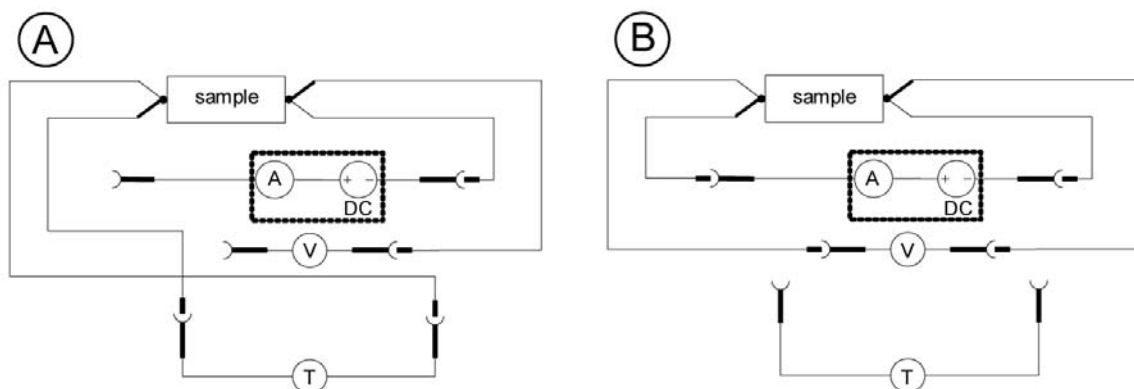


Figure 3.3: Block diagram of the electrical circuit for resistivity measurement. Measurements were both made without (A) and with (B) an applied constant current of 40mA

from the thermocouple junction. To isolate the sample signal from that of the remaining circuit components, measurements were made both with and without an applied current of 40 mA, from a constant current DC power supply. Once at the desired pressure, measurements were made at temperature steps of ~ 50 K during both heating and cooling. The resistivity of the sample was calculated by:

$$\rho = a/[x(V_I - V_0)/I] \quad (3.1)$$

whereas a and x are the cross-sectional area and length of the sample cylinder (as measured after the experiment), and V_I and V_0 are the voltages measured with and without the applied current (I), respectively. After the experiments, the pressure cell was cut in half and polished for optical examination. Material from most experiments was made into thin sections and then prepared for further TEM investigation by Ar ion milling.

3.3. Results and Discussion

3.3.1. The measurements

Results are presented as a function of temperature (each experiment at a particular

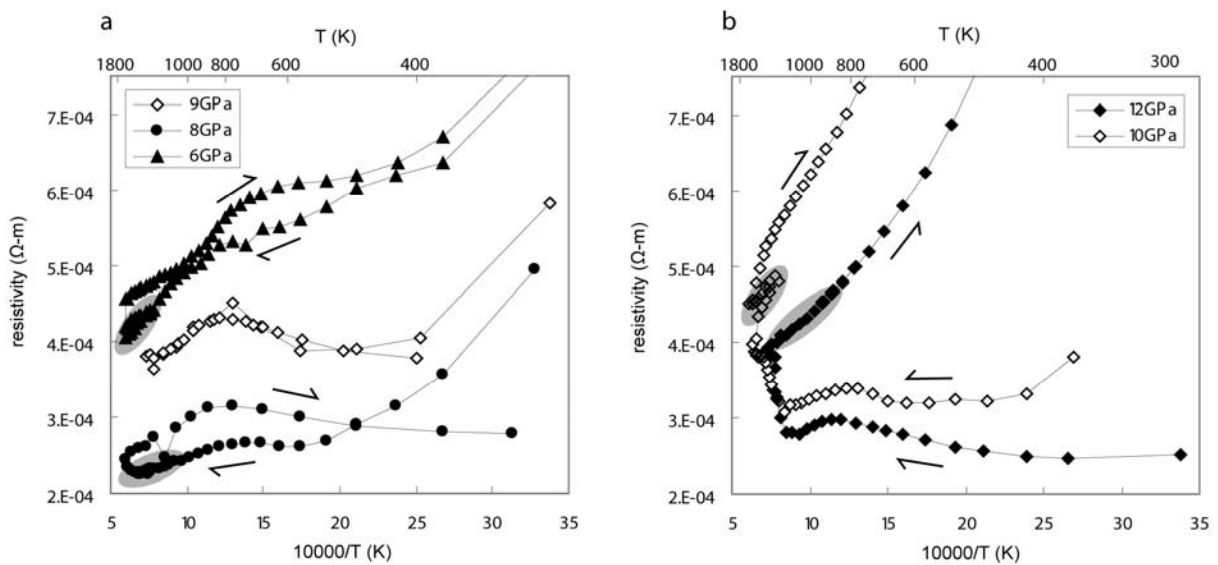


Figure 3.4a/b: Electrical resistivity plotted as a function of T at a) lower pressures of 6, 8 and 9 GPa, and b) higher pressures of 10 and 12 GPa. Arrows indicate experimental sequence and the grey areas illustrate re-heating and cooling cycles. Note the different behaviour in b) implying a phase transition at these pressures.

pressure) in Fig. 3.4a and 3.4b. All experiments at pressures ≤ 9 GPa show similar resistivity paths during heating and cooling (Fig. 3.4a). Obtained values of $2\text{-}6 \times 10^{-4} \Omega\text{-m}$ are consistent with literature values for magnetite, obtained under different P-T conditions (e.g., Parker and Tinsley 1976; Morris and Williams 1997). The resistivities measured during the initial heating cycles at 10 and 12 GPa also exhibit identical behaviour (Fig. 3.4b). A reversible small maximum in resistivity occurs between ~ 700 and 1000 K. Such behaviour has been observed at 1 atm for magnetite and other oxides and attributed to a spin-order-induced increase in conductivity at temperatures below the Curie point, T_c (Parker and Tinsley 1976; Parker 1958). Although this is an attractive explanation, the position of this maximum implies that T_c does not vary much between 8 and 12 GPa, which is inconsistent with Schult (1970), who reports a $dT_c/dP = 18.5$ K/GPa.

All experiments performed at ≤ 9 GPa exhibit reversible behaviour during the initial heating cycle up to 1723 K and the subsequent cooling cycle to room temperature. In several experiments, a short reheating sequence was performed during the cooling cycle to assure reproducibility (Fig. 3.4a, 3.4b). We conclude that magnetite remained stable in these experiments (see below).

During heating at 10 and 12 GPa, a distinctive jump in resistivity occurred that was not reversible upon cooling (Fig. 3.4b). At 12 GPa, the jump occurred at ~ 1270 K. At 10 GPa, the nature of the increase is more complex, with an initial gradual increase beginning at ~ 1270 K, followed by a further increase in resistivity at ~ 1620 K. In both

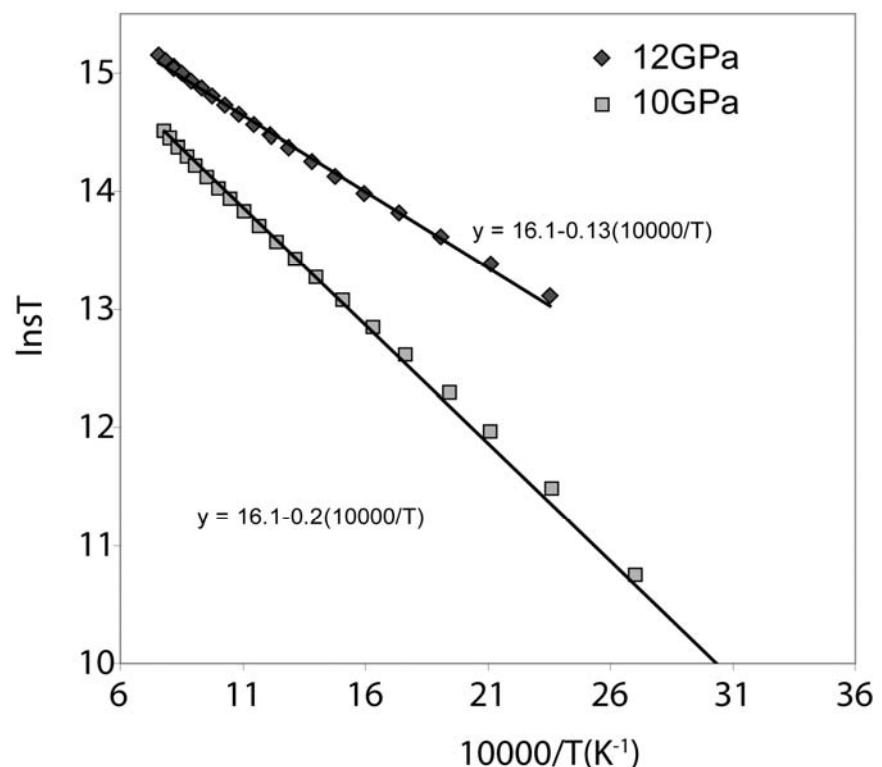


Figure 3.5: Assessment of the conductivity of h-Fe₃O₄.

experiments, subsequent cooling led to systematically higher resistivities, producing a

completely different trajectory as a function of temperature than observed at ≤ 9 GPa. Note that measured resistivities track this new trajectory even during short reheating sequences (Fig. 3.4b). We interpret the jump in resistivity to record the transformation of magnetite to h-Fe₃O₄, with the post-spinel phase exhibiting a higher resistivity. This is consistent with Xu et al. (2004), who observed a large increase in resistivity at $P > 25$ GPa and room temperature in a diamond anvil cell, which they also attributed to the appearance of the h-Fe₃O₄ phase. The temperature dependence of the resistivity of h-Fe₃O₄ confirms that it is a semiconductor (Fig. 3.5). Thus, the metallic-type behaviour observed by Dubrovinsky et al. (2003) and Xu et al. (2004) and at much higher pressures means that a further transition in the post-spinel phase may also occur.

3.3.2. TEM investigations

Microstructural investigation revealed that although all of the recovered samples had the spinel structure (i.e. reconverted to magnetite), microtwins on the (311) plane (Fig. 3.6) and extensive planar defects such as stacking faults (Fig. 3.7) were present in samples from the 10 and 12 GPa experiments, implying that the magnetite has back-reacted from a phase of lower symmetry (Frost et al. 2001). On the other hand, such defect microstructures were completely absent in the samples run at ≤ 9 GPa. This supports our interpretation that only magnetite was present at ≤ 9 GPa and that h-Fe₃O₄ formed in the experiments above 9 GPa.

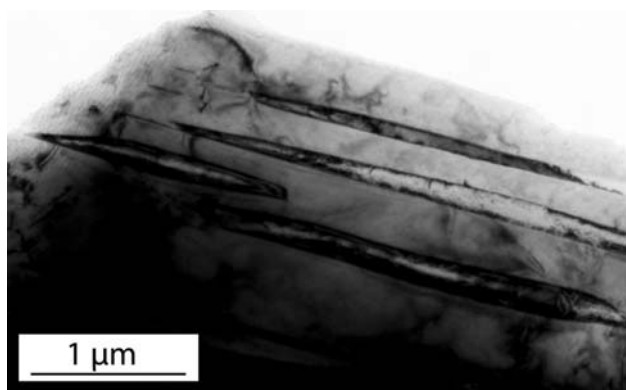


Figure 3.6: Twin lamella in magnetite after 12 GPa and 1100 °C indicate a reversible martensitic phase transformation.

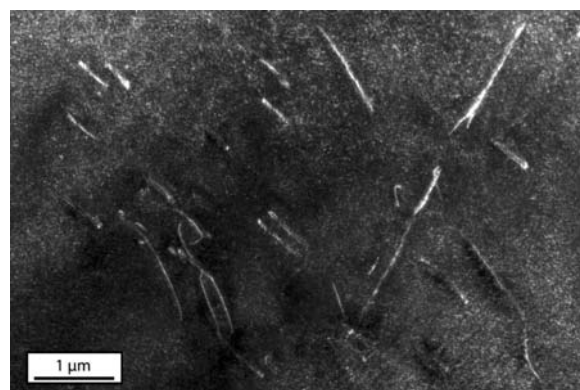


Figure 3.7: Numerous defect structures in magnetite after 12 GPa and 1100 °C.

3.3.3. The phase boundary

Our resistivity measurements allow us to place important constraints on the position of the magnetite–h-Fe₃O₄ phase boundary at high pressures and temperatures: magnetite remains stable up to 1673 K and 9 GPa and h-Fe₃O₄ must become stable between 9 and 10 GPa (Fig.

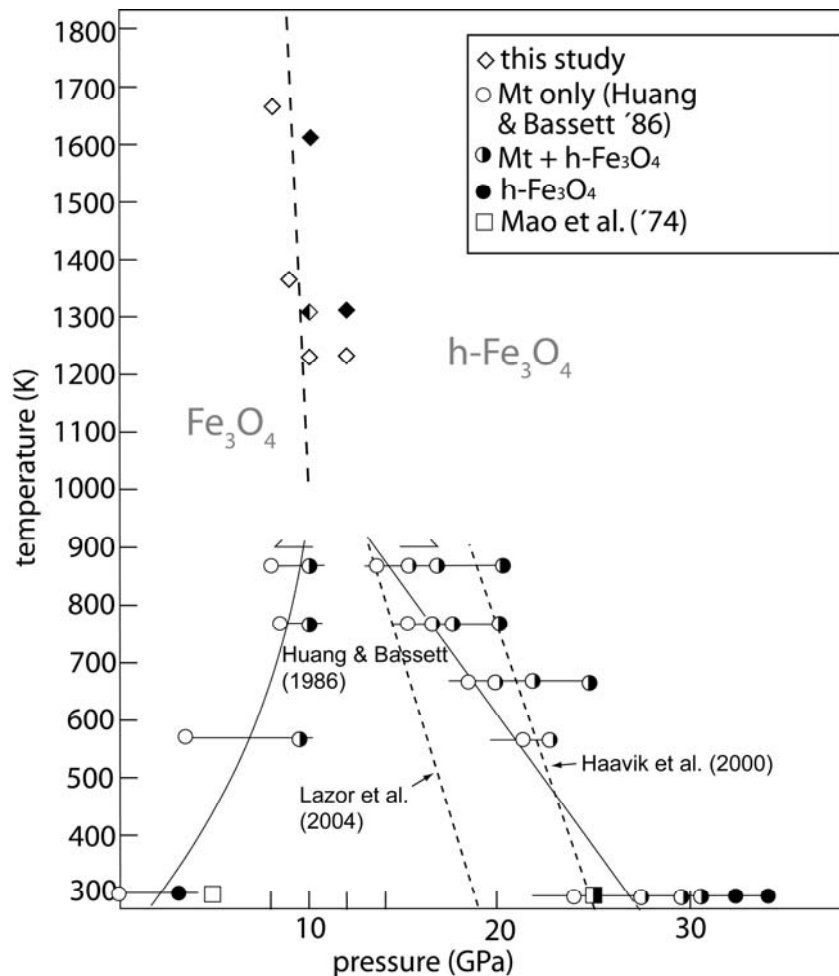


Figure 3.8: Phase boundary for the magnetite–h-Fe₃O₄ transition. Open symbols: pure magnetite, full symbols: pure h-Fe₃O₄.

3.8). The somewhat different behaviour in resistivity between the 10 and 12 GPa experiments can be understood in terms of reaction kinetics and the degree of overstep of the phase boundary. The rather sharp jump in resistivity at 12 GPa suggests the phase boundary must have been significantly overstepped and that the transformation reaction was thermally driven. The more complex behaviour observed at 10 GPa would then be due to a closer proximity to the phase boundary where pressure buffering from the ~7% volume reduction

attending the transformation (Fei et al. 1999) could cause small variations in pressure. Temperatures >1250 K appear to be necessary to drive the transformation reaction at these pressures. Our results imply that the magnetite–h- Fe_3O_4 phase boundary is nearly isobaric and must lie just below 10 GPa (Fig. 3.8). Extrapolation of this boundary to lower temperatures is consistent with results of Huang and Bassett (1986) during the decompression cycle of their experiments. The re-appearance of magnetite at 9.04 GPa and 923 K observed by Fei et al. (1999) is also consistent with our data. On the other hand, the phase boundary proposed by Huang and Bassett (1986), as well as those derived by Haavik et al. (2000) and Lazor et al. (2004) are inconsistent with our results (Fig. 3.8). Our measurements emphasise the very sluggish reaction kinetics of the magnetite–h- Fe_3O_4 transition, requiring ~ 1273 K to drive the reaction near to the phase boundary.

This study demonstrates the utility of in situ resistivity measurements to monitor phase transitions at high pressures and temperatures. In the case of magnetite, the near isobaric nature of the phase boundary represents a worst-case situation for the method since the pressure calibration of the multi-anvil press requires pressurisation prior to heating. As a result, the boundary was not directly measurable during a given experiment. However, combining results from several experiments still could provide important constraints on the position and slope of the boundary.

3.4. References

- Dieckmann, R. (1982) Defects and cation diffusion in magnetite (IV) - nonstoichiometry and point-defect structure of magnetite $\text{Fe}_{3-\delta}\text{O}_4$. *Berichte der Bunsen Gesellschaft* (86), pp 112-118.
- Dubrovinsky, L.S., Dubrovinskaia, N.A., McCammon, C., Rozenberg, G.Kh., Ahuja, R., Osorio-Guillen, J.M., Dmitriev, V., Weber, H.-P., Le Bihan, T., and Johansson, B. (2003) The structure of the metallic high-pressure Fe_3O_4 polymorph: experimental and theoretical study. *Journal of Physics and Condensed Matter* (15), pp 7697-7706.
- Fei, Y.W., Frost, D.J., Mao, H.-K., Prewitt, C.T., and Häusermann, D. (1999) In situ structure determination of the high-pressure phase of Fe_3O_4 *American Mineralogist* (84), pp 203-206.

- Frost, D.J., Langenhorst, F., and van Aken, P.A. (2001) Fe-Mg partitioning between ringwoodite and magnesiowustite and the effect of pressure, temperature and oxygen fugacity. *Physics and Chemistry of Minerals* (28), pp 455-470.
- Frost, D.J., Poe, B.T., Trønnes, R.G., Liebske, C., Duba, A., and Rubie, D.C. (2004) A New Large-Volume Multianvil System. *Physics of the Earth and Planetary Interior*, (143-44), pp 507-514.
- Haavik, C., Stølen, S., Fjellvag, H., Hanfland, M., and Häusermann, D. (2000) Equation of state of magnetite and its high-pressure modification: Thermodynamics of the Fe-O system at high pressure. *American Mineralogist* (85), pp 514-523.
- Huang, E. and Bassett, W.A. (1986) Rapid-determination of Fe₃O₄ phase-diagram by synchrotron radiation. *Journal of Geophysical Research [Solid Earth]* (91), pp 4697-4703.
- Kündig, W. and Hargrove, R.S. (1969) Electron hopping in magnetite. *Solid State Communications* (7), pp 223-227.
- Lazor, P., Shebanova, O.N., and Annersten, H. (2004) High-pressure study of stability of magnetite by thermodynamic analysis and synchrotron X-ray diffraction. *Journal of Geophysical Research [Solid Earth]* (109) DOI 10.1029/2003JB002600
- Mason, T.O. and Bowen, H.K. (1981) Electronic conduction and thermopower of magnetite and iron-aluminate spinels. *Journal of the American Ceramic Society* (64), pp 237-242.
- Morris, E.R. and Williams, Q. (1997) Electrical resistivity of Fe₃O₄ to 48 GPa: Compression-induced changes in electron hopping at mantle pressures. *Journal of Geophysical Research [Solid Earth]* (102), pp 18139-18148.
- Parker, R. (1958) Electrical resistivity of compounds with ordered spin arrangements. *Philosophical Magazine* (3), pp 853-861.

Parker, R. and Tinsley, C.J. (1976) Electrical conduction in magnetite. *Physica Status Solidi A* (33), pp 189-194.

Schult, A. (1970) Effect of pressure on the Curie temperature of titanomagnetites [(1-x) · Fe₃O₄ · x · TiFe₂O₄]. *Earth and Planetary Science Letters* (10), pp 81-86.

Stachel, T., Harris, J.W. and Brey, G.P. (1998) Rare and unusual mineral inclusions in diamonds from Mwadui, Tanzania. *Contributions to Mineralogy and Petrology* (132), pp 34-47.

Xu, W.M., Machavariani, G.Y., Rozenberg, G.K., and Pasternak, M.P. (2004) Mössbauer and resistivity studies of the magnetic and electronic properties of the high-pressure phase of Fe₃O₄. *Physical Review B* (70) DOI 10.1103/PhysRevB.70.174106

4. In situ determination of the spinel – post-spinel transition in Fe_3O_4 at high temperature and pressure by synchrotron X-ray diffraction

Schollenbruch K¹, Woodland AB¹, Frost DJ², Wang Y³, Sanehira T³, Langenhorst F²

¹ Institut für Geowissenschaften, Universität Frankfurt, 60438 Frankfurt, Germany

² Bayerisches Geoinstitut, Universität Bayreuth, 94550 Bayreuth, Germany

³ Center for Advanced Radiation Sources, The University of Chicago, 5640 S. Ellis Avenue, Chicago, IL 60637, U.S.A.

Submitted: American Mineralogist

4.1. Introduction

Magnetite (FeFe_2O_4) belongs to the large group of spinel-structured minerals with the general formula AB_2O_4 . It is an important accessory mineral in many magmatic and metamorphic rocks and occurs as a component in spinels of the spinel peridotite facies of the upper mantle (e.g., Wood and Virgo 1989), as well as in $(\text{Mg,Fe})_2\text{SiO}_4$ ringwoodite, which is expected to be stable in the mantle transition zone (e.g., O'Neill et al. 1993). Nearly pure magnetite has also been found as inclusions in diamonds (Meyer 1987; Stachel et al. 1998). Hence the stability and high-pressure properties of Fe_3O_4 have direct relevance to geochemical processes in the deep earth as magnetite and its polymorphs provide important structural models for understanding the behaviour of Fe^{3+} bearing components in the mantle. Furthermore knowledge about its high-pressure behaviour is fundamental for the understanding of the phase relations in the simple Fe-O system. For these reasons, magnetite has been the subject of many studies over the years. Magnetite is known to undergo an unquenchable phase transition at ~ 21 GPa at room temperature to a high pressure polymorph (hereafter denoted as h- Fe_3O_4) (Mao et al. 1974; Huang and Bassett 1986; Pasternak et al. 1994; Fei et al. 1999). The h- Fe_3O_4 polymorph was found by Fei et al. (1999) to have the Pbcm space group (CaMn_2O_4 -type structure) with cell parameters $a = 2.7992(3)$ Å, $b = 9.4097(15)$ Å, and $c = 9.4832(9)$ Å at 24 GPa and 650 °C. However, more recent studies suggest that a CaTi_2O_4 -type structure (with space group Bbmm) is more consistent with the available diffraction data from room temperature experiments between

21.8 GPa and 43 GPa (Haavik et al. 2000) or experiments up to 930 °C and 60 GPa (Dubrovinsky et al. 2003). The unquenchable nature of h-Fe₃O₄ complicates direct crystallographic analysis of this phase. A further difficulty in studying this transition is the apparent sluggishness of the reaction and the persistence of magnetite at pressures significantly above that where h-Fe₃O₄ first appears (e.g., Huang and Bassett 1986). In addition, there is a large hysteresis in the back-reaction to magnetite, even at temperatures up to ~800° C (e.g., Huang and Bassett 1986; Woodland et al. 2001). For these reasons, the actual position and slope of the phase boundary in P-T space remains poorly constrained. In this contribution we report the results of in situ diffraction measurements at high pressures and temperatures using synchrotron radiation that provide further important constraints on the position of the magnetite – h-Fe₃O₄ phase boundary. Our new experiments significantly expand the temperature range investigated by earlier studies. The current results are consistent with our recent electrical resistivity study (Schollenbruch et al. 2009), but provide a more definitive delineation of the boundary.

4.2. Experimental methods

Magnetite starting material was produced by sintering Fe₂O₃ powder in a gas mixing furnace at one atmosphere, 1573 K and $\log f_{\text{O}_2} = -5.5$. Under these conditions the magnetite should be essentially stoichiometric (Dieckmann 1982). X-ray diffraction analysis revealed single-phase magnetite with a unit cell parameter of $a_0 = 8.3966(6) \text{ \AA}$, which is in good agreement with that of Haavik et al. (2000).

High-pressure, high-temperature experiments were performed using the GSECARS on-line multi-anvil press at beamline 13-ID-D at the Advanced Photon Source at Argonne National Laboratory, U.S.A.. The 1000t Kawai-type multi-anvil press and the beamline setup is described in detail by Wang et al. (1998, 2009). A major advantage of using a multi-anvil press combined with synchrotron radiation is that pressure can

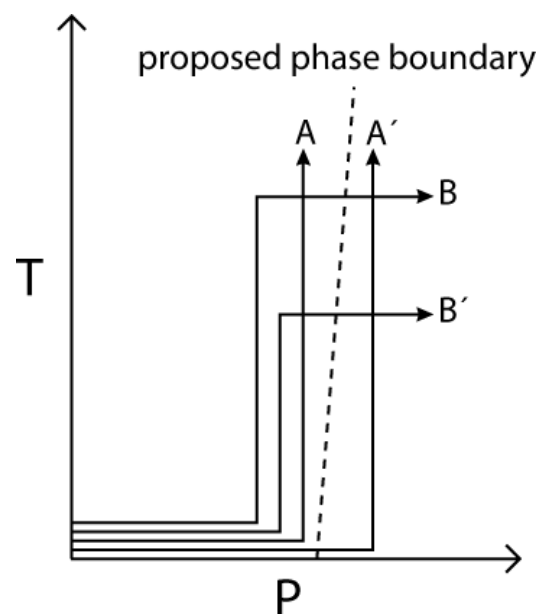


Figure 4.1: Problem of determination of a near-isobaric phase boundary with a conventional MA-apparatus (A, A'). To cross the phase boundary perpendicular independent pressure-temperature profiles are required (B-B').

be monitored during the experiment by measuring the unit cell parameter of a standard material located next to the sample. In conventional laboratory multi-anvil experiments, pressure determination is based on a series of calibrations at both room temperature and high temperature, using electrical resistance or quenchable phase transitions as pressure markers (the so-called fixed points). These calibrations typically are performed such that the sample is pressurised to the target pressure prior to heating (such as paths A and A' in Fig. 4.1). In reality, the pressures achieved at high temperature are path dependent, hence it is difficult to intersect a phase boundary that has a weak temperature dependence, based on fixed point pressure calibration. With an on-line multi-anvil press, the pressure can be varied (and monitored) during the experiment, even at high temperatures, permitting other P-T trajectories to be explored (e.g., paths B or B' in Fig. 4.1).

Each sample was pressed to a ~1mm long cylinder and placed in a COMPRES 10/5 (octahedral edge length/truncation edge length in mm) standard pressure assembly (Fig. 4.2). The pressure cell has a Re foil furnace, surrounded by a LaCrO_3 sleeve (Leinenweber, p.c.). Slits in the sleeve and Re foil filled with B-epoxy plugs provided a window for the incident and diffracted radiation, which was detected by an energy dispersive Ge solid-state detector located at a fixed diffraction angle of 6.1° (Wang et al. 2009). The beam was collimated to a linear dimension of $\sim 100\mu\text{m}$. The geometry of the sample with respect to the synchrotron beam is illustrated in Fig. 4.2.

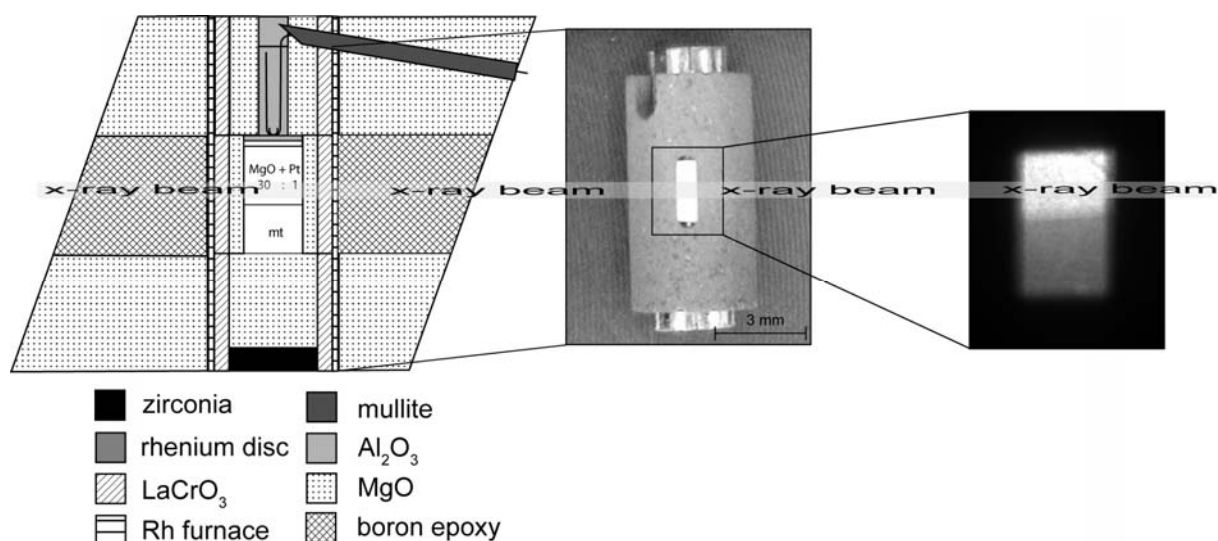


Figure 4.2: Schematic sketch of the COMPRES 10/5 Pressure cell with a picture of the inner part of the cell and a X-ray photograph of the pressure medium and the sample.

Temperature was monitored by a $W_{74}Re_{26}/W_{95}Re_5$ thermocouple, without correcting the effects of pressure on the emf. The magnetite sample was packed in an MgO sleeve to separate it from the furnace. Approximately half of the available sample chamber volume was used for a mixture of fine-grained MgO and Pt or Au powder (mixing ratio 30:1), which served as pressure standard. The equation of state (EoS) for MgO from Dewaele et al. (2000) and those for Pt given by Jamieson et al. (1982) were used to convert the molar volumes of these phases obtained from diffraction patterns into working pressures. Values derived from the equations of state of MgO and Pt are in good agreement with each other, with a maximum deviation of 1 GPa. Differences between the two calibrations are not systematic, however, pressures derived from the Pt EoS tended to be more variable. For this reason, all pressures quoted here are based on the EoS of MgO.

Before each experiment, the radiation wavelength was calibrated using an $\alpha-Al_2O_3$ diffraction standard (Formal NBS XRD intensity standard 674a). Energy dispersive diffraction patterns were obtained during the experiments and were analysed by LeBail refinement using the GSAS software package (Larson and von Dreele 1988) and the EXPGUI interface of Toby (2001). An imaging system was used to help position the sample and pressure standards with respect to the incident beam, allowing accurate tracking of the sample position during the course of the experiment (i.e., after changing temperature or pressure). This assured that the diffraction patterns were acquired from the central region of either the sample or the pressure standards. The diffraction and imaging setups can be quickly switched back and forth. The experiments were performed between room temperature and 1400 °C and pressures up to 16 GPa (Tab. 4.1). After the experiments, the samples were recovered and prepared as polished sections for investigations by microprobe (JEOL JXA-8900RL), transmission electron microscopy (Philips CM20 FEG scanning TEM operating at 200kV) and Raman spectroscopy (Renishaw RM-1000).

4.3. Results and Discussion

4.3.1. In situ observations

Several experiments were performed following different P-T trajectories (e.g., Fig. 4.3). Generally, our strategy was to pressurise the sample to ~8 GPa, a pressure where magnetite was known to remain stable from previous experiments (Schollenbruch et al. 2009) and then heat to a target temperature. Once at high temperature, the load in the hydraulic ram was again changed in

steps with the resulting change in pressure monitored by measuring the unit cell parameter of the MgO standard adjacent to the sample. In this way, pressure could be effectively increased or decreased while at high temperature. Diffraction patterns of the Fe_3O_4 sample were collected both during changes in ram load and once pressure had stabilised at a new value. Thus, we could follow the dynamic response of the sample during a change in pressure and assess how the sample behaved under new P-T conditions.

In experiment T0933, at 9.5 GPa and 800°C, new diffraction peaks (d-spacings at 1.846 Å, 1.43 Å, 1.18 Å) appeared, which are attributable to h- Fe_3O_4 . The first appearance of h- Fe_3O_4 was also marked by a decrease in intensity of the diffraction peaks from magnetite. Diffraction patterns collected in a time series over several minutes revealed that some peaks of either h- Fe_3O_4 or magnetite would grow in intensity and then diminish, only to change intensity at a later point in time (Fig. 4.4). Similar behaviour was reported by Haavik et al. (2000) during their room temperature measurements using a diamond

anvil cell and an image plate detector. They suggested that this could also be due to atom motion or lattice strain which reduces long-range order and thus reduces the sample's ability to diffract radiation. Although these effects could indeed be operative, our observations suggest that a combination of grain growth and changing grain orientation in the sample during the phase transition also plays important roles. This is especially the case when using a fixed energy dispersive detector and a narrow beam diameter ($\sim 100 \mu\text{m}$ in linear dimension), which may only illuminate a relatively small number of grains at any one time. Only after a further step in pressure did the h- Fe_3O_4 -related diffraction peaks become more numerous and intense. The same type of behaviour was also observed in experiment T0935 at 1300°C once reaching a pressure of ~ 10.5 GPa. In these two experiments, as well as in experiment T0932, the phase transformation was accompanied by a constant pressure or a small drop in pressure even though the ram load was increased constantly (see Fig. 4.3). This could reflect pressure buffering since the volume change of the magnetite to h- Fe_3O_4 transition is $\sim -6.5\%$ (Fei et al. 1999). Thus as h- Fe_3O_4 is formed, the sample volume decreases causing a local lowering of pressure, which temporarily re-

Table 4.1: Range of P and T of the different investigations.

experiment	temperature	pressure
T0930	800 °C	~ 9 GPa
	1200 °C	10 GPa
T0931	1000 °C	9-11 GPa
	1300 °C	8-11 GPa
T0932	900 °C	6-9 GPa
	1200 °C	7-12 GPa
T0933	800 °C	9-11 GPa
	1300 °C	14 GPa
T0935	1300 °C	7-15 GPa
	1400 °C	9-11 GPa

stabilises magnetite and drives the reverse reaction. The intensities of the h-Fe₃O₄ reflections increased with further increases in pressure. However, complete transformation to single-phase h-Fe₃O₄ was never attained, even after reaching 16 GPa at 1300°C (Fig. 4.4). A reversal of the transition was performed at 1300°C by progressively reducing pressure from 16 to 8 GPa. The same type of low-intensity diffraction pattern described previously was observed in a narrow pressure range approaching the phase boundary (Fig. 4.4).

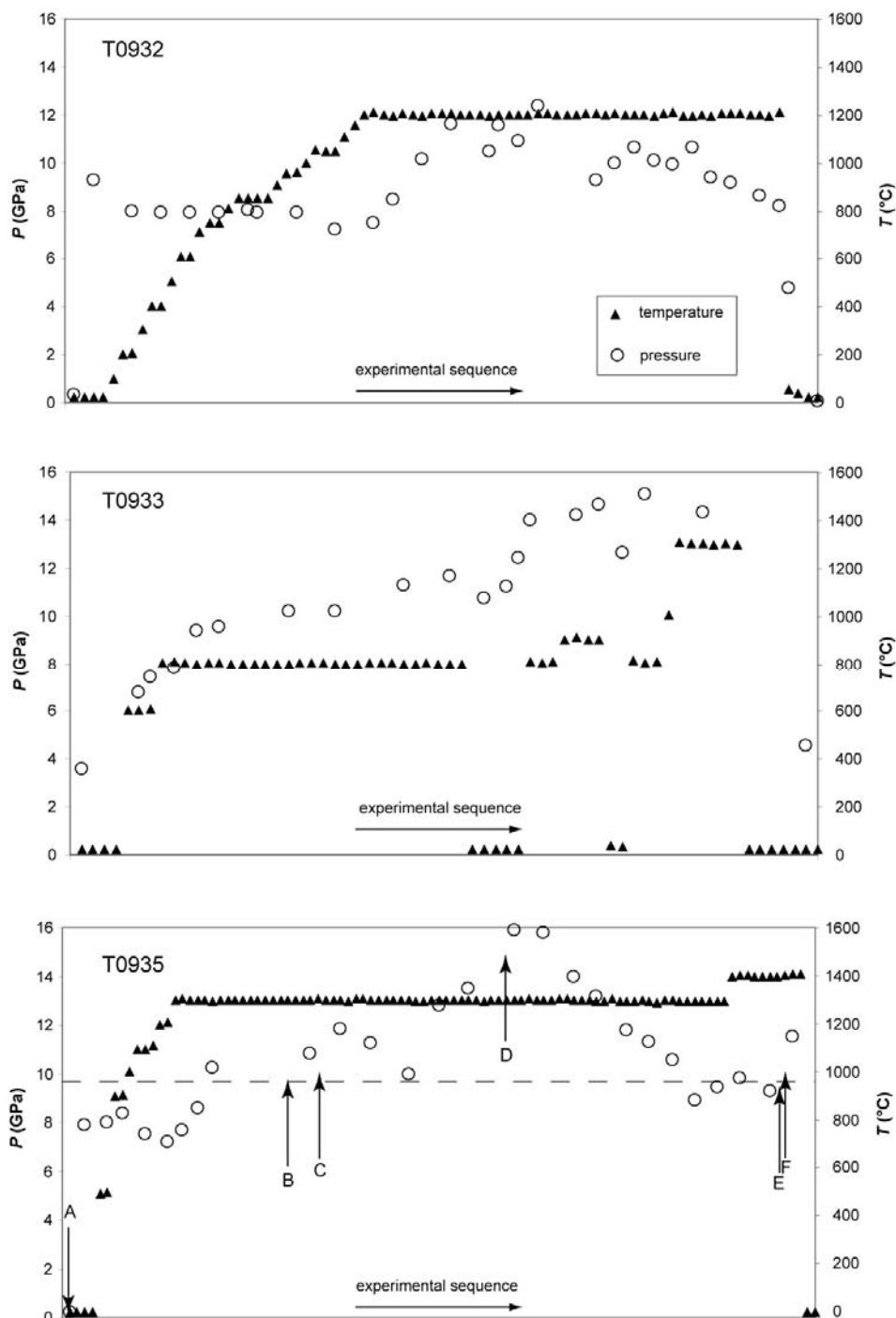


Figure 4.3: Pressure (GPa) and temperature (°C) trajectory of experiments T0932, T0933 and T0935. Dashed line symbolizes the position of the phase boundary. The letters represent the measurements illustrated in Figure 4.4.

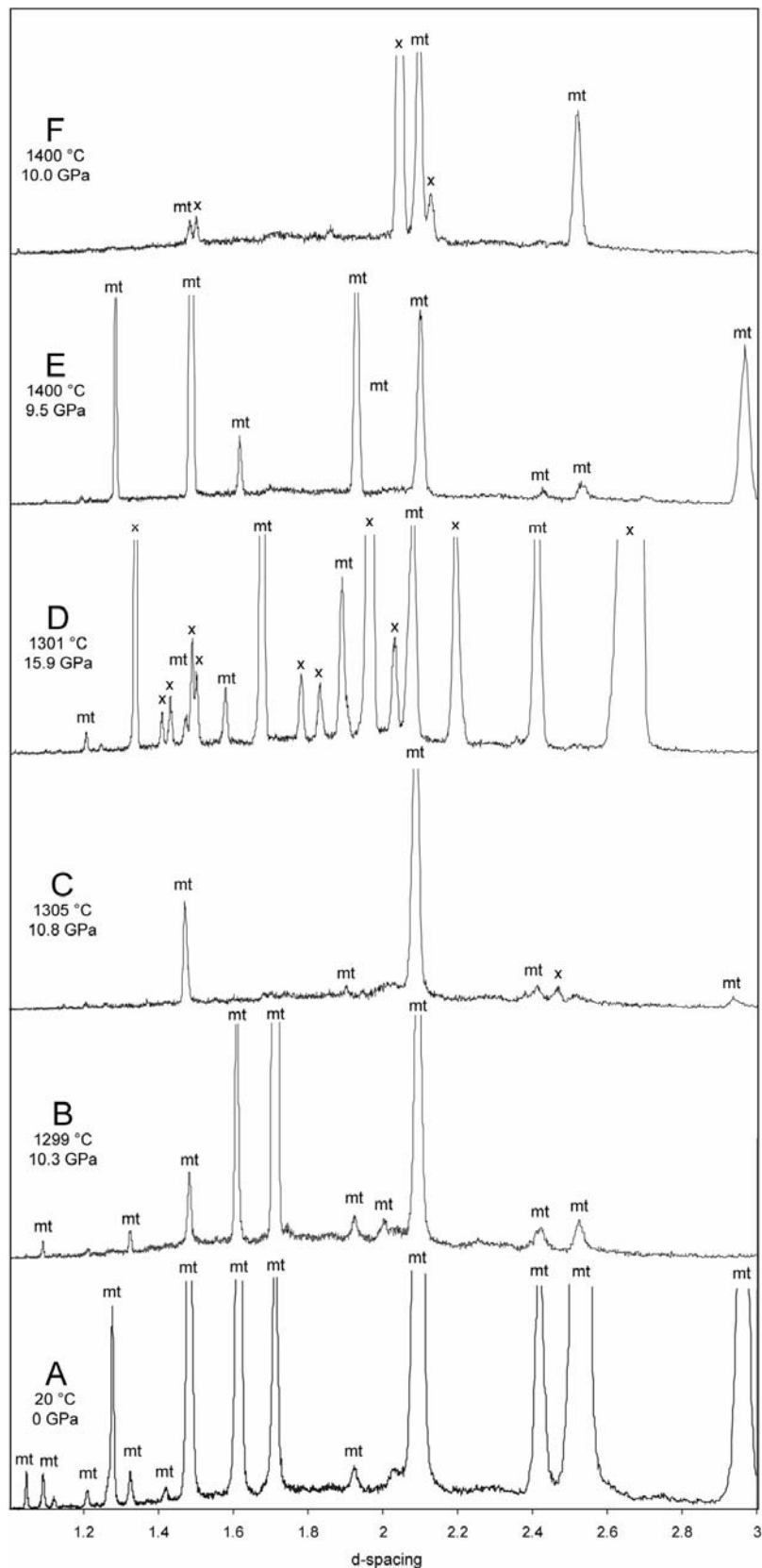


Figure 4.4: Phase development during experiment T0935. Note that A-G represents a time series. A: start of the experiment, only magnetite. B: change in peak intensities, but no additional peaks. C: first appearance of $h\text{-Fe}_3\text{O}_4$. D: maximum pressure, still magnetite peaks present. E: below 10 GPa only magnetite peaks. F: first reappearance of $h\text{-Fe}_3\text{O}_4$. G: last measurement at room temperature, possible hematite formation. mt: magnetite; x: $h\text{-Fe}_3\text{O}_4$; hem: hematite.

In total, the magnetite - h-Fe₃O₄ phase boundary was intersected at 700 °C, 800 °C, 1200 °C, 1300 °C, and 1400 °C (Tab. 4.2). Over this temperature range of 700° C, the diffraction peaks of h-Fe₃O₄ always appeared between ~9 and ~11.5 GPa implying a nearly isobaric phase boundary.

Table 4.2: P and T of the first emergence of h-Fe₃O₄-peaks.

exp. number	T (°C)	unit cell (MgO)	pressure*
T0930	800	4.1704(6)	9.5 ± 0.6
T0931	700	4.1496(3)	9.3 ± 0.6
T0932	1200	4.1852(6)	11.6 ± 0.8
T0933	800	4.1707(2)	9.0 ± 0.6
T0935a	1300	4.1854(4)	10.8 ± 0.8
T0935b	1400	4.2033(7)	10.0 ± 0.9

* Pressure and error range are calculated on the basis of the EoS for MgO from Dewaele et al. (2000)

4.3.2. Post-experiment analysis

After the experiments, the pressure cell was mounted in epoxy, cut in half and polished for study by electron microprobe. Texturally, significant grain growth was apparent, particularly around the periphery of the sample (Fig. 4.5). This coarsening is consistent with observations made

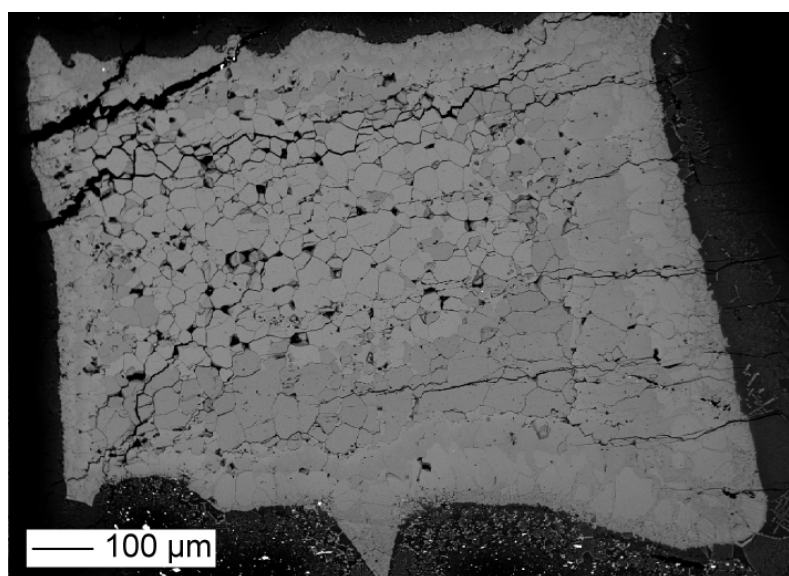


Figure 4.5: BSE-picture of a recovered sample. On the right rim Fe was incorporated in the MgO of the sleeve material. On the bottom Pt-grains of the pressure medium are visible.

during the acquisition of some diffraction patterns during the experiments where certain reflections exhibited unexpectedly strong intensities. Chemical analysis revealed that some reaction had occurred between the sample and the MgO sleeve, producing a Fe₃O₄-MgFe₂O₄ solid solution. However, reaction was limited to a thin, 20 – 50 μm rim region and should not have influenced any of the diffraction patterns obtained during the experiments since the beam was centred on the sample using the imaging mode.

4.3.3. Additional phases

In two experiments (T0930, T0935) a few hematite grains were observed by microprobe analysis. In T0930 the amount of hematite remained below the resolution of the X-ray diffraction patterns, whereas in T0935 the first hematite peaks appeared during the last stage of the experiment, during heating to 1400°C and pressurizing above 10 GPa. No hematite was detected in the other experiments.

4.3.4. The h-Fe₃O₄ phase

Unfortunately, the nature of diffraction patterns collected in energy dispersive mode does not allow an unequivocal determination of the crystal structure of h-Fe₃O₄ in our experiments. This is primarily because peak intensities are too unreliable for a proper Rietveld analysis; changing relative peak intensities due to local grain growth was observed during collection of many diffraction patterns. In addition, the apparent persistence of magnetite up to the highest pressures caused peak overlap, as did the appearance of hematite towards the end of one experiment. A prominent diffraction peak with a d-spacing of ~ 2.64 Å is observable in all patterns obtained above 10 GPa, which agrees with the highest intensity reflection reported for h-Fe₃O₄ by Fei et al. (1999). However, refinements of the best-resolved diffraction patterns that were dominated by the h-Fe₃O₄ phase revealed that neither of the recently proposed structures, the CaTi₂O₄-type (Haavik et al. 2000, Dubrovinsky et al. 2003) or the CaMn₂O₄-type (Fei et al. 1999), were consistent with the set of reflections observed in our experiments. Although several peaks are indeed consistent with the CaMn₂O₄-structure (e.g., the strongest peak at $d = 2.624$ and four other strong peaks at $d = 2.040, 1.777, 1.567$ and 1.405), other observed peaks are not. In addition, a number of d-spacings expected for the CaMn₂O₄-structure (Fei et al. 1999) were not found in our diffraction patterns. The set of d-spacings we observed at 15.1 GPa and 1301 °C (see pattern “D” in Fig. 4.4) are compared with literature data for a variety of Fe-oxide structures in Tab. 4.3.

A similar set of diffraction peaks was observed by Koch et al. (2004) in samples quenched from 9 – 16 GPa and 1100 °C in the system Fe₃O₄-Fe₂SiO₄-Mg₂SiO₄ (Tab. 4.3). These reflections appear to belong to a Fe₃O₄-MgFe₂O₄ solid solution, but could not be attributed to any known phase in this chemical system. They were unable to unequivocally determine the structure of this phase, referring to it as a “mystery phase”.

Table 4.3: D-values (in Å) of our h-Fe₃O₄-phase compared with other Fe-oxide structures. Where available, the numbers in brackets represent the relative intensities.

h-Fe ₃ O ₄ at 15.1 GPa and 1301 °C (this study)	"mystery phase" at 0 GPa and RT (Koch et al 2004)	h-Fe ₃ O ₄ at 24 GPa and 650 °C (Fei et al. 2000)*	h-Fe ₃ O ₄ at 25 GPa and RT (Mao et al. 1974)	Hematite at 0 GPa and RT (JCPDS file 33-664)	Magnetite at 0 GPa and RT (Fleet, 1984)
		4.705 (4)			4.848 (10)
2.670		3.340 (3)		3.684 (30)	
2.643	2.708 (28)	2.683 (10)		2.700 (100)	2.9688 (30)
2.409 (?)	2.643 (100)	2.624 (100)	2.60 (10)	2.519 (7)	2.5317 (100)
	2.444 (24)	2.582 (34)	2.44 (1)		2.424 (8)
	2.236 (15)	2.352 (14)	2.35 (3)	2.292 (3)	
2.195	2.133 (33)	2.335 (18)		2.207 (20)	
		2.117 (8)	2.14 (1)	2.0779 (3)	2.0992 (20)
2.031	2.046 (54)	2.040 (27)	2.03 (4)		
1.964		1.911 (29)			
1.889		1.887 (2)	1.90 (4)	1.8406 (40)	
1.829					
1.780					
		1.777 (12)	1.79 (2)	1.6941 (45)	1.714 (9)
1.577	1.672 (9)			1.6033 (5)	1.6160 (28)
	1.570 (15)	1.581 (14)		1.5992 (10)	
	1.512 (11)	1.567 (20)			
1.501	1.507 (12)	1.549 (7)	1.55 (4)	1.4859 (30)	
1.430	1.448 (10)	1.541 (17)		1.4538 (30)	1.4844 (37)
1.408		1.405 (14)	1.40 (5)	1.3497 (3)	
1.336		1.400 (8)		1.3115 (10)	1.3277 (3)
		1.312 (8)		1.3064 (6)	1.2805 (7)
		1.235 (16)	1.23 (1)	1.2592 (8)	1.2659 (3)
1.18		1.203 (6)		1.2278 (4)	1.2120 (2)

* calculated with xpow (Downs et al. 1993)

Our results indicate that magnetite also transforms to this “mystery phase” and, considering previous studies performed at yet higher pressures (Fei et al. 1999; Haavik et al. 2000; Dubrovinsky et al. 2003), more than one high-P polymorph of Fe_3O_4 may exist. The occurrence of an additional high P polymorph is also supported by electrical resistivity measurements of Xu et al. (2004) and Schollenbruch et al. (2009), who reported strong increases in resistivity for h- Fe_3O_4 , in contrast to the metallic behaviour observed by Dubrovinsky et al. (2003) at > 24 GPa. The exact structure of this “mystery phase” awaits further investigation.

4.3.5. TEM observations

At the end of two experiments, the final diffraction patterns suggested the persistence of h- Fe_3O_4 at ambient conditions. In another experiment we directly quenched our sample from 1400°C and 11 GPa in the hope of preserving h- Fe_3O_4 for subsequent structural investigation. However, TEM investigation of these samples revealed reconversion to the spinel structure had occurred during final recovery of the sample. The magnetite was found to have numerous twins on $\{311\}$ planes (Fig. 4.6), as is obvious from high-resolution TEM images and electron diffraction patterns. Thereby, the $[110]^*$ -directions of twins are rotated by 62° with respect to the host lattice. Such a twin law is so far not known for magnetite. The lamellar to needle-like shape of the twins suggests that they may be caused by a transformation from a high symmetry phase to one with a lower symmetry, as could happen during the transformation of cubic magnetite to orthorhombic h- Fe_3O_4 . Such microstructures have also been found in magnetite samples recovered from normal quench experiments (Frost et al. 2001) and after in situ electrical resistivity measurements at high pressures and temperatures (Schollenbruch et al. 2009), and were likewise considered to indicate the magnetite to h- Fe_3O_4 transition. This interpretation was further supported by the absence of such microstructures in the starting material and in samples from experiments performed at ≤ 9 GPa (Schollenbruch et al. 2009), which argues against them being deformation twins. Considering that the samples investigated in this study are known to have contained h- Fe_3O_4 during the experiments, we are able to unequivocally confirm the link between the formation of these microstructures and the magnetite to h- Fe_3O_4 transition. Whether the twins actually formed during the transition from magnetite to the lower symmetry h- Fe_3O_4 or during the reverse reaction forming magnetite upon decompression, remain open. In the later case, twins could develop in magnetite if there was more than one transformation path from the h- Fe_3O_4 to the spinel structure. In principle, such extensive twinning should cause certain

diffraction peaks to exhibit significant broadening, reflecting the structural repeat in a particular crystallographic direction. However, we find no convincing evidence for selective peak broadening either in the set of diffraction peaks attributable to h-Fe₃O₄ or in the magnetite that formed upon decompression (e.g., Fig. 4.4).

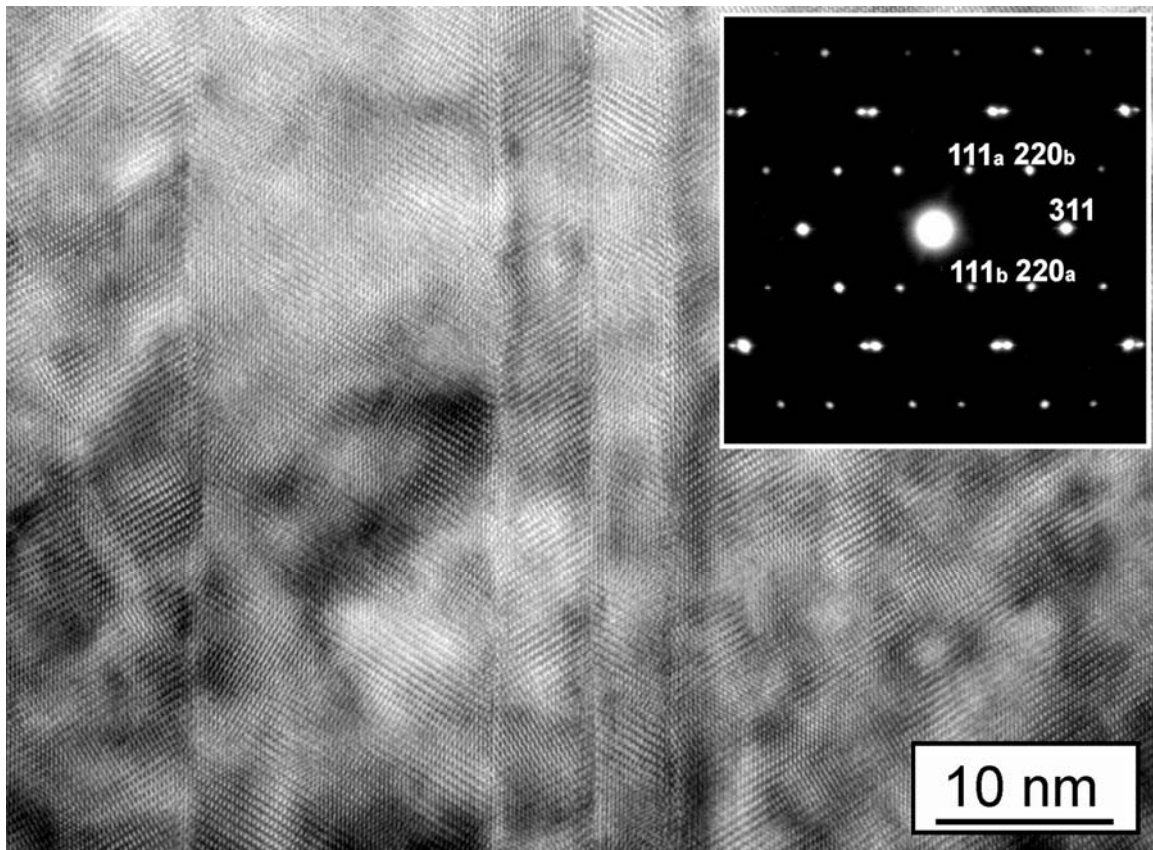


Figure 4.6: High-resolution TEM image and corresponding selected area electron diffraction pattern of magnetite recovered from run TO933. Both images reveal the presence of multiple twins parallel to the (311) plane. The zone axes of host magnetite and twins are $[-112]$ and $[1-1-2]$, respectively.

4.3.6. The transition

A major goal of this study was to investigate the nature of the transformation of magnetite to its high-P polymorph and to determine the position of the phase boundary. At room temperature, magnetite has been observed to coexist with h-Fe₃O₄ at pressures up to 60 GPa (Dubrovinsky et al. 2003; Pasternak et al. 1994). Experiments by Huang and Bassett (1986) and

Woodland et al. (2001) also indicated magnetite co-existing with h-Fe₃O₄ over a significant pressure interval, even at moderate temperatures (Fig. 4.7). Likewise, the reversion of h-Fe₃O₄ to

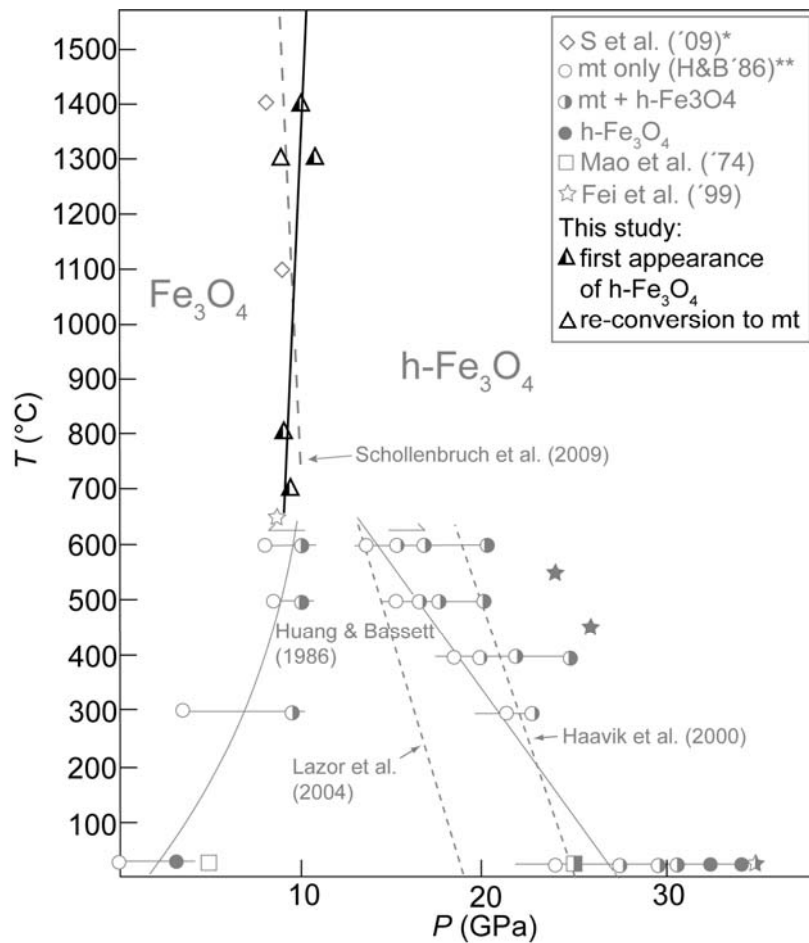


Figure 4.7: Position of the phase boundary in P-T-space and comparison with literature data. Open symbols represent the stability of magnetite, solid symbols stand for the stability of h-Fe₃O₄ and half-filled symbols the coexistence of magnetite + h-Fe₃O₄. * = Schollenbruch et al. (2009), ** = Huang and Bassett (1986).

magnetite was considered to be sluggish as well (Huang and Bassett 1986). Our in situ experiments at >1000°C were intended to overcome the apparent hysteresis in the reaction kinetics encountered at lower temperatures. However, even at 1300 °C and 16 GPa significant amounts of magnetite were present in diffraction patterns, even after remaining at these conditions for 30 minutes (see pattern D in Fig. 4.4). On the other hand, h-Fe₃O₄ disappears quite readily during pressure release, suggesting the reverse reaction to magnetite is rather rapid.

The observed low-intensity nature of diffraction patterns collected during crossing of the phase boundary both during pressure increase and pressure release suggests that nucleation and growth are important mechanisms for the transition. However, this behaviour occurs over a very large temperature range, implying that athermal processes are also involved. The persistence of

magnetite co-existing with h-Fe₃O₄ even at high temperatures also points to athermal processes being important (i.e., a diffusionless transformation mechanism). Chen et al. (2001) proposed that the olivine-spinel transition in fayalite is of a pseudomartensitic type, where the oxygen sublattice remains essentially stationary and the cations undergo short-range diffusional reordering. This mechanism is also partly related to that recently proposed for the transition in CdCr₂O₄ spinel at high pressures and temperatures (Arévalo-López et al. 2010). For this spinel, a two-stage process was proposed with an intermediate structure formed by cation diffusion across shared edges of octahedra (i.e., short-range reordering), followed by a reconstructive reorganisation of the new octahedra to produce the CaFe₂O₄-type structure. Such types of transformation mechanisms could also be operative in the case of magnetite and would be consistent with our observations that point to elements of both diffusional as well as diffusionless mechanisms. Such a transformation would still be stress-sensitive, hence the appearance of more and stronger reflections from h-Fe₃O₄ during subsequent pressure increases (at constant T). However, since our energy-dispersive diffraction patterns preclude rigorous refinement, we are unable to directly test this hypothesis presently. This is further complicated by the fact that the exact crystal structure of h-Fe₃O₄ remains unknown, making discussion of possible displacement vectors premature. However, it is likely that the oxygen sublattices in two oxide phases like magnetite and h-Fe₃O₄ can be related through some displacement vector or vectors. These conclusions are consistent with earlier in situ observations made at lower temperatures (600 – 800°C) using an externally heated diamond anvil cell and an image plate collector that allowed better quality diffraction patterns to be obtained (Woodland et al. 2001). In this study, broadening of the magnetite diffraction peaks occurred when coexisting with h-Fe₃O₄. The peak broadening was also reversible and disappeared once h-Fe₃O₄ became unstable during decompression at pressures below 10 GPa. This behaviour was interpreted as indicating that the phase transition is coherent or semi-coherent in nature and causes strain in the magnetite structure when h-Fe₃O₄ begins to form (Woodland et al. 2001).

4.3.7. The phase boundary

Based upon the kinetic behaviour described above, we chose to define the position of the phase boundary by the first appearance of diffraction peaks belonging to h-Fe₃O₄ when increasing pressure from within the magnetite stability field. In our five experiments, we were able to observe the appearance of h-Fe₃O₄ diffraction peaks at 700°C and 9.3 GPa, 800°C and

9.5 GPa (9.0 GPa), 1200°C and 11.6 GPa, 1300°C and 10.8 GPa, and at 1400°C and 10 GPa (Tab. 4.2). During experiment T0935, pressure was also decreased while at 1300°C (see Fig. 4.3). Nearly immediately upon reaching ~10 GPa the diffraction peaks from h-Fe₃O₄ disappeared and magnetite reflections grew in intensity. This provides a rather tight reversal for the appearance and disappearance of h-Fe₃O₄ at 1300°C. In addition, results from the recent resistivity experiments of Schollenbruch et al. (2009) provide further information concerning the position of the phase boundary. These experiments followed the P-T path marked “A” and “A’” in Fig. 4.1 and an experiment at 9 GPa revealed that magnetite was stable up to 1400°C, with no evidence for h-Fe₃O₄ having formed. In total, we have constraints on the position of the magnetite-h-Fe₃O₄ phase boundary that span 700° and indicate that it is nearly isobaric (Fig. 4.7). These constraints yield the following estimate for the position of the phase boundary:

$$P \text{ (GPa)} = 1.5 \times 10^{-3} T \text{ (K)} + 8.0 \quad (4.1)$$

At this point, a rigorous assessment of the uncertainties in the slope of the phase boundary is compromised by 1) the low-intensity diffraction patterns obtained at conditions near the boundary, 2) the variably-sized pressure steps during the experiments, and 3) uncertainties related to using the EoS of MgO as a pressure monitor (see Dewaele et al. 2000). A qualitative assessment suggests an overall uncertainty in the position of the phase boundary of ~1 GPa. However, the appearance of h-Fe₃O₄ at slightly higher pressures at 1400°C and 1300°C compared to that at 700°C and 800°C does indeed imply that the boundary has a slightly positive dP/dT slope (Fig. 4.7). The results of the resistivity study of Schollenbruch et al. (2009) are consistent with our phase boundary within the uncertainties of pressure measurement; no h-Fe₃O₄ was present at 9 GPa, but it appeared in the experiment at 10 GPa. The temperature at which h-Fe₃O₄ first appeared in the latter experiment was no doubt controlled by the different P-T trajectory of the experiment (Fig. 4.1), the heating rate and the slower reaction kinetics at lower temperatures.

The fact that the structure of h-Fe₃O₄ remains to be resolved means that we are currently unable to perform a meaningful thermodynamic analysis of this transformation. Qualitatively, the nearly isobaric nature of the boundary indicates that the ΔV of the transformation is the deciding factor in driving the reaction. The slightly positive slope of the boundary implies that the entropy change of this reaction must also be negative.

Our observations on the nature of the transition suggest that the kinetics of the reverse reaction from h-Fe₃O₄ to magnetite is more rapid than the forward reaction. Thus, the

disappearance of h-Fe₃O₄ might be a more reliable indicator of the phase boundary, particularly at low temperatures, where the reaction kinetics becomes less favourable. Huang and Bassett (1986) performed several experiments in a diamond anvil cell at 300 – 600°C that involved compression and decompression segments. During their decompression segment, they found that h-Fe₃O₄ disappeared at pressures below 10 GPa. Fei et al. (1999) also observed that h-Fe₃O₄ had completely reacted to magnetite at 650°C and ~9 GPa. Our preferred position for the phase boundary is consistent with these results (Fig. 4.7).

Several in situ studies performed at room temperature suggested the phase boundary to lie at 19 – 25 GPa and to have a strongly negative dP/dT slope (Lazor et al. 2004; Haavik et al. 2000). Extrapolation of these results to higher temperatures reveals that they are inconsistent with our observations (Fig. 4.7). The most obvious explanation for this is that these authors based the position of their boundary for the most part on the first appearance of h-Fe₃O₄ and a significant overstep in pressure was necessary to nucleate the high-pressure phase at such low temperatures. Similar behaviour was observed by Zhang et al. (1996) for the coesite – stishovite transition, where slow kinetics at low temperatures suggested a negative P-T slope, but a definitely positive slope was apparent from measurements made above 1000 °C. Based upon a thermodynamic analysis, Lazor et al. (2004) also proposed that magnetite breaks down to a mixture of FeO and Fe₂O₃ before converting to h-Fe₃O₄ at higher pressures. Their theoretical stability field for FeO + Fe₂O₃ pinches out at ~580°C and above this temperature magnetite should transform directly to h-Fe₃O₄. Considering the unfavourable kinetics of this system, it is questionable whether the existence of a FeO + Fe₂O₃ stability field can be reliably tested experimentally. However, we note that the position of our phase boundary lies at lower pressures than the stability field for FeO + Fe₂O₃ proposed by Lazor et al. (2004), indicating that their assumptions related to the thermodynamic properties of h-Fe₃O₄ require reassessment. No evidence of FeO was ever observed in any diffraction pattern acquired during our experiments, even those where hematite reflections were present. This further suggests that minor oxidation was the cause of hematite appearing in several of our experiments.

4.4. Implications

Although our diffraction data for h-Fe₃O₄ do not permit an unambiguous refinement of its crystal structure at this time, the apparent discovery of a post-spinel polymorph of Fe₃O₄ additional to those previously proposed (e.g., Fei et al. 1999; Haavik et al. 2000; Dubrovinsky et

al. 2003), indicates the necessity for further study of the phase relations and thermodynamics in this system at high pressures and temperatures. This is particularly the case since this phase exhibits very different electronic behaviour compared to either magnetite or that reported for the CaTi_2O_4 -structured polymorph (Schollenbruch et al. 2009; Morris and Williams 1997; Dubrovinsky et al. 2003).

Although the presence of magnetite in samples from the Earth's mantle is quite limited, its occurrence as inclusions in diamond suggests that it may play a role during diamond formation (Meyer 1987; Stachel et al. 1998; Logvinova et al. 2010). The nearly isobaric nature of the magnetite – $\text{h-Fe}_3\text{O}_4$ phase boundary could permit its use as an indicator of whether a diamond originated at pressures > 10 GPa or not. The presence of microtwins on the (311) plane would be indicative of the grain having undergone the transition to $\text{h-Fe}_3\text{O}_4$. Even if the microstructures of the inclusion equilibrated on the way to the surface, it is possible that evidence for the volume increase during the reversion to magnetite would be preserved around the interface between the inclusion and the surrounding diamond.

The study of Koch et al. (2004) indicates that the high-pressure polymorph identified here is stable in Mg-bearing compositions, also at similar pressures. However, its stability field was not defined in this system. Clearly further work is required to understand the influence of the post-spinel transition on the stabilities of solid solutions involving a Fe_3O_4 component.

4.5. Acknowledgements

This study was supported by a grant from the Deutsche Forschungsgemeinschaft within the aegis of Schwerpunkt Program 1236. R. Angel and T. Boffa Ballaran are thanked for their help with analysis of the in situ diffraction patterns. This study benefited from numerous discussions with L. Dubrovinsky. Portions of this work were performed at GeoSoilEnviroCARS (GSECARS; Sector 13), Advanced Photon Source (APS), Argonne National Laboratory. GSECARS is supported by the National Science Foundation - Earth Sciences (EAR-0622171) and Department of Energy - Geosciences (DE-FG02-94ER14466). Use of the Advanced Photon Source was supported by the U. S. Department of Energy, Office of Science, Office of Basic Energy Sciences, under Contract No. DE-AC02-06CH11357.

4.6. References

- Arévalo-López, A.M., Dos Santos-Garcia, A.J., Catillo-Martinez, E., Durán, A., Alario-Franco, M.A. (2010) Spinel to CaFe_2O_4 transformation: Mechanism and properties of B- CdCr_2O_4 . *Inorganic Chemistry*, 49, pp 2827-2833.
- Chen, J.C., Weidner, D.J., Parise, J.B., Vaughn, M.T., Raterron, P. (2001) Observation of cation reordering during the olivine-spinel transition in fayalite by in situ synchrotron X-ray diffraction at high pressure and temperature. *Physical Review letters*, 86, pp 4072-4075.
- Dewaele, A., Fiquet, G., Andrault, D., and Häusermann, D. (2000) P-V-T equation of state of periclase from synchrotron radiation measurements. *Journal of Geophysical Research*, 105(B2), pp 2869-2877.
- Downs, R.T., Bartelmehs, K.L., Gibbs, G.V., and Boisen, M.B. (1993) Interactive software for calculating and displaying X-ray or neutron powder diffractometer patterns of crystalline materials. *American Mineralogist*, 78(9-10), pp 1104-1107.
- Dieckmann, R. (1982) Defects and cation diffusion in magnetite (IV) - nonstoichiometry and point-defect structure of magnetite $\text{Fe}_{3-\delta}\text{O}_4$. *Berichte der Bunsen-Gesellschaft-Physical Chemistry Chemical Physics*, 86(2), pp 112-118.
- Dubrovinsky, L.S., Dubrovinskaia, N.A., McCammon, C., Rozenberg, G.K., Ahuja, R., Osorio-Guillen, J.M., Dmitriev, V., Weber, H.P., Le Bihan, T., and Johansson, B. (2003) The structure of the metallic high-pressure Fe_3O_4 polymorph: experimental and theoretical study. *Journal of Physics-Condensed Matter*, 15(45), pp 7697-7706.
- Fei, Y.W., Frost, D.J., Mao, H.K., Prewitt, C.T., and Häusermann, D. (1999) In situ structure determination of the high-pressure phase of Fe_3O_4 . *American Mineralogist*, 84(1-2), pp 203-206.
- Frost, D.J., Langenhorst, F., and van Aken, P.A. (2001) Fe-Mg partitioning between ringwoodite and magnesiowustite and the effect of pressure, temperature and oxygen fugacity. *Physics and Chemistry of Minerals*, 28(7), pp 455-470.

- Haavik, C., Stolen, S., Fjellvag, H., Hanfland, M., and Häusermann, D. (2000) Equation of state of magnetite and its high-pressure modification: Thermodynamics of the Fe-O system at high pressure. *American Mineralogist*, 85(3-4), pp 514-523.
- Huang, E., and Bassett, W.A. (1986) Rapid-determination of Fe₃O₄ phase-diagram by synchrotron radiation. *Journal of Geophysical Research-Solid Earth and Planets*, 91(B5), pp 4697-4703.
- Jamieson, J.C., Fritz, J.N., and Manghnani, M.H. (1982) Pressure measurement at high temperature in X-ray diffraction studies: Gold as a primary standard. In S. Akimoto, and M.H. Manghnani, Eds. *High-Pressure Research in Geophysics Pressure*, pp 27-48. Center for Academic Publications, Tokyo, Japan.
- Koch, M., Woodland, A.B., and Angel, R.J. (2004) Stability of spinelloid phases in the system Mg₂SiO₄-Fe₂SiO₄-Fe₃O₄ at 1000 °C and up to 10.5 GPa. *Physics of The Earth and Planetary Interiors*, 143, pp 171-183.
- Larson, A.C., and von Dreele, R.B. (1988) GSAS manual. Los Alamos National Laboratory, report LAUR, pp 86-748.
- Lazor, P., Shebanova, O.N., and Annersten, H. (2004) High-pressure study of stability of magnetite by thermodynamic analysis and synchrotron X-ray diffraction. *Journal of Geophysical Research-Solid Earth*, 109.
- Logvinova, A.M., Wirth, R., and Sobolev, N.V. (2010) Fluid/melt inclusions in alluvial Northeast Siberian diamonds: new approach on diamond formation. *Geophysical Research Abstracts*, (12), EGU2010-1236.
- Mao, H.K., Takahashi, T., Bassett, W.A., Kinsland, G.L., and Merrill, L. (1974) Isothermal compression of magnetite to 320 Kbar and pressure-induced phase-transformation. *Journal of Geophysical Research*, 79(8), pp 1165-1170.
- Meyer, H.A.O. (1987) Inclusions in diamond, in Nixon, P.H. (ed.) *Mantle Xenoliths*, Wiley and Sons, pp 501-522.

- O'Neill, H. S. C., Rubie, D.C., Canil, D., Geiger, C.A., Ross, II C.R., Seifert, F. and Woodland, A.B. (1993) Ferric iron in the upper mantle and in transition zone assemblages: implications for relative oxygen fugacities in the mantle, *Geophysical Monograph 74, IUGG Volume 14, American Geophysical Union, Washington D.C., pp 73-88.*
- Pasternak, M.P., Nasu, S., Wada, K., and Endo, S. (1994) High-pressure phase of magnetite. *Physical Review B, 50(9), pp 6446-6449.*
- Schollenbruch, K., Woodland, A.B., Frost, D.J. and Langenhorst, F. (2009) Detecting the spinel-post-spinel transition in Fe_3O_4 by in situ electrical resistivity measurements. *High Pressure Research, 29 (4), pp 520-524.*
- Stachel, T., Harris, J.W., and Brey, G.P. (1998) Rare and unusual mineral inclusions in diamonds from Mwadui, Tanzania (vol 132, pg 34, 1998). *Contributions to Mineralogy and Petrology, 132(3), pp 307-307.*
- Toby, B.H. (2001) EXPGUI, a graphical user interface for GSAS. *Journal of Applied Crystallography, 34, pp 210-213.*
- Wang, Y., Rivers, M., Sutton, S., Eng, P., Shen, G., and Getting, I. (1998) A multi-anvil, high-pressure facility for synchrotron radiation research at GeoSoilEnviroCars at the advanced photo source. *The Review of High Pressure Science and Technology, 7, pp 1490-1495.*
- Wang, Y., Rivers, M., Sutton, S., Nishiyama, N., Uchida, T., and Sanehira, T. (2009) The large-volume high pressure facility at GSECARS: A "Swiss-army-knife" approach to synchrotron-based experimental studies. *Physics of the Earth and Planetary Interiors, 174, pp 270-281.*
- Wood, B.J. and Virgo, D. (1989) Upper mantle oxidation state: Ferric iron contents of lherzolite spinels by ^{57}Fe Mössbauer spectroscopy and resultant oxygen fugacities. *Geochimica et Cosmochimica Acta, 53(6), pp 1277-1291.*

Woodland, A.B., Angel, R.J., Frost, D.J., and Koch, M. (2001) Determination of the post-spinel phase boundary in magnetite and Si-bearing spinel at high pressures and temperatures. ESRF Report HS1214, European Synchrotron Radiation Facility, Grenoble, France.

Xu, W.M., Machavariani, G.Y., Rozenberg, G.K., and Pasternak, M.P. (2004) Mössbauer and resistivity studies of the magnetic and electronic properties of the high -pressure phase of Fe₃O₄. *Physical Review B*, 70(17), DOI: 10.1103/PhysRevB.70.174106.

Zang, J., Li, B., Utsumi, W., and Liebermann, R.C. (1996) In situ X-ray observations of the coesite-stishovite transition: reversed phase boundary and kinetics. *Physics and Chemistry of Minerals*, 23(1), pp 1-10.

5. Phase transformations of Fe_3O_4 - Fe_2SiO_4 solid solutions and Fe_3O_4 - FeCr_2O_4 solid solutions at high temperature and pressure

5.1. Introduction

Minerals with spinel structure are common accessory minerals in the Earth's crust and widespread in the Earth's upper mantle. At these P-T conditions many spinels undergo a phase transformation. These phase transformations have been extensively studied by diamond-anvil cell and multi-anvil cell apparatus (e.g., Irifune et al. 2002; Dubrovinsky et al. 2003; Chen et al. 2003a). At least three general types of transformations are known. A spinel mineral can decompose to its oxides (e.g. FeAl_2O_4 ; Schollenbruch et al. 2009). An orthorhombic phase can form at higher pressures (MgAl_2O_4 ; Irifune et al. 2002). Alternatively a spinel can convert directly to an orthorhombic structure like chromite (Chen et al. 2003b) or magnetite (e.g., Fei et al. 1999). Most experiments on magnetite were carried out at room temperature resulting in a transformation to a CaTi_2O_4 -structured high pressure polymorph (h- Fe_3O_4) at ~ 20 GPa (Dubrovinsky et al. 2003; Haavik et al. 2000). However, the high pressure polymorph is not quenchable and transforms back to magnetite at several GPa. *In situ* high P-T experiments (chapters 3 and 4) reveal the magnetite – h- Fe_3O_4 phase boundary lies at ~ 10 GPa at temperatures > 1000 °C. In the same pressure range (12.5 GPa) chromite (FeCr_2O_4) converts to the CaFe_2O_4 -type phase xieite (Chen et al. 2008). In contrast to h- Fe_3O_4 , this polymorph is stable at ambient conditions.

The nearly pure Fe-endmember spinel (magnetite) as well as Cr-rich Fe spinels are observed in nature under mantle conditions as inclusions in diamonds (Stachel et al. 1998; Logvinova et al. 2010) and in shock veins in meteorites (Chen et al. 2003b). Being quenchable to ambient conditions makes the high-pressure phase of chromite attainable for structural analysis by conventional XRD or transmission electron microscopy (TEM) techniques. Chromite undergoes a two-stage transformation at high pressures. At 12.5 GPa it transforms to a CaTi_2O_4 -structured high pressure polymorph, which transforms to a CaFe_2O_4 -structured phase > 20 GPa. Both high pressure phases are quenchable to ambient P-T conditions (Chen et al. 2003a). This behaviour makes high P-T experiments on magnetite-chromite solid solutions interesting because of the possibility of finding a quenchable high-

pressure phase. This phase could reveal more information on the high pressure behaviour of Fe_3O_4 .

In addition, the role of SiO_2 as a minor component in spinels is of petrological interest as Si is a widespread element in the upper mantle and solid solutions between Fe_3O_4 and Fe_2SiO_4 seem to be likely. Secondary, the high pressure phase of Fe_2SiO_4 is also quenchable, facilitating structural studies of the high pressure modification. In this study the analyses are focused on the effect of Cr and Si on the stability and structure of h- Fe_3O_4 . Based on the critical pressure range from 10-15 GPa, we expect new insights on the phase boundary of magnetite and its shift with additional elements. Due to the stability of xieite and ringwoodite at ambient conditions in contrast to the unquenchable nature of h- Fe_3O_4 , we hope to detect a stable high pressure polymorph in a Fe_3O_4 - FeCr_2O_4 and Fe_3O_4 - Fe_2SiO_4 solid solution.

5.2. Experimental

Starting materials for the high pressure experiments were various Fe_3O_4 - Fe_2SiO_4 solid solutions (mtfay) and Fe_3O_4 - FeCr_2O_4 solid solutions (mtcr). Magnetite and two different magnetite-chromite solid solutions (mt80chr20, mt50chr50) were synthesized from Fe_2O_3 and Cr_2O_3 powder under controlled oxygen fugacity ($f\text{O}_2 = -6.5$) in a gas mixing furnace at 1300 °C. Repeated sintering and grinding cycles were performed until homogeneity was achieved. X-ray analysis yielded an unit cell parameter for magnetite of 8.3966(6) Å, which is in good agreement with Haavik et al. (2000). The unit cell parameters for mt80chr20 and mt50chr50 are 8.3856(8) Å and 8.3973(8) Å, respectively, which are in very good agreement with data from Robbins et al. (1971) (Fig. 5.1). Experiments with mtfay were performed with stoichiometric mixtures of Fe_3O_4 and Fe_2SiO_4 (mt90fay10) as well as with spinel solid solutions. Producing the spinel solid solutions required high temperature and high pressure synthesis. The P-T conditions chosen for the syntheses were based on the phase diagram of Fe_3O_4 - Fe_2SiO_4 by Woodland and Angel (2000). The starting material was a mt85fay15 mixture, treated at 6 GPa and 1100 °C in a belt apparatus using a Pt-capsule (see supplementary material). The product, a single phase spinel, had a unit cell of 8.3762(8) Å, which is in perfect agreement with Woodland and Angel (2000). Experiments with a mt70fay30 spinel required a presynthesis on a multianvil press at 8 GPa and 1100 °C. One experiment was started with a stoichiometric mixture of hematite and metallic iron.

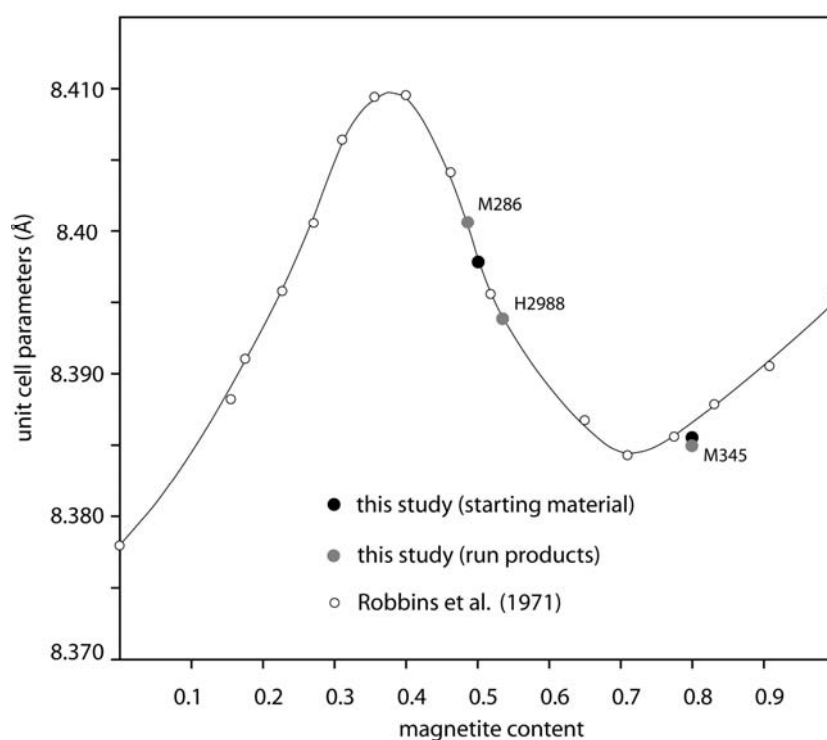


Figure 5.1: Unit cell parameters of different magnetite-chromite starting materials and three samples (modified from Robbins et al. 1971).

High-pressure experiments were performed at the Department of Geosciences at the Goethe University Frankfurt am Main in a 800 t Walker-type multianvil apparatus (Walker et al. 1990) in a P-T range of 8 – 13 GPa and 1000 – 1300 °C. Two experiments at 10 GPa and 1200 °C were conducted in the HYMAG MA-6/8 1000 ton multianvil press at the Bayerisches Geoinstitut in Bayreuth. A 0.05 mm thick silver foil was folded and cold-welded to form a ~1.6 mm long capsule with a diameter of 1.2 mm, containing the compacted, fine-grained powder sample. Cr₂O₃-doped MgO pressure assemblies with an octahedral edge length of 14 mm and a truncation edge length of the tungsten carbide cubes of 8 mm were used for all experiments. Heat was provided by a Re-furnace and temperature was measured by a W₅/Re₉₅ – W₂₆/Re₇₄ thermocouple with the emf uncorrected for pressure. To avoid metal-metal contact between capsule and furnace, the capsule was covered by a thin sleeve of MgO. The thermocouple, separated by a 0.2 mm thin layer of ceramic cement, is placed directly above the sample. Below the sample a MgO spacer ensures the central position of the capsule. Detailed instructions for sample preparation as well as technical details are provided and in the appendix and in Hanrahan et al. (2009).

During an experiment the pressure was first increased to the desired value with a rate of 1500 kN/h and then the temperature was increased with a rate of 50 °C/min. The sample

was quenched by turning off the power of the furnace. The experimental conditions and the run duration are summarized in Table 5.1. The calibration of the multianvil apparatus was done by Buhre (2005) and Steinberg (2005) using the phase transformation α -Mg₂SiO₄ – β -Mg₂SiO₄ at 1200 °C and 13.6 GPa (Morishima et al. 1994).

All samples were recovered and cut into three parts, which were then prepared for TEM analysis, electron microprobe analysis (EMPA) and powder XRD analysis. TEM analyses were carried out at the Bayerisches Geoinstitut, Bayreuth on a FEG transmission electron microscope. The EMPA measurements were performed on a JEOL JXA-8900RL at the Goethe University, Frankfurt. Photographs were taken in the back-scattered electron (BSE) modus to get a better differentiation between the phases. A beam current of 20 nA, accelerating voltage of 15 keV, and a beam spot size of 1 μ m were used. The elemental calibration was based on fayalite for the mtfay samples and on fayalite and chromite for the mtchr samples. BSE images were taken of every sample, pointing out the difference between the coexisting phases. The powder XRD analyses were conducted on a Philips X'Pert PRO diffractometer using Cu-radiation ($\lambda = 1.54056$). Metallic Si was added as an internal standard. The diffraction patterns were analysed by leBail refinement using the GSAS software package by Larson and von Dreele (1988) and the EXPGUI interface of Toby (2001). The run products were characterized additionally using a Renishaw Microraman 1000 spectrometer.

5.2. Results

5.2.1. Fe₃O₄ – Fe₂SiO₄

The experiments covered a temperature range from 1100 °C – 1300 °C and a pressure range from 8 GPa – 13 GPa (Tab. 5.1). The experiments were conducted with two different spinel solid solutions (mt85fay15, mt70fay30) and one mixture of magnetite and fayalite (mt90fay10).

5.2.1.1. X-ray diffraction

All experiments (except M354) reacted to more than one phase. The diffraction peaks from a spinel structure occur in all experiments ≤ 10 GPa. Due to the linear relation between

the unit cells of different $\text{Fe}_3\text{O}_4\text{-Fe}_2\text{SiO}_4$ solid solutions, the size of the unit cells reveals the Fe_2SiO_4 -content in the spinel solid solution (Woodland and Angel 2000). This information was confirmed by more detailed microprobe analyses (Tab. 5.1). In all experiments conducted at 10 GPa and 13 GPa with mt85fay15, small diffraction peaks of stishovite were identified. The coexisting Fe-oxide phase with stishovite and spinel, respectively had always a similar set of patterns, impossible to allocate to a known mineral. This phase has reflections that are inconsistent with magnetite, spinelloid II, spinelloid III, spinelloid V, maghemite, hematite or wüstite as well as with the post-spinel structures proposed by Fei et al. (1999) (CaMn_2O_4 -structure) and Haavik et al. (2000) and Dubrovinsky et al. (2003) (CaTi_2O_4 -structure) for h- Fe_3O_4 . However, the set of diffraction peaks do coincide with those identified by Koch et al. (2004) for a phase in the system $\text{Fe}_3\text{O}_4\text{-Fe}_2\text{SiO}_4\text{-Mg}_2\text{SiO}_4$ stable at 1100 °C and ≥ 9 GPa. Since Koch et al. (2004) were unable to identify the phase, they called it “mystery phase”. This term has been preliminary adopted for the unknown phase in our experiments until its structure can be determined. The diffraction pattern of sample m304 is shown in Figure 5.2 as an example for the “mystery phase”

In a few samples (H2988, M287, M304) an additional weak peak with $d = 2.787(79)$ Å is present, which is consistent with the strongest peak of siderite (Fig. 5.2). Another peak at $d = 2.538(93)$ Å, which occurs in all samples ≥ 10 GPa, coincides with the 100% peak of magnetite.

Table 5.1: Experimental conditions and run products of the experiments from the mtfay system

exp. number	starting material	P (GPa)	T (°C)	duration (hours)	products**	spinel cell edge (Å)	spinel composition (R_3O_4 stoichiometry)
M344	mt85fay15	8	1250	17.5	sp+mp	8.367(8)	$\text{Fe}_{1.2}\text{Fe}_{1.6}\text{Si}_{0.2}\text{O}_4$
M354	mt70fay30	8	1100	15.0	sp+x	8.338(5)	-
M348	mt70fay30	8	1100	17.0	sp+mp	-	-
M346	mt70fay30	8	1200	16.0	sp+mp	8.324(2)	-
M283	mt90fay10	10	1300	18.0	mp+sp	-	$\text{Fe}_{1.2}\text{Fe}_{1.7}\text{Si}_{0.2}\text{O}_4$
	*						
H2988	mt85fay15	10	1200	10.0	mp+hem+sti	-	$\text{Fe}_{1.1}\text{Fe}_{1.8}\text{Si}_{0.1}\text{O}_4$
M287	mt85fay15	10	1300	16.5	mp+sti+ sid	-	-
M351	mt70fay30	10	1200	17.0	sp+mp	8.290(2)	$\text{Fe}_{1.7}\text{Fe}_{0.6}\text{Si}_{0.7}\text{O}_4$
M282	mt90fay10	13	1300	7.5	mp+sti	-	-
	*						
M304	mt85fay15	13	1300	9.0	mp+sti	-	-

* stoichiometric mixture of $\text{Fe}_3\text{O}_4 + \text{Fe}_2\text{SiO}_4$

** sp: spinel; mp: “mystery phase”; hem: hematite; sid: siderite; sti: stishovite; x: unidentified peaks

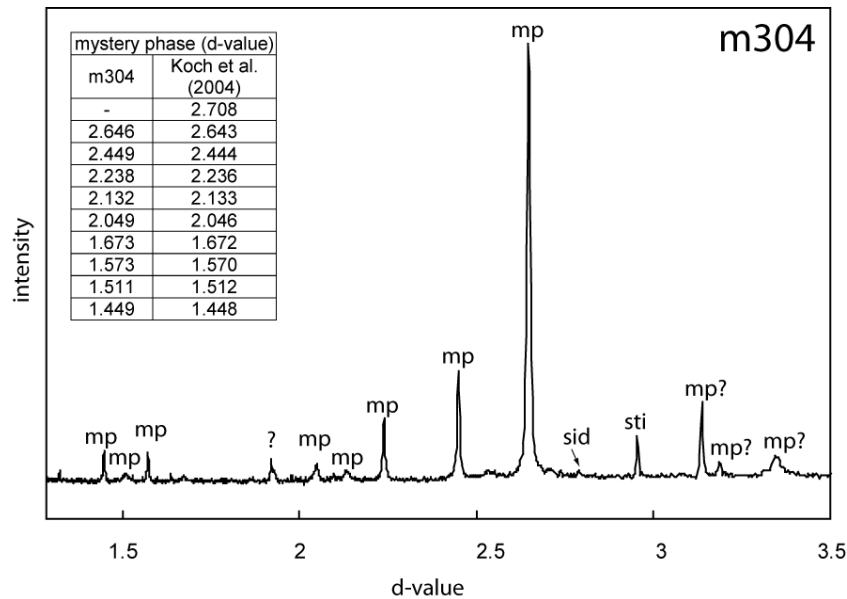


Figure 5.2: XRD pattern of sample M304 and comparison of the “mystery phase” peaks with the data of Koch et al. (2004).
 mp = “mystery phase”; sti = stishovite; sid = siderite

5.2.1.2. EMPA

The amount of SiO_2 in the “mystery phase” varies between 0 – 0.2 wt%, independent of the starting composition. The iron content, calculated as FeO, is between 93% – 95% corresponding to a Fe^{3+} content of 45 mol% – 60 mol%. This is very similar to the $\text{Fe}^{2+}/\text{Fe}^{3+}$ ratio of the employed spinel and indicates, in the case of a stoichiometric composition that the “mystery phase” has a composition of endmember $\text{Fe}^{2+}\text{Fe}_2^{3+}\text{O}_4$. The samples run at ≥ 10 GPa reacted to a mixture of “mystery phase” and stishovite, occurring as small, xenomorphic crystals, with an average size of 1 – 5 μm . Analysis of a few grains > 5 μm in size confirm stishovite being Fe-free. In the presence of spinel, the “mystery phase” forms 10 – 20 μm long tabular crystals. Some of these grains exhibit a distinctive cleavage structure (Fig. 5.3).

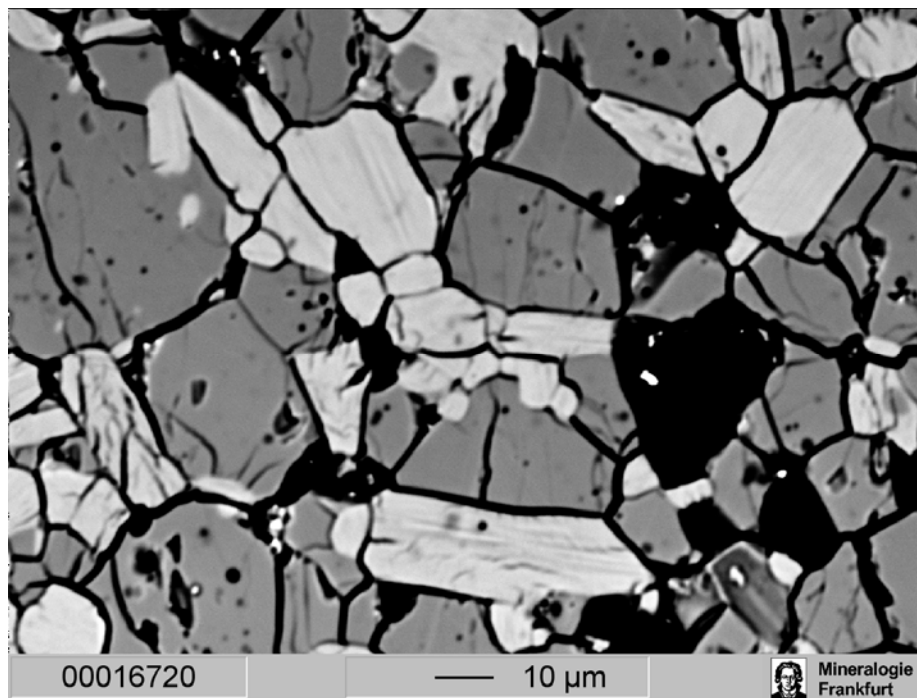


Figure 5.3: BSE image of the “mystery phase” (light grey) together with Si-rich spinel (darker grey) and some wholes (black) from sample M283. Some of the tabular “mystery phase” grains exhibit a distinctive cleavage structure.

Traces of siderite were identified in two samples (M304, M287) with amounts < 5 vol%. This phase could be due to a possible contamination by insufficient evaporation of solvents during sample preparation or due to traces of carbon in the fayalite synthesised in a CO – CO₂ atmosphere. Single grains (< 5 vol%) of hematite occur in sample H2988. The oxygen to produce hematite must have originated from outside the capsule, since hematite grains only occur near the rim of the sample.

5.2.2. Fe₃O₄ – FeCr₂O₄

Quench experiments with Fe₃O₄-FeCr₂O₄ solid solutions were conducted between 8 – 13 GPa and 1200 °C and 1300 °C and covered the same pressure range as the mtfay experiments. The experiment conditions and run products are summarized in Tab. 5.2. In contrast to the Si-bearing spinels, all starting materials were spinel solid solutions with compositions of mt50chr50 or mt80chr20.

Table 5.2: Experimental conditions and run products of the experiments in the mtrcr-system

exp. number	starting material	P (GPa)	T (°C)	duration (hours)	products*	spinel cell edge (Å)	spinel composition (R ₃ O ₄ stoichiometry)	mp composition (R ₃ O ₄ stoichiometry)
M345	Mt80Cr20	8	1250	19	sp	8.385(4)	FeFe _{1.6} Cr _{0.4} O ₄	-
M288	Mt80Cr20	10	1300	15	mp+sid	-	-	FeFe _{1.6} Cr _{0.4} O ₄
M319	Mt50Cr50	8	1250	10	sp+esk	-	FeFe _{0.9} Cr _{1.1} O ₄	-
H2988	Mt50Cr50	10	1200	10	sp+mp+x	8.393(6)	FeFeCrO ₄	FeFe _{1.5} Cr _{0.5} O ₄
M286	Mt50Cr50	10	1300	16.5	sp+mp	8.401(7)	FeFe _{0.9} Cr _{1.1} O ₄	FeFe _{1.5} Cr _{0.5} O ₄
M257	Mt50Cr50	13	1300	7	mp + esk	-	-	FeFe _{1.3} Cr _{0.7} O ₄

*sp: spinel solid solution; esk: eskolaite solid solution; mp: “mystery phase”; sid: siderite

5.2.2.1. X-ray diffraction

Spinel was the only phase present at 8 GPa and 1250 °C, reacted from a mt80cr20 starting material. The peak positions coincide with the starting material indicating the stability of mt80cr20 at these conditions. At 10 GPa and 1300 °C the peaks of spinel are not detectable and peaks of the “mystery phase” are apparent together with three small peaks attributable to siderite.

Treated at 8 GPa and 1250 °C, the mt50cr50 solid solution exhibited peaks attributable to spinel. Additional diffraction peaks revealed the presence of a hematite-eskolaite solid solution with a unit cell of a, b: 5.009(0) Å, c: 13.624(2) Å. These cell parameters indicate a hematite content of ~ 50 mol% (Di Cerbo and Seybolt 1959; Grygar et al. 2003). The first peaks of the “mystery phase” appeared after 10 GPa and 1250 °C, together with peaks of spinel and an unidentified phase. The unit cell of the spinel has a size of 8.393(6), corresponding to a spinel with either 20% or 55% chromite-content (Robbins et al. 1971) (also see Fig. 5.1). An experiment at the same pressure (10 GPa), but at 1300 °C (m286) resulted in the formation of two phases. The predominant phase is a magnetite with an unit cell of 8.401(7) Å, indicating a chromite-content of 28 mol% or 48 mol%, respectively (Fig. 5.1). The peaks of the second phase coincide with the ones of the “mystery phase”. The X-ray analysis of a mt50chr50 solid solution, treated at 13 GP and 1300 °C, yield two phases, one of them being the “mystery phase”, the other one being an eskolaite-hematite solid solution with an unit cell of a, b: 4.995 Å, c:13.607 Å. This corresponds to an eskolaite-component of ~ 60 mol% (DiCerbo et al. 1959).

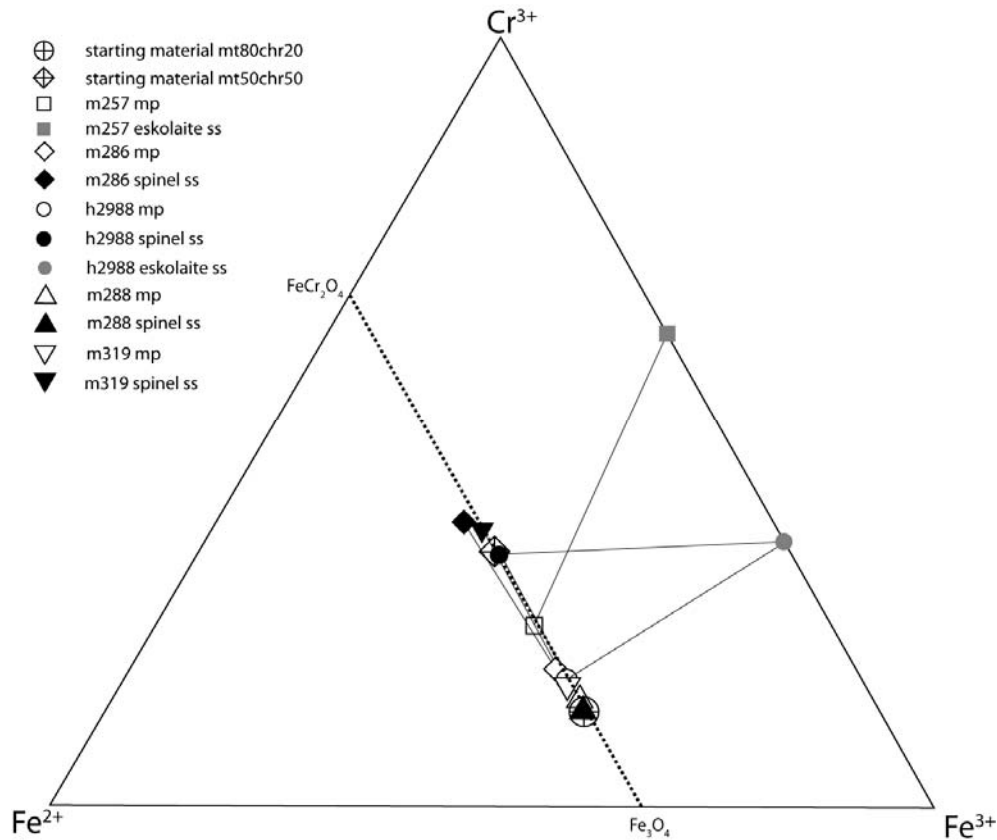


Figure 5.4: Composition of the mtchr samples, estimated by EMPA data. The trend to Fe^{3+} , without a corresponding phase on the Fe^{3+} -poor side points to oxidation of the samples. The eskolaite was calculated without any Fe^{2+} . R_3O_4 stoichiometry is assumed for spinel (black symbols) and the “mystery phase” (open symbols) and R_2O_3 stoichiometry for hematite-eskolaite s.s. (grey symbols).

5.2.2.2. EMPA

Samples M257, M286, and M319 (all mt50chr50) reacted to a mixture of two phases. Both phases contain Fe and Cr in different proportions. The phase poorer in Fe is either spinel or eskolaite. The second phase is “mystery phase” with a Cr_2O_3 -content ranging from 15 – 23 wt%. One of the experiments with mt80chr20 starting material (M288) yielded only pure “mystery phase” with 13 wt% Cr_2O_3 -component, consistent with the starting composition (Fig.5.4). The other experiment with a mt80chr20 composition produced a spinel with also 13 wt% Cr_2O_3 (i.e. no reaction). Three phases appeared in experiment H2988. BSE imaging and EMPA analyses revealed the incomplete formation from mt50chr50 (33 mol% Cr_2O_3) to a phase with 36 mol% Cr_2O_3 and 16 mol% Cr_2O_3 , respectively (Fig. 5.5).

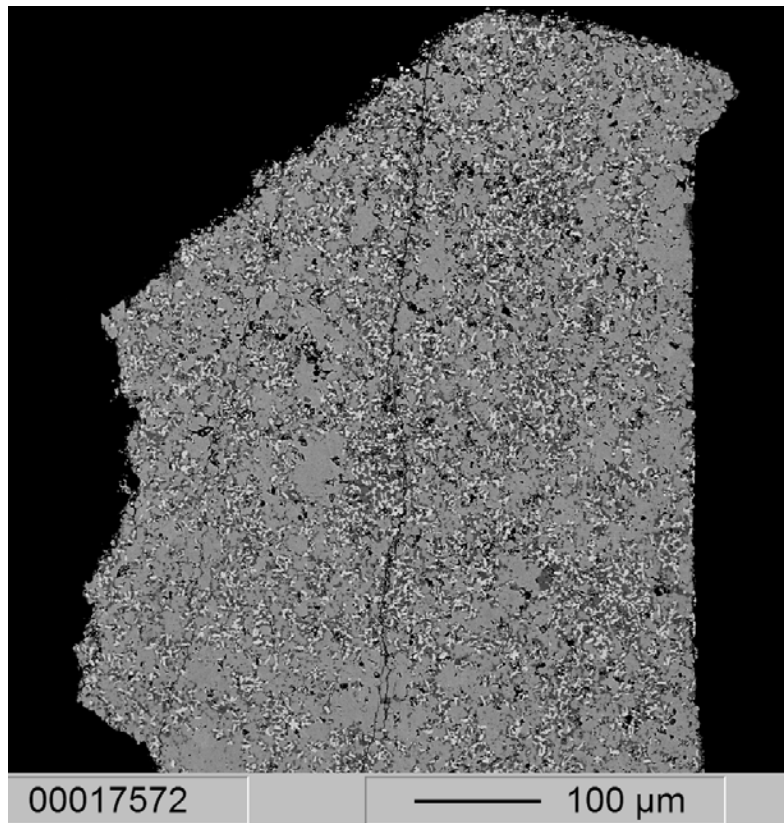


Figure 5.5: BSE-image of H2988chr50. Spinel (grey) reacted to eskolaite-eskolaite (darker grey) + “mystery phase” (light grey).

This experiment delivered a “snap shot” of the transformation from spinel to “mystery phase” (Cr-rich) and eskolaite (Cr-poor). In M288 a minor phase (~ 5 vol%) occurred, whose composition and the XRD data points to siderite (FeCO_3). The siderite grains have a size of 1 – 5 μm and occur mainly at the rim of the Fe-Cr-oxide. The incorporation of Cr in the “mystery phase” structure contrasts with the mtfay-system, where Si is not incorporated

5.2.3. Further characterisation of run-products

The analysis of the structure of the “mystery phase” requires additional methods like Raman spectroscopy and TEM analysis. Raman spectroscopy was chosen, because it allows a quick distinction of different polymorphs. Detailed and more complex TEM investigations on single crystals of the “mystery phase” are probably the most powerful tool to reveal the structure of the “mystery phase”.

5.2.3.1. Raman spectroscopy – preliminary measurements

All run-products were analysed by a Renishaw 1000 microraman. The Renishaw 1000 microraman of the Department of Geosciences at the Goethe University, Frankfurt is equipped with a 532 nm laser (green laser), having an output-power of 200mW. It is also equipped with a 633 nm laser (red laser) with a maximum output-power of 17 mW. The focussing of the laser beam to maximal 5 μm on the surface may cause a temperature increase. This will lead to a possible thermally excited alteration of the laser spot area (Shebanova and Lazor 2003a).

To test for thermally induced alteration, the same powdery starting material as for the multianvil experiments was used for a series of measurements to systematically study the thermal stability of magnetite with increasing laser power. Freshly synthesized, fine-grained magnetite was pressed into pellets, to have a direct comparison with the samples from the multianvil press. All measurements were performed between 60 and 120 sec in the wavenumber range of 200 cm^{-1} – 1200 cm^{-1} with a 50x objective, focussing the laser beam to $\sim 5 \mu\text{m}$ diameter. Prior to the first measurement of a sample, the peak position was calibrated with the 520 cm^{-1} peak of crystalline Si and also checked with a Ne-lamp.

Spectra obtained using the 633 nm laser with up to 33% laser power revealed vibrations attributable to magnetite (A_{1g} vibration at 664 cm^{-1} , T_{2g} vibration at 536 cm^{-1} , E_g vibration at 304 cm^{-1}) (Shebanova and Lazor 2003b). Additional vibrations were not observed (Fig. 5.6a). A laser power increase to 50% led to no significant changes in peak intensity or growth of new peaks. This supports the stability of magnetite at 50% of the 17 mW laser. An increase to 100% laser power led to the broadening of the A_{1g} peak and to a shift to lower wavenumbers. The T_{2g} peak is no longer visible and the E_g peak is masked by a strong peak at

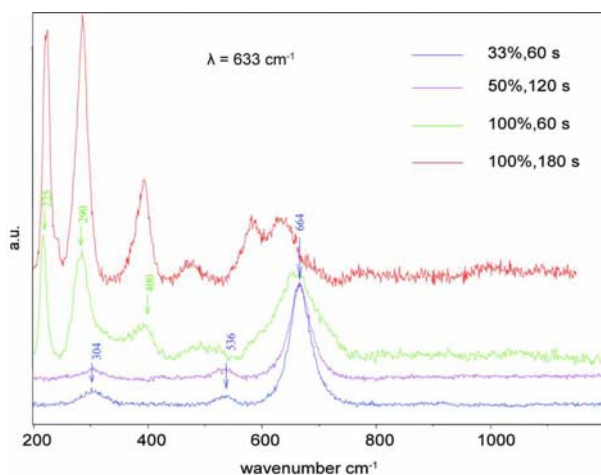


Figure 5.6a: Test series with the 633 nm laser on magnetite powder with different laser intensities.

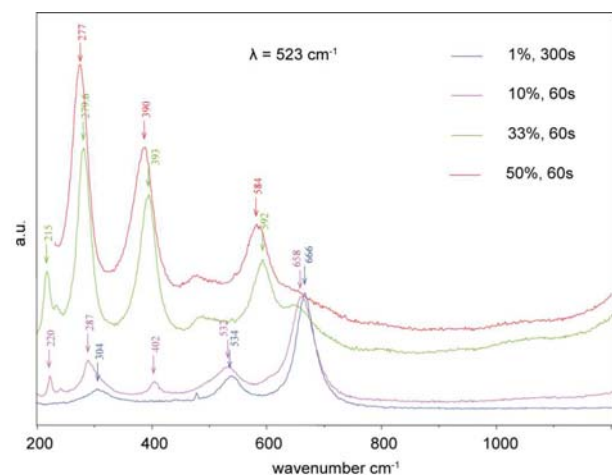


Figure 5.6b: Test series with the 532 nm laser on magnetite powder with different laser intensities.

290 cm^{-1} . Two additional peaks appeared at 225 cm^{-1} and $\sim 400 \text{ cm}^{-1}$. These peaks can be attributed to hematite, indicating the beginning oxidation of magnetite. Extending the exposure time to 180 sec caused an intensity increase of the hematite peaks along with a simultaneous decrease in the intensity of the remaining magnetite peaks. The continuous shift of the peaks to lower wavenumbers with increasing laser intensity can be explained by a temperature increase of the sample (Shebanova and Lazor 2003a).

A similar series of measurements was performed with the 532 nm laser on the same starting material with an average exposure time of 60 s. Only three peaks of magnetite at 666 cm^{-1} , 536 cm^{-1} , and 304 cm^{-1} are visible with 1% laser power in the same spectral range (Fig. 5.6b; Tab. 5.3). After an increase to 10%, several peaks of hematite appeared (220 cm^{-1} (A_{1g}), 241 cm^{-1} (E_g), 287 cm^{-1} (E_g), and 402 cm^{-1} (E_g)) (Tab. 5.3). With 33% laser power an additional hematite peak at 592 cm^{-1} emerges (Fig. 5.6b). Simultaneously, the 666 cm^{-1} peak of magnetite shifted to 650 cm^{-1} and decreased in intensity. At 50% laser power, magnetite completely reacted to hematite. Again the transformation of the sample was clearly visible and was only focused on the area of the laser spot.

Lasers with both wavelengths caused oxidation of magnetite to hematite, when used at 100% power. Due to its different output energy the transformation started at 100% power with the 633nm laser. On the other hand, the 10 times stronger 532 nm laser caused oxidation with only 10% output power. The required temperature to start the oxidation of magnetite with a Raman laser was estimated by Shebanova and Lazor (2003a) to a minimum of 250 °C. The exposure time of the sample to the laser had a subordinate influence.

Table 5.3: Frequencies and vibrational modes (in brackets) of magnetite and hematite

Peak positions of magnetite* (in cm^{-1})	Peak positions of hematite** (in cm^{-1})
193 (T_{2g})	226 (A_{1g})
	245 (E_g)
	292 (E_g)
306 (E_g)	299 (E_g)
	411 (E_g)
538 (T_{2g})	497 (A_{1g})
668 (A_{1g})	612 (E_g)
Shebanova and Lazor (2003b)	** de Faria et al. (1997)

5.2.3.2. Raman measurements on experimental products

To avoid any oxidation, every sample of the mt-fay and mt-cr experiments was measured with the 633 nm laser with max. 10% output power. With a linear relation between laser power and temperature of the sample (Shebanova and Lazor, 2003a), the warming of the sample was estimated to $< 50 \text{ }^\circ\text{C}$.

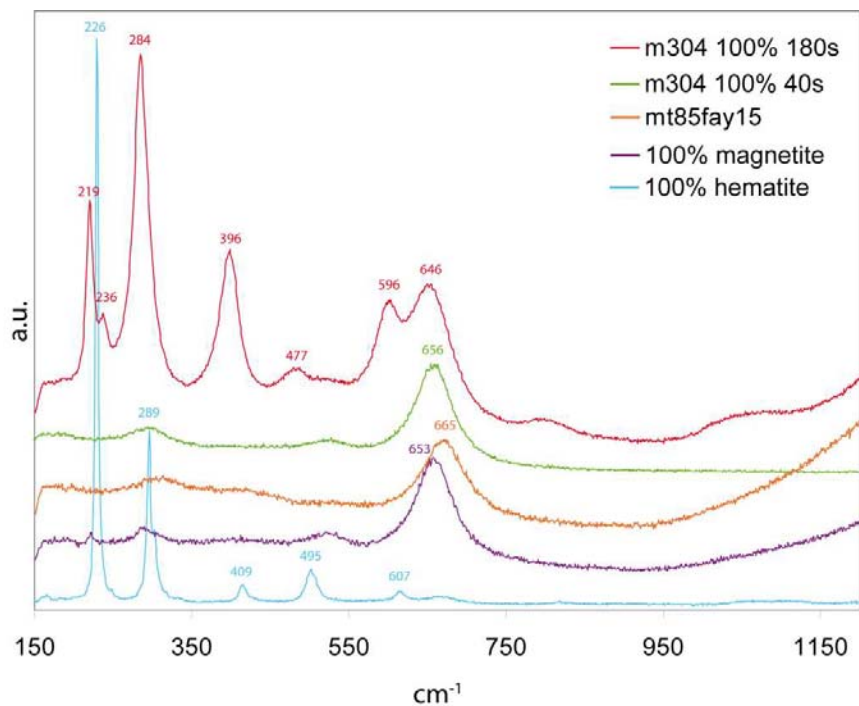


Figure 5.7: Raman spectra of the “mystery phase” (green) in comparison to the starting material (orange) and pure magnetite (purple). After 180 sec with 100% output power of the 633 nm laser, the “mystery phase” starts to transform to hematite (red).

Spectra were taken from samples M282 and M304, containing only the “mystery phase”. All measurements had a similar pattern with generally weak peak intensity (Fig. 5.7). They all exhibit one single broad peak at 660 cm^{-1} , with slight changes in exact position among the different samples. These shifts might be due to thermal or compositional differences. The spectrum from the “mystery phase” is very similar to that of magnetite, which has a strong A_{1g} vibration at 668 cm^{-1} (Shebanova and Lazor 2003b). On the other hand, the T_{2g} vibration at 538 cm^{-1} and the E_g vibration at 306 cm^{-1} are absent in the “mystery phase” (Fig. 5.7). The thermal stability of the “mystery phase”, the sample m304 (pure “mystery phase”) was tested with 100% output power of the 633 nm laser for 180 sec. After 40 sec no reaction was observed, but after 180 sec the unknown phase started to transform to hematite, identifiable at the most prominent peaks of Fe_2O_3 . This indicates a similar temperature stability of the “mystery phase” and magnetite.

5.2.3.3. TEM

One (Si-bearing) sample (M304) was chosen for TEM analysis due to its complete transformation to the “mystery phase”. Preliminary TEM-analysis of the “mystery phase” suggested a possible hexagonal crystal structure (Fig. 5.8), but being inconsistent with that of hematite. It could be indexed only with a strongly distorted hematite structure. However, this structure was already excluded by XRD and Raman measurements. Further analyses on single crystals are required to provide more information about the “mystery phase”.

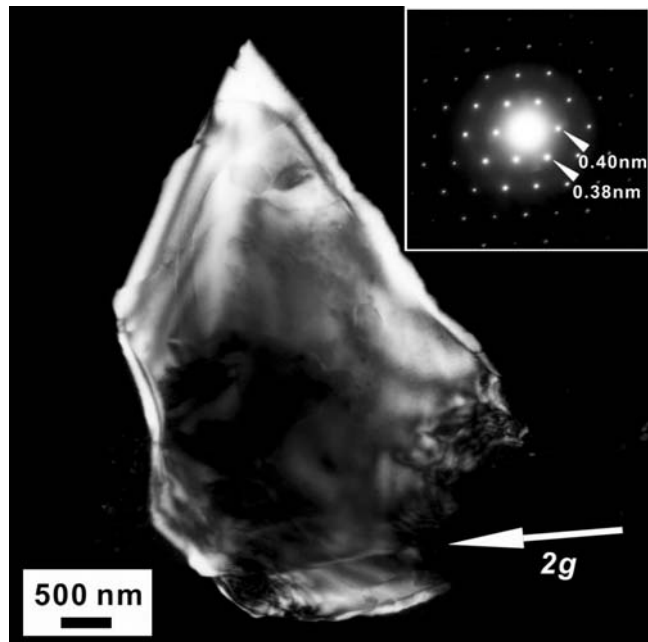


Figure 5.8: Dark-field TEM image and corresponding diffraction pattern (inset) of an unidentified iron oxide phase in sample M304.

5.3. Discussion

5.3.1. Mt-Fay solid solutions

The composition of the magnetite-fayalite solid solution products is strongly dependent on temperature, pressure and starting material (Fig. 5.9). During an experiment at 8 GPa and 1100 °C no reaction was observed. A subsequent experiment at the same conditions (M348) resulted in the formation of significant amounts of “mystery phase”. Since neither starting material nor run conditions were changed, these P-T conditions seem close to the phase boundary. A third experiment at the same pressure but at 1200 °C also yielded the formation of “mystery phase”. The corresponding phase at this pressure is a spinel, which incorporates Si, released from the formation of “mystery phase”. The more of the unknown phase is created, the Si-richer the spinel becomes. Above 10 GPa, the Si-rich spinel is no longer stable and completely reacts to “mystery phase”. The released Si forms at these conditions the stable SiO₂-modification stishovite. However, the stability of spinel seems to

depend of the starting composition. Only solid solutions with 15 mol% Fe_2SiO_4 component reacted at 10 GPa to stishovite and “mystery phase”. With a starting composition of mt70fay30, Si-rich spinel and “mystery phase” coexist together at 10 GPa and 1200 °C, although the pre-synthesised spinel starting material already contained small amounts of the “mystery phase”, which could have promoted the transformation.

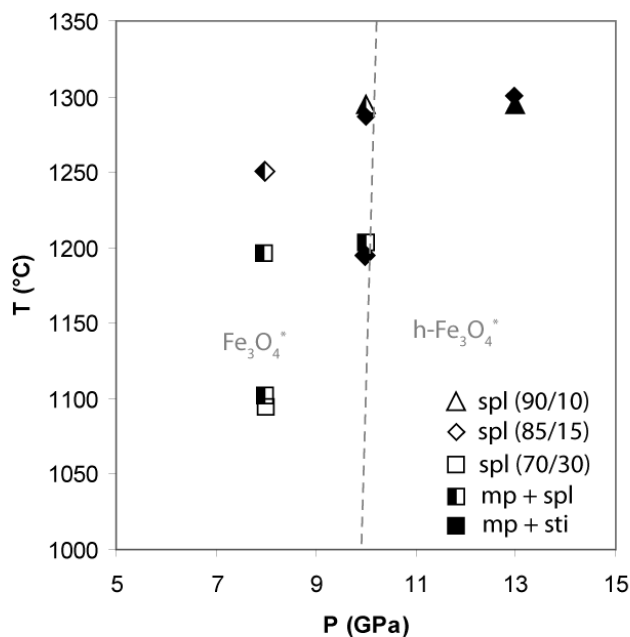


Figure 5.9: Position of the mtfay experiments in P-T space. The different symbols represent the different starting compositions; the filling represents the resulting products. spl: spinel, mp: “mystery phase”. *Phase boundary between magnetite and h- Fe_3O_4 determined by Schollenbruch et al. (2009).

A mixture of 90 vol% magnetite and 10 vol% fayalite also reacted at 10 GPa and 1300 °C to stishovite + “mystery phase”. Mt85fay15 solid solution also reacted to stishovite + “mystery phase” at these conditions. The first appearance of the “mystery phase” was observed at 9 GPa and 1200 °C for Mg-bearing compositions (Koch et al. 2004). Differences in the stability of the “mystery phase” between our data and data from Koch et al. (2004) are most likely due to different composition of the starting materials. All educts from Koch et al. (2004) contained significant amounts of Mg, influencing the stability of the products. On the other hand, Ohtaka et al. (1997) demonstrated the existence of pure spinel solid solutions between magnetite and fayalite at 10 GPa and 1200 °C. These different results cannot be explained by a variable composition, as they also worked with pure magnetite-fayalite solid solutions. The absence of “mystery phase” at these conditions is more likely due to kinetic effects because

Ohtaka et al. (1997) ran the experiments for only five hours. Experiments by Woodland and Angel (2000) indicate a complete solid solution series between magnetite and fayalite at 1100 °C and 8 GPa. But they did not conduct experiments with samples containing ≥ 70 mol% magnetite. This enables the possibility of a phase boundary at Fe-rich spinels (≥ 70 % Fe-content).

Another reason for the formation of “mystery phase” at 8 GPa could be oxidation. Referring to the composition of our products a partial oxidation seems likely. On the one hand, the $\text{Fe}^{2+}/\text{Fe}^{3+}$ ratio of the “mystery phase” is similar to that of magnetite according to stoichiometry and element totals of the EMPA. But on the other hand, the formation of stishovite as a corresponding phase requires extra oxygen. However, the findings of siderite in some samples contradicts the theory of a broad oxidation, as siderite contains only Fe^{2+} and reacts

The results suggest a phase boundary of $\text{Fe}_3\text{O}_4\text{-Fe}_2\text{SiO}_4$ solid solutions between 9 and 11 GPa and temperatures > 1100 °C. Temperature dependence was not observed. However, an exact definition of the slope needs more experiments at different P and T.

5.3.2. Mt-Chr solid solutions

The first occurrence of the unknown phase is documented at 8 GPa and 1250 °C (Fig. 5.10). Mt50cr50 resulted in the formation of “mystery phase” together with spinel at these conditions. A mt80cr20 solid solution reacted to spinel with the same unit cell size as the starting material.

At 10 GPa spinel reacts to eskolaite (Cr_2O_3) and “mystery phase”. However, the reaction depends on the composition of the solid solution. In the products of mt50chr50, significant amounts of spinel were found at 10 GPa. In mt80chr20 the reaction to eskolaite + “mystery phase” was accomplished. At 13 GPa mt50chr50 also completely transformed to eskolaite + “mystery phase”. The position of the phase boundary is strongly pressure dependent and is located between 8 GPa and 10 GPa, although the phase boundary requires more data-points for an exact definition. Both phases, eskolaite + “mystery phase” form solid solution with different amounts of Fe and Cr, respectively. This is in clear contrast to the mtfay spinels. To reveal the definite reasons why Cr can be incorporated into the structure of the “mystery phase”, but Si cannot, extensive structural analyses are necessary. However, some general features of the involved cations deliver first results. Cr^{3+} and Fe^{3+} are equal concerning their

charge and ionic radius (67 pm, 64 pm), whereas Si^{4+} has a different charge and a much smaller radius (26 pm). This simplifies a substitution between Fe and Cr and requires a coupled substitution between Si and a divalent cation.

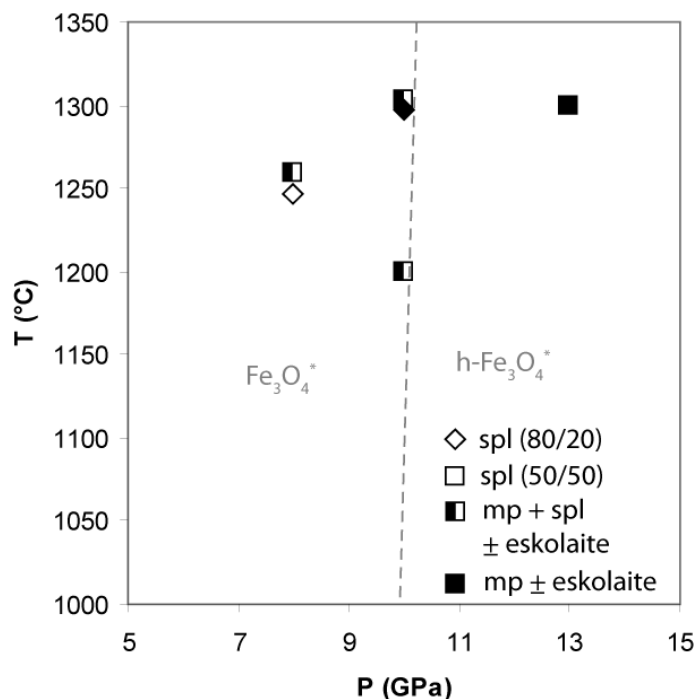


Figure 5.10: Position of the experiments on mtchr solid solutions. The dashed line represents the estimated position of the phase boundary between spinel and „mystery phase“ + eskolaite.

In some experiments with mtchr oxidation occurred. If the $\text{Fe}^{2+}/\text{Fe}^{3+}$ ratio in the „mystery phase“ stays constant compared to magnetite, the produced eskolaite can only be Fe^{2+} -free at constant redox conditions as eskolaite only contains Fe^{3+} . However, all produced eskolaite is a solid solution between hematite and eskolaite and therefore oxidation must have occurred. The oxidation in “mystery phase” containing samples cannot be estimated, since the ratio between the two phases is unknown. The only method to estimate the ratio of the products is by optical microscopy of thin sections. But the error of this appraisal is larger than the rate of oxidation.

A hint for an oxidation during the phase transformation is sample M345, treated at 8 GPa and 1250 °C, and yielding no transformation. The produced spinel has the same lattice parameter (8.385(4) Å) as the starting material (8.3855 Å), indicating that no reaction occurred and the $\text{Fe}^{2+}/\text{Fe}^{3+}$ ratio did not change.

5.4. Further Work

In additional experiments between 7 GPa and 13 GPa with smaller pressure intervals, the maximum amount of Si and Cr in spinel could be investigated, before the spinel solid solution reacts completely to “mystery phase”. This would also reveal the maximum spinel stability with increasing Fe₂SiO₄/chromite content. To define the stability field of the “mystery phase”, experiments at higher pressures are necessary. Occurring in pure magnetite, in magnetite- Fe₂SiO₄ and magnetite-chromite solid solutions, and in the Fe-Mg-Si system, further systems have to be checked for the occurrence of the “mystery phase”. Electron energy loss spectroscopy (EELS) would provide important information on the Fe²⁺/Fe³⁺ ratio of the “mystery phase”. This ratio is crucial for the evidence of a possible oxidation during the experiments and for the formula of the new phase. But first of all, the structure of the “mystery phase” has to be identified. Electron diffraction measurements on single crystals could help to solve the crystal class and its structure.

5.5. References

- Buhre, S. (2005) Experimentelle Bestimmung der Löslichkeit von Al und SEE und Reaktionskinetik im CaSiO₃-System unter Bedingungen des Oberen Erdmantels, Ph.D.dissertation, p. 153. J.W. Goethe-Universität, Frankfurt am Main.
- Chen, M., Shu, J.F., and Mao, H.K. (2008) Xieite, a new mineral of high-pressure FeCr₂O₄ polymorph. Chinese Science Bulletin, 53(21), pp 3341-3345.
- Chen, M., Shu, J.F., Mao, H.K., Xie, X.D., and Hemley, R.J. (2003a) Natural occurrence and synthesis of two new postspinel polymorphs of chromite. Proceedings of the National Academy of Sciences of the United States of America, 100(25), pp 14651-14654.
- Chen, M., Shu, J.F., Xie, X.D., and Mao, H.K. (2003b) Natural CaTi₂O₄-structured FeCr₂O₄ polymorph in the Suizhou meteorite and its significance in mantle mineralogy Geochimica Et Cosmochimica Acta, 67(20), pp 3937-3942.

- De Faria, D.L.A., Venâncio Silva, S., and de Oliveira, M.T. (1997) Raman microspectroscopy of some iron oxides and oxyhydroxides. *Journal of Raman Spectroscopy*, 28(11), pp 873-878.
- Di Cerbo, R.K., and Seybolt, A.U. (1959) Lattice parameters of the α -Fe₂O₃-Cr₂O₃ solid solution. *Journal of the American Ceramic Society*, 42(9), pp 430-431.
- Dubrovinsky, L.S., Dubrovinskaia, N.A., McCammon, C., Rozenberg, G.K., Ahuja, R., Osorio-Guillen, J.M., Dmitriev, V., Weber, H.P., Le Bihan, T., and Johansson, B. (2003) The structure of the metallic high-pressure Fe₃O₄ polymorph: experimental and theoretical study. *Journal of Physics-Condensed Matter*, 15(45), pp 7697-7706.
- Fei, Y.W., Frost, D.J., Mao, H.K., Prewitt, C.T., and Häusermann, D. (1999) In situ structure determination of the high-pressure phase of Fe₃O₄. *American Mineralogist*, 84(1-2), pp 203-206.
- Grygar, T., Bezduka, P., Dedecek, J., Petrovsky, E., and Schneeweiss, O. (2003) Fe₂O₃-Cr₂O₃ system revised. *Ceramics-Silikaty*, 47(1), pp 32-39.
- Haavik, C., Stolen, S., Fjellvag, H., Hanfland, M., and Häusermann, D. (2000) Equation of state of magnetite and its high-pressure modification: Thermodynamics of the Fe-O system at high pressure. *American Mineralogist*, 85(3-4), pp 514-523.
- Hanrahan, M., Brey, G.P., Woodland, A.B., Altherr, R., and Seitz, H.-M. (2009) Towards a Li barometer for bimineraleclogites: experiments in CMAS. *Contributions to Mineralogy and Petrology*, 112, pp 992-1001.
- Irifune, T., Naka, H., Sanhira, T., Inoue, T., and Funakoshi, K. (2002) In situ X-ray observations of phase transitions in MgAl₂O₄ spinel to 40 GPa using multianvil apparatus with sintered diamond anvils. *Physics and Chemistry of Minerals*, 29(10), pp 645-654.

- Koch, M., Woodland, A.B., and Angel, R.J. (2004) Stability of spinelloid phases in the system $\text{Mg}_2\text{SiO}_4\text{-Fe}_2\text{SiO}_4\text{-Fe}_3\text{O}_4$ at 1100 °C and up to 10.5 GPa. *Physics of the Earth and Planetary Interiors*, 143, pp 171-183.
- Larson, A.C., and von Dreele, R.B. (1988) GSAS manual. Los Alamos National Laboratory, report LAUR, pp 86-748.
- Logvinova, A.M., Wirth, R., and Sobolev, N.V. (2010) Fluid/melt inclusions in alluvial Northeast Siberian diamonds: new approach on diamond formation. *Geophysical Research Abstracts*, (12), EGU 2010-1236.
- Morishima, H., Kato, T., Suto, M., Ohtani, E., Urakawa, S., Utsumi, W., Shimomura, O., and Kikegawa, T. (1994) The phase boundary between α - and β - Mg_2SiO_4 determined by in situ X-ray observation. *Science*, 265(5176), pp 1202-1203.
- Ohtaka, O., Tobe, H., and Yamanaka, T. (1997) Phase equilibria for the $\text{Fe}_2\text{SiO}_4\text{-Fe}_3\text{O}_4$ system under high pressure. *Physics and Chemistry of Minerals*, 24(8), pp 555-560.
- Robbins, M., Wertheim, G.K., Sherwood, R.C., and Buchanan, D.N. (1971) Magnetic properties and site distributions in system $\text{FeCr}_2\text{O}_4\text{-Fe}_3\text{O}_4(\text{Fe}^{2+}\text{Cr}_{2-x}\text{Fe}_x^{3+}\text{O}_4)$. *Journal of Physics and Chemistry of Solids*, 32(3), pp 717-729.
- Shebanova, O.N., and Lazor, P. (2003a) Raman study of magnetite (Fe_3O_4): laser induced thermal effects and oxidation. *Journal of Raman Spectroscopy*, 34, pp 845-852.
- Shebanova, O.N., and Lazor, P. (2003b) Raman spectroscopic study of magnetite (FeFe_2O_4): a new assignment for the vibrational spectrum. *Journal of Solid State Chemistry*, 174, pp 424-430.
- Schollenbruch, K., Woodland, A.B., Frost, D.J. and Langenhorst, F. (2009) Detecting the spinel-post-spinel transition in Fe_3O_4 by in situ electrical resistivity measurements. *High Pressure Research*, 29 (4), pp 520-524.

- Stachel, T., Harris, J.W., and Brey, G.P. (1998) Rare and unusual mineral inclusions in diamonds from Mwadui, Tanzania (vol 132, pg 34, 1998). *Contributions to Mineralogy and Petrology*, 132(3), pp 307-307.
- Steinberg, H.K. (2005) Hochdruckexperimente an Calciumsilikatphasen zur Rekonstruktion der Aufstiegs Geschichte von Diamanten, Ph.D. dissertation, p. 141. J.W. Goethe-Universität, Frankfurt am Main.
- Toby, B.H. (2001) EXPGUI, a graphical user interface for GSAS. *Journal of Applied Crystallography*, 34, pp 210-213.
- Walker, D., Carpenter, M.A., and Hitch, C.M. (1990) Some simplifications to multianvil devices for high pressure experiments *American Mineralogist*, 75(9-10), pp 1020-1080.
- Woodland, A.B., and Angel, R.J. (2000) Phase relations in the system fayalite-magnetite at high pressures and temperatures. *Contributions to Mineralogy and Petrology*, 139(6), pp 734-747.

6.a Summary and outlook

6.1.a Hercynite

A single experiment at 12 GPa and 1000 °C by Ringwood and Reid (1968) suggested, that hercynite (FeAl_2O_4) may decompose to its oxides at high P and T. Since detailed information about its high pressure behaviour are missing, a series of systematic multianvil quench experiments were performed between 7 – 24 GPa and 950 – 1720 °C. The experimental setup allowed determining the stability of each phase at the corresponding P and T. The primary assumption of Ringwood and Reid (1968) of hercynite decomposing to its oxides was confirmed. Despite the addition of metallic iron, a minor formation of Fe^{3+} occurred, leading to a shift of the stability of hercynite. To correct this shift, the magnetite fraction was calculated by the size of the unit cell. The stability of pure hercynite was determined by the equation of state of the involved phases. In the range of 7 – 9 GPa pure (calculated) hercynite is stable at about 0.4 – 0.8 GPa lower pressures than hercynite comprising 4 – 7 % magnetite. The high P and T experiments, together with the correction for Fe^{3+} , yield a slope of the phase boundary of:

$$6.0(9) \times 10^{-4} T (\text{K}) + 6.2(1) = P (\text{GPa}) \quad (6.1)$$

The phase boundary is in perfect agreement with the thermodynamically calculated phase boundary of Holland and Powell (1990) and the S_{298}° for hercynite from Klemme and Van Miltenburg (2003). The slope of the phase boundary is similar to that of spinel (MgAl_2O_4) (Akaogi et al. 1999), which also decomposes to its oxides at high pressure. However, the phase boundary of hercynite is at ~ 5 – 6 GPa lower pressures compared to MgAl_2O_4 . This is most likely due to the general effect, that oxides or silicates, containing Fe^{2+} , have a lower pressure stability compared to analogue Mg^{2+} systems.

The oxides of spinel (MgO and Al_2O_3) react to an orthorhombic high-pressure structure (h- MgAl_2O_4) of MgAl_2O_4 at pressures above 28 GPa. To test the analogy between FeAl_2O_4 and MgAl_2O_4 , two single experiments were performed with hercynite at 18 GPa and 24 GPa. The chosen pressure is adapted to the shift in pressure between the two systems. FeO and Al_2O_3 would react to a high pressure modification at 18 – 20 GPa, if the behaviour of hercynite is analogue to MgAl_2O_4 . However, both experiments resulted in the formation of

FeO and Al₂O₃. Hence the existence of h-FeAl₂O₄ seems unlikely, although the formation of a high-P polymorph at > 24 may still be possible.

As the high pressure behaviour of these two spinels is completely different experiments with magnetite-hercynite solid solutions should be performed in a next step. With experiments on these solid solutions it could be possible to determine a stable high pressure polymorph or even to stabilize the “mystery phase”, occurring in solid solutions of mtchr and mtfay at high P and T as described in chapter 5.

6.2.a Magnetite

Due to the unquenchable nature of the high pressure polymorph of magnetite sophisticated methods were applied to measure the *in situ* phase transformation of magnetite. Two independent methods were chosen. The structural change was analyzed indirectly by electrical resistivity experiments and directly by synchrotron measurements at high P and T.

6.2.1.a Resistivity measurements

During *in situ* multianvil experiments, the phase transition was determined by a change in the electrical resistivity of Fe₃O₄ via the four-electrode-method. Four measurements were conducted at 8 GPa, 9 GPa, 10 GPa, and 12 GPa, at which the resistivity was measured during heating as well as during cooling.

The resistivity curves of the 8 GPa and 9 GPa experiment are very similar during heating and cooling. After a small primary drop, the resistivity stayed constant up to 1400 °C and followed the same path during cooling. At 10 GPa the characteristics of the resistivity were comparable to the 8 GPa and 9 GPa experiment below 1000 °C, but reaching 1000 °C, the resistivity sharply increased and also rose nearly logarithmic during cooling. This rapid increase was also monitored at 12 GPa, this time starting at 1300 °C.

With electrical resistivity measurements it was possible to determine the exact position of the phase boundary of magnetite for the first time at high P and T. The irreversible change in resistivity at 10 GPa and 12 GPa is interpreted as the beginning of the phase transformation into a non-metallic phase. Present results are in contrast to results from Dubrovinsky et al. (2003), who report of a metallic high pressure phase of magnetite at much higher pressures.

This points to the existence of a second high pressure phase of magnetite being inconsistent with the one described by Dubrovinsky et al. (2003). During subsequent TEM analysis only magnetite was detected in all samples. However, in the 10 GPa and 12 GPa experiments twin lamella were identified in magnetite, being absent in the two lower pressure experiments. These twin lamella are interpreted as a relict of a reaction from a phase with low symmetry back to magnetite (Frost et al. 2001) or from the reaction from magnetite to a phase with lower symmetry (chapter 4). By crossing the phase boundary at two different pressures and temperatures it is possible to plot it in P-T space. It has a nearly isobaric, slightly negative slope. Furthermore it is shifted to ~ 10 GPa lower pressures compared to literature data (e.g., Mao et al. 1974; Huang and Bassett 1986; Lazor et al. 2004). This observation is due to the reduced kinetics at > 1000 °C. To maintain the pressure calibration of the multianvil press, it was only possible to conduct the experiments at constant pressure. This led to a kinetically induced delay of the transformation. To overcome this problem, further experiments were conducted on a multianvil press and analyzed in situ by synchrotron radiation, gaining more structural information.

6.2.2.a Synchrotron measurements

For a direct *in situ* analysis of the transition magnetite – h-Fe₃O₄ multianvil experiments were conducted at the Advanced Photon Source in Chicago, Illinois. Due to direct measurements of pressure, it was possible to change temperature and pressure independently, allowing an isothermal transition of the phase boundary. A P-T range up to 1400 °C and 15 GPa was covered during five experiments during which the phase boundary was crossed six times over a range in temperature of 700–1400 °C and between 9 GPa and 11.5 GPa. The determined phase boundary is nearly identical with the one identified during the resistivity experiments and has the equation:

$$P \text{ (GPa)} = 1.5 \times 10^{-3} T \text{ (K)} + 8.0 \quad (6.2)$$

A small drop in pressure was monitored during the appearance of the high pressure phase (h-Fe₃O₄). This may be related to a volume reduction of 6.5% during the transformation to h-Fe₃O₄ (Fei et al. 1999).

The beamline was equipped with energy-dispersive radiation, which made a structural analysis of the high pressure phase impossible. However, the CaMn_2O_4 -structure suggested by Fei et al. (1999) or the CaTi_2O_4 -structure by Dubrovinsky et al. (2003) seem unlikely. It is more consistent with the pattern of a “mystery phase” detected in quenched samples (>10 GPa) by Koch et al. (2004) in the system Fe_3O_4 - Fe_2SiO_4 - Mg_2SiO_4 . It may be an intermediate phase, reacting at higher pressures to an orthorhombic CaMn_2O_4 - or CaTi_2O_4 -structure.

TEM analyses of the experimental products yield a complete re-conversion to magnetite. According to the resistivity experiments, numerous twin lamella on the {311} plane were found, indicating a phase transformation.

To gain more structural information of h- Fe_3O_4 , multianvil experiments with angle-dispersive synchrotron radiation should be performed. The results of the electrical resistivity measurements and the synchrotron measurements indicate the existence of a high pressure phase inconsistent with the h- Fe_3O_4 described in literature (Haavik et al. 2000; Fei et al. 1999; Dubrovinsky et al. 2003). To determine the stability field of this phase, experiments at higher pressure are recommended, especially in the P-T range near the first occurrence of the high pressure modification of magnetite described in literature. This would also solve the question, how many h- Fe_3O_4 phases exist. To cover the stability field at the beginning growth of the CaMn_2O_4 -structured high pressure phase, a laser heated diamond anvil cell or a multianvil apparatus with sintered diamonds can be an appropriate tool.

The experimental data deliver an important contribution for the phase relations in the Fe-O system. The position of the phase boundary at 10 GPa lies within the stability field of diamond formation. The nearly isobaric slope of this phase boundary makes magnetite a possible barometer in diamondiferous rocks. Twin lamella or relicts of volume changes of magnetite inclusions in a diamond indicates a formation of this diamond at pressures > 10 GPa.

6.3.a Spinel solid solutions

Based on the defined phase boundary of pure Fe_3O_4 , the phase boundary of petrological more relevant spinels such as magnetite-fayalite (mt-fay) and magnetite-chromite (mt-chr) solid solutions was investigated by multianvil quench experiments. Additionally, the stability of a possible high pressure mt-chr phase at ambient conditions was checked, as the

high pressure polymorph of chromite (Xieite, h-FeCr₂O₄) is quenchable (Chen et al. 2003; Chen et al. 2008).

16 experiments were conducted between 8 GPa and 13 GPa and 1100 °C and 1300 °C with different fayalite- and chromite concentrations. All samples were X-rayed afterwards and analysed with electron microprobe. The solid solution mt70fay30 started to react to a Si-rich spinel and a Si-free iron oxide at 1100 °C and 8 GPa. With increasing temperature, the amount of the pure Fe-oxide increased together with the Si-content in the spinel. At pressures ≥ 10 GPa the Si-rich spinel (mt85fay15) reacts to a Si-free iron oxide + stishovite. X-ray analysis of the Si-free iron oxide yield the same pattern as for the “mystery phase” from Koch et al. (2004).

Chromite-bearing spinels show a similar behaviour at high P and T. From 10 GPa on, a new iron oxide emerges, which has the same reflexes as the “mystery phase” and can incorporate up to 20 wt% Cr₂O₃. At 13 GPa and 1300 °C mt50chr50 reacts to an eskolaite-hematite solid solution and to “mystery phase”.

Raman and preliminary TEM analysis could not reveal the structure of the “mystery phase”. It is magnetic, not cubic, and has neither the structure of a known high pressure modification of magnetite, nor a common iron oxide (wüstite, magnetite, hematite, maghemite). It seems likely to be an unknown, quenchable high pressure phase of magnetite, but for a reliable structural analysis, additional TEM single crystal experiments will be necessary.

In further experiments the h-Fe₃O₄ detected by Schollenbruch et al. (2009) in the same P-T range should be compared to the “mystery phase”. If the phases have different structures, the role of Si and Cr for the formation of the “mystery phase” must be investigated. Additional experiments on spinels with $> 50\%$ chromite could reveal the maximum amount of Fe₃O₄-component of Xieite, the high pressure polymorph of chromite (Chen et al., 2008).

6.4.a References

Akaogi, M., Hamada, Y., Suzuki, T., Kobayashi, M., and Okada, M. (1999) High pressure transitions in the system MgAl₂O₄-CaAl₂O₄: a new hexagonal aluminous phase with implication for the lower mantle. *Physics of the Earth and Planetary Interiors*, 115(1), pp 67-77.

- Chen, M., Shu, J.F., and Mao, H.K. (2008) Xieite, a new mineral of high-pressure FeCr_2O_4 polymorph. *Chinese Science Bulletin*, 53(21), pp 3341-3345.
- Chen, M., Shu, J.F., Mao, H.K., Xie, X.D., and Hemley, R.J. (2003) Natural occurrence and synthesis of two new postspinel polymorphs of chromite. *Proceedings of the National Academy of Sciences of the United States of America*, 100(25), pp 14651-14654.
- Dubrovinsky, L.S., Dubrovinskaia, N.A., McCammon, C., Rozenberg, G.K., Ahuja, R., Osorio-Guillen, J.M., Dmitriev, V., Weber, H.P., Le Bihan, T., and Johansson, B. (2003) The structure of the metallic high-pressure Fe_3O_4 polymorph: experimental and theoretical study. *Journal of Physics-Condensed Matter*, 15(45), pp 7697-7706.
- Fei, Y.W., Frost, D.J., Mao, H.K., Prewitt, C.T., and Hausermann, D. (1999) In situ structure determination of the high-pressure phase of Fe_3O_4 . *American Mineralogist*, 84(1-2), pp 203-206.
- Frost, D.J., Langenhorst, F., and van Aken, P.A. (2001) Fe-Mg partitioning between ringwoodite and magnesiowustite and the effect of pressure, temperature and oxygen fugacity. *Physics and Chemistry of Minerals*, 28(7), pp 455-470.
- Haavik, C., Stolen, S., Fjellvag, H., Hanfland, M., and Hausermann, D. (2000) Equation of state of magnetite and its high-pressure modification: Thermodynamics of the Fe-O system at high pressure. *American Mineralogist*, 85(3-4), pp 514-523.
- Holland, T.J.B., and Powell, R. (1990) An enlarged and updated internally consistent thermodynamic dataset with uncertainties and correlations - the system $\text{K}_2\text{O}-\text{Na}_2\text{O}-\text{CaO}-\text{MgO}-\text{MnO}-\text{FeO}-\text{Fe}_2\text{O}_3-\text{Al}_2\text{O}_3-\text{TiO}_2-\text{SiO}_2-\text{C}-\text{H}_2-\text{O}_2$. *Journal of Metamorphic Geology*, 8(1), pp 89-124.
- Huang, E., and Bassett, W.A. (1986) Rapid-determination of Fe_3O_4 phase-diagram by synchrotron radiation. *Journal of Geophysical Research-Solid Earth and Planets*, 91(B5), pp 4697-4703.

- Klemme, S., and Van Miltenburg, J.C. (2003) Thermodynamic properties of hercynite (FeAl_2O_4) based on adiabatic calorimetry at low temperatures *American Mineralogist*, 88(1), pp 68-72.
- Koch, M., Woodland, A.B., and Angel, R.J. (2004) Stability of spinelloid phases in the system $\text{Mg}_2\text{SiO}_4\text{-Fe}_2\text{SiO}_4\text{-Fe}_3\text{O}_4$ at 1100 °C and up to 10.5 GPa. *Physics of the Earth and Planetary Interiors*, 143, pp 171-183.
- Lazor, P., Shebanova, O.N., and Annersten, H. (2004) High-pressure study of stability of magnetite by thermodynamic analysis and synchrotron X-ray diffraction. *Journal of Geophysical Research-Solid Earth*, 109.
- Mao, H.K., Takahashi, T., Bassett, W.A., Kinsland, G.L., and Merrill, L. (1974) Isothermal compression of magnetite to 320 Kbar and pressure-induced phase-transformation. *Journal of Geophysical Research*, 79(8), pp 1165-1170.
- Ringwood, A.E., and Reid, A.F. (1968) High pressure transformations of spinels (I). *Earth and Planetary Science Letters*, 5(4), pp 245-250.
- Schollenbruch, K., Woodland, A.B., Frost, D.J. and Langenhorst, F. (2009) Detecting the spinel-post-spinel transition in Fe_3O_4 by in situ electrical resistivity measurements. *High Pressure Research*, 29 (4), pp 520-524.

6.b Zusammenfassung und Ausblick

6.1.b Hercynit

Aus einem einzelnen Experiment ist bekannt, dass Hercynit (FeAl_2O_4) bei hohem Druck in seine Oxide zerfällt (Ringwood & Reid 1968). Da genauere Informationen fehlen, wurde eine Reihe systematischer Multianvil-Quench-Experimente zwischen 7 – 24 GPa und 950 – 1720 °C durchgeführt. Der experimentelle Aufbau erlaubte die Bestimmung, der bei ausgewählter Temperatur und Druck stabilen Phase. Die ursprüngliche Annahme von Ringwood & Reid (1968), dass Hercynit zu Wüstit und Korund zerfällt wurde bestätigt. Auch die Zugabe von Eisen konnte eine geringe Bildung von Magnetitkomponente im Hercynit nicht verhindern, was eine Verschiebung der Stabilität von Hercynit zur Folge hatte. Um diese Verschiebung zu korrigieren wurde mit Hilfe der Größe der Elementarzelle der Magnetitanteil errechnet und über die Zustandsgleichungen der beteiligten Phasen die Stabilität von reinem Hercynit bestimmt. Zwischen 7 GPa und 9 GPa ist reiner (berechnet) Hercynit bei 0.4 GPa bis 0.8 GPa niedrigeren Drücken stabil als Hercynit der 4-7 Gewichtsprozent Eisen enthält. Daraus ergibt sich eine Phasengrenze von:

$$6.0(9) \times 10^{-4} T (\text{K}) + 6.2(1) = P (\text{GPa}) \quad (6.1)$$

Die Phasengrenze stimmt genau mit der thermodynamisch berechneten von Holland und Powell (1990) und dem S°_{298} für Hercynit von Klemme and Van Miltenburg (2003) überein. Die Steigung der Phasengrenze ist der von Spinel (MgAl_2O_4) (Akaogi et al. 1999) sehr ähnlich. MgAl_2O_4 zerfällt bei hohem Druck ebenfalls in seine Oxide, allerdings erst bei 5 – 6 GPa höheren Drücken, im Vergleich zu Hercynit. Hierbei handelt es sich aller Wahrscheinlichkeit nach um den generellen Effekt, dass Oxide oder Silikate, die Fe^{2+} enthalten im Vergleich zu analogen Mg^{2+} -Systemen eine niedrigere Druckstabilität besitzen.

Da sich die Oxide von Spinel ($\text{MgO} + \text{Al}_2\text{O}_3$) ab 28 GPa zu einer orthorhombischen Hochdruckstruktur (h- MgAl_2O_4) von MgAl_2O_4 umwandeln, wurden mit Hercynit zusätzlich einzelne Experimente bei hohen Drücken (18, 24 GPa) durchgeführt. Bei einem analogen Verhalten von Hercynit und MgAl_2O_4 und unter Berücksichtigung der Stabilitätsverschiebung zwischen Fe- und Mg-System würde Hercynit zuerst in $\text{FeO} + \text{Al}_2\text{O}_3$ zerfallen, um dann bei 18 – 20 GPa zu einer orthorhombischen Hochdruckphase zu reagieren. Während beiden Experimenten wurde jedoch ein Zerfall von Hercynit in seine Oxide beobachtet. Aus dem

Grund erscheint eine orthorhombische Hochdruckphase von FeAl_2O_3 unwahrscheinlich. Allerdings kann nicht ausgeschlossen werden, dass sich h- FeAl_2O_3 ab einem Druck > 24 GPa bildet.

Da das Verhalten von MgAl_2O_4 und FeAl_2O_4 bei sehr hohem Druck komplett unterschiedlich ist, sollten in einem nächsten Schritt Experimente mit Hercynit-Spinel-Mischkristallen durchgeführt werden. Dadurch könnten stabile Mischkristall-Polymorphe der Hochdruckphase gefunden werden oder vielleicht sogar die „mystery phase“ stabilisiert werden, welche bei hohem Druck und Temperatur in mtchr und mtfay Mischkristallen auftaucht (siehe Kapitel 5).

6.2.b Magnetit

Aufgrund der Eigenschaft, dass die Hochdruckphase von Magnetit nicht abschreckbar ist, musste aufwendige Methoden verwendet werden um die Phasenumwandlung *in situ* zu messen. Dafür wurden zwei unabhängige Methoden verwendet. Die strukturelle Umwandlung wurde indirekt über elektrische Widerstandsmessungen analysiert und direkt durch Synchrotron-Messungen bei hohem Druck und Temperatur.

6.2.1.b Widerstandsmessungen

Während *in situ* Multianvil Experimente konnte die Phasenumwandlung in Magnetit durch die Änderung der elektrischen Leitfähigkeit mittels der Vier-Elektroden-Methode verfolgt werden. Es wurden vier Experimente bei 8 GPa, 9 GPa, 10 GPa und 12 GPa durchgeführt, bei denen der Widerstand sowohl bei der Temperaturerhöhung als auch bei der schrittweisen Abkühlung aufgezeichnet wurde.

Die Widerstandskurven bei 8 GPa und 9 GPa ähneln sich sowohl während des Heiz- als auch während der Abkühlphase. Nach einem anfänglichen leichten Abfall des Widerstands pendelt dieser sich bis 1400 °C auf ein konstantes Niveau ein und folgt dem gleichen Verlauf während des Abkühlens. Bei einem Druck von 10 GPa zeigt sich bei niedrigen Temperaturen zunächst ein vergleichbares Bild. Allerdings steigt der Widerstand bei ~ 1000 °C sprunghaft an und erhöht sich auch während des Abkühlens nahezu logarithmisch. Dieser abrupte

Anstieg ist auch während des 12 GPa Experimentes zu beobachten, diesmal jedoch bei ~ 1300 °C.

Mit den elektrischen Widerstandsexperimenten war es erstmals möglich die Position der Phasengrenze bei hohem Druck und Temperatur zu bestimmen. Die irreversible Änderung des elektrischen Widerstandes bei 10 und 12 GPa wird als die beginnende Phasenumwandlung in eine nicht-metallische Phase interpretiert. Das steht im Gegensatz zu den Ergebnissen von Dubrovinsky et al. (2003), die eine metallische Hochdruckphase von Magnetit postulieren. In anschließenden TEM Untersuchungen wurde in allen vier Proben nur Magnetit identifiziert. Allerdings konnte in den Proben der 10 und 12 GPa Experimente Zwillinglamellen im Magnetit nachgewiesen werden, die von Frost et al. (2001) als Hinweis für eine Umwandlung einer niedrigsymmetrischen Phase zu Magnetit oder aber für eine Umwandlung von Magnetit zu einer niedrigsymmetrischeren Phase (Kapitel 4) gesehen werden. Im Magnetit der 8 GPa und 9 GPa Experimente wurden keine Zwillinglamellen identifiziert. Durch eine Phasenumwandlung bei zwei unterschiedlichen Temperaturen und Drücken kann die Phasengrenze im P-T Raum dargestellt werden. Sie ist nahezu isobar mit einer leicht negativen Steigung. Außerdem ist sie im Vergleich zur bisherigen Literatur (e.g. Mao et al. 1974, Huang & Bassett 1986, Lazor et al. 2003) um ~ 10 GPa zu niedrigeren Drücken verschoben. Dies wird auf die beschleunigte Kinetik bei > 1000 °C zurück geführt. Um die Kalibration der Multianvil Presse beizubehalten waren nur Experimente bei konstantem Druck möglich, was zu einer kinetisch verursachten Verzögerung der Reaktion führen kann. Um dieses Problem zu beheben wurden weitere Multianvil Experimente an einer Synchrotronanlage durchgeführt, wo es möglich ist in situ genauere strukturelle Informationen zu sammeln.

6.2.2.b Synchrotron-Experimente

Um die Phasengrenze bei hohen Temperaturen direkt zu bestimmen wurden Multianvil-Experimente an der Advanced Photon Source in Chicago, Illinois durchgeführt. Aufgrund direkter Druckmessung können Druck und Temperatur unabhängig voneinander verändert werden, was eine isotherme Überschreitung der Phasengrenze ermöglicht. Bei insgesamt fünf Experimenten wurde ein P-T Bereich bis 1400 °C und 15 GPa abgedeckt und die Phasengrenze sechs Mal in einem Temperaturintervall von 700 °C zwischen 9 und 11.5 GPa überschritten.

Die daraus resultierende fast isobare Phasengrenze stimmt mit den Ergebnissen der Widerstandsexperimente nahezu überein. Im P-T Raum ist die Phasengrenze folgendermaßen definiert:

$$P \text{ (GPa)} = 1.5 \times 10^{-3} T \text{ (K)} + 8.0 \quad (6.2)$$

Zusammen mit dem ersten Auftreten der Hochdruckphase (h-Fe₃O₄) wurde ein leichter Druckabfall festgestellt. Laut Fei et al. (1999) kann dies auf eine Volumenreduktion von 6,5 % während der Transformation zurückzuführen sein.

Da aus technischen Gründen Energie-dispersive Strahlung verwendet wurde, war eine Strukturanalyse der Hochdruckphase nicht möglich. Dennoch erscheint eine CaTi₂O₄- oder eine CaMn₂O₄- Struktur wie sie von Fei et al. (1999) und Dubrovinsky et al. (2003) vorgeschlagen wird als unwahrscheinlich. Das gemessene Beugungsmuster ähnelt vielmehr einer abgeschreckten Phase (>10 GPa) aus dem System Fe₃O₄-Fe₂SiO₄-Mg₂SiO₄ (Koch et al. 2004). Es handelt sich wahrscheinlich um eine Zwischenphase, die bei höheren Drücken vermutlich in eine orthorhombische CaMn₂O₄-Struktur übergeht.

TEM Analysen der untersuchten Proben bestätigten die vollständige Umwandlung der Hochdruckphase zurück zu Magnetit. Wie schon bei den Widerstandsexperimenten wurde eine Vielzahl von Zwillingslamellen auf der {311} Ebene gefunden.

Bei reinem Magnetit bieten sich Multianvil-Experimente mit Wellen-dispersiver Synchrotronstrahlung an, um nähere Informationen zur Struktur von h-Fe₃O₄ zu erhalten. Die Ergebnisse der elektrischen Widerstandsversuche und der Synchrotronmessungen deuten auf eine Hochdruckphase hin, welche nicht mit der, in der Literatur beschriebenen, übereinstimmt (Fei et al. 1999; Haavik et al. 2000; Dubrovinsky et al. 2003). Um das Stabilitätsfeld dieser Phase mehr einzuengen werden Experimente bei höherem Druck vorgeschlagen, vor allem in dem Druck-Temperatur-Bereich, in welchem die, in der Literatur beschriebene Hochdruckmodifikation von Magnetit GPa auftritt. Das würde auch die Frage klären wie viele h-Fe₃O₄ Phasen existieren. Um den Bereich abzudecken, bei dem die Hochdruckphase mit CaMn₂O₄-Struktur stabil ist, bieten sich als geeignetes Werkzeug Laser geheizte Diamantstempelzellen an.

Die experimentellen Daten liefern einen wichtigen Beitrag zum Verständnis der Phasenbeziehungen im Fe-O System. Die Position der Phasengrenze bei 10 GPa ist konsistent mit der tiefen Region der Diamantformation. Die fast isobare Steigung der Phasengrenze lässt Magnetit ein mögliches Barometer in Diamant führenden Gesteinen werden.

Zwillingslamellen oder Spuren von Volumenänderungen in Magnetiteinschlüssen könnten Informationen über Phasenumwandlung(en) liefern und somit auch über die minimale Bildungstiefe.

6.3.b Mischkristalle

Basierend auf den Ergebnissen der Magnetit-Experimente und Literaturdaten (Chen et al. 2003) wurde die Phasengrenze in petrologisch relevanteren Spinell-Mischkristallen untersucht. Dazu wurden Multianvil-Abschreckversuche mit Magnetit-Fayalit- (Mt-Fay) und Magnetit-Chromit- (Mt-Chr) Mischkristallen durchgeführt. Da die Hochdruckmodifikation von Chromit (Xieite, $h\text{-FeCr}_2\text{O}_4$) abschreckbar ist (Chen et al. 2008), soll die Stabilität einer möglichen Hochdruck-Mt-Cr Phase bei Raumbedingungen untersucht werden.

Es wurden 16 Versuche zwischen 8 und 13 GPa und zwischen 1100 °C und 1300 °C mit unterschiedlichen Fayalit- und Chromitkonzentrationen durchgeführt. Alle Proben wurden anschließend geröntgt und mit der Mikrosonde untersucht. Der Mischkristall Mt70Fay30 begann bei 1100 °C und 8 GPa zu einem Si-reichen Spinel und einem Si-freien Eisenoxid zu reagieren. Bei einer isobaren Temperaturerhöhung um 100 °C nahmen der Anteil des Eisenoxides und der Si-Gehalt im Spinel zu. Ab Drücken ≥ 10 GPa reagierte der Si-haltige Spinel (Mt85Fay15) komplett zu der Si-freien „mystery phase“ von Koch et al. (2004) + Stishovit.

Für chromithaltigen Magnetit wurde ein ähnliches Verhalten wie bei Mt-Fay beobachtet. Ab 10 GPa entstand neben einem Cr-haltigen Spinel ein weiteres Eisenoxid mit vergleichbaren Röntgenreflexen wie die „mystery phase“. Im Gegensatz zum Si-haltigen System konnte es aber bis zu 20 wt% Cr_2O_3 einbauen. Bei 13 GPa und 1300 °C reagierte Mt50Chr50 zu einem Eskolait-Hämatit Mischkristall und der „mystery phase“.

Eine eindeutige Identifizierung der „mystery phase“ war auch mit Raman-, und vorläufigen TEM-Messungen nicht möglich. Es handelt sich weder um eine bekannte Hochdruckmodifikation von Magnetit, noch um ein gewöhnliches Eisenoxid (Wüstit, Magnetit, Hämatit, Maghemit). Die Unvereinbarkeit mit Röntgenspektren bekannter Eisenoxide deutet darauf hin, dass es sich um eine noch unbekannte, abschreckbare Hochdruckmodifikation von Magnetit handelt. Zur Bestätigung sind jedoch umfangreiche Einkristallmessungen notwendig.

In weiteren Experimenten sollte die, von Schollenbruch et al. (2009) im gleichen Druck-Temperatur-Bereich entdeckte, $h\text{-Fe}_3\text{O}_4$ Phase mit der „mystery phase“ verglichen

werden. Falls die Phasen unterschiedliche Beugungsmuster aufweisen muss die Rolle von Si und Cr bei der Bildung der „mystery phase“ untersucht werden. Zusätzlich könnte man mit Experimenten mit > 50% Chromitanteil im Mischkristall die maximale Stabilität von Xieit, der Hochdruckmodifikation von Chromit (Chen et al. 2008), bestimmen.

6.4.b Referenzen

- Akaogi, M., Hamada, Y., Suzuki, T., Kobayashi, M., and Okada, M. (1999) High pressure transitions in the system $MgAl_2O_4$ - $CaAl_2O_4$: a new hexagonal aluminous phase with implication for the lower mantle. *Physics of the Earth and Planetary Interiors*, 115(1), pp 67-77.
- Chen, M., Shu, J.F., and Mao, H.K. (2008) Xieite, a new mineral of high-pressure $FeCr_2O_4$ polymorph. *Chinese Science Bulletin*, 53(21), pp 3341-3345.
- Chen, M., Shu, J.F., Mao, H.K., Xie, X.D., and Hemley, R.J. (2003) Natural occurrence and synthesis of two new postspinel polymorphs of chromite. *Proceedings of the National Academy of Sciences of the United States of America*, 100(25), pp 14651-14654.
- Dubrovinsky, L.S., Dubrovinskaia, N.A., McCammon, C., Rozenberg, G.K., Ahuja, R., Osorio-Guillen, J.M., Dmitriev, V., Weber, H.P., Le Bihan, T., and Johansson, B. (2003) The structure of the metallic high-pressure Fe_3O_4 polymorph: experimental and theoretical study. *Journal of Physics-Condensed Matter*, 15(45), pp 7697-7706.
- Fei, Y.W., Frost, D.J., Mao, H.K., Prewitt, C.T., and Hausermann, D. (1999) In situ structure determination of the high-pressure phase of Fe_3O_4 . *American Mineralogist*, 84(1-2), pp 203-206.
- Frost, D.J., Langenhorst, F., and van Aken, P.A. (2001) Fe-Mg partitioning between ringwoodite and magnesiowüstite and the effect of pressure, temperature and oxygen fugacity. *Physics and Chemistry of Minerals*, 28(7), pp 455-470.

- Haavik, C., Stolen, S., Fjellvag, H., Hanfland, M., and Hausermann, D. (2000) Equation of state of magnetite and its high-pressure modification: Thermodynamics of the Fe-O system at high pressure. *American Mineralogist*, 85(3-4), pp 514-523.
- Holland, T.J.B., and Powell, R. (1990) An enlarged and updated internally consistent thermodynamic dataset with uncertainties and correlations - the system K_2O - Na_2O - CaO - MgO - MnO - FeO - Fe_2O_3 - Al_2O_3 - TiO_2 - SiO_2 - C - H_2 - O_2 . *Journal of Metamorphic Geology*, 8(1), pp 89-124.
- Huang, E., and Bassett, W.A. (1986) Rapid-determination of Fe_3O_4 phase-diagram by synchrotron radiation. *Journal of Geophysical Research-Solid Earth and Planets*, 91(B5), pp 4697-4703.
- Klemme, S., and Van Miltenburg, J.C. (2003) Thermodynamic properties of hercynite ($FeAl_2O_4$) based on adiabatic calorimetry at low temperatures *American Mineralogist*, 88(1), pp 68-72.
- Koch, M., Woodland, A.B., and Angel, R.J. (2004) Stability of spinelloid phases in the system Mg_2SiO_4 - Fe_2SiO_4 - Fe_3O_4 at 1100 °C and up to 10.5 GPa. *Physics of the Earth and Planetary Interiors*, 143, pp 171-183.
- Lazor, P., Shebanova, O.N., and Annersten, H. (2004) High-pressure study of stability of magnetite by thermodynamic analysis and synchrotron X-ray diffraction. *Journal of Geophysical Research-Solid Earth*, 109.
- Mao, H.K., Takahashi, T., Bassett, W.A., Kinsland, G.L., and Merrill, L. (1974) Isothermal compression of magnetite to 320 Kbar and pressure-induced phase-transformation. *Journal of Geophysical Research*, 79(8), pp 1165-1170.
- Ringwood, A.E., and Reid, A.F. (1968) High pressure transformations of spinels (I). *Earth and Planetary Science Letters*, 5(4), pp 245-250.

Schollenbruch, K., Woodland, A.B., Frost, D.J. and Langenhorst, F. (2009) Detecting the spinel – post-spinel transition in Fe_3O_4 by in situ electrical resistivity measurements. *High Pressure Research*, 29 (4), pp 520-524.

Supplementary material

Gas mixing furnace manual

Belt-apparatus manual

Multianvil apparatus manual

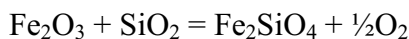
Acknowledgement

Curriculum Vitae

Gas mixing furnace manual

1. Calculation of the amounts of Si and Fe₂O₃

Synthesis of 3g Fe₂SiO₄



oxides	mole weight (A)	Mole (B)	(A)x(B)	ratio	normalized to 3g
SiO ₂	60.0843	1	60.0843	0.2734	0.8202
Fe ₂ O ₃	159.687	1	159.687	0.7266	2.1798g

- use material from the chemistry lab
- the balance is in the Mössbauer lab
- always use weighing paper
- mix and grind the materials carefully

2. Pressing the pills

- the pressure assembly (Fig.1) in the cupboard in the Raman-preparation lab
- set the different parts together in the correct order (Fig.1)



Figure 1: Assembly to press pills

- use the grey press in the MA-preparation lab (Fig. 2)
- do not press harder than ~10Kn
- the result should be a stable pill (Fig. 3)

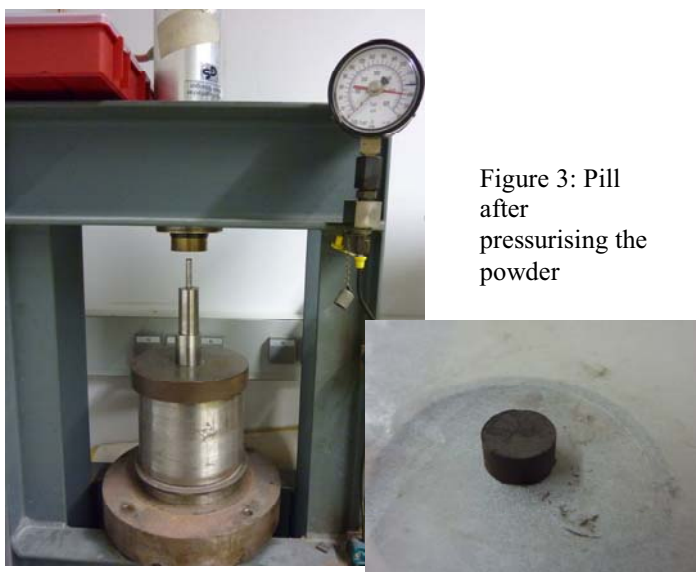


Figure 3: Pill after pressurising the powder

Figure 2: Pressing a pill

3. Gas mixing furnace

- the gas mixing furnace (Fig.4) is water cooled and to buffer the fugacity CO and CO₂ are used
- the heating zone is in the middle of the white ceramic tube of the furnace
- the thin ceramic tube (+ the platinum wire) is used to hold the sample in the middle of the heating zone
- depending on the temperature the heating zone varies (table next to the door)



Figure 4: The gas mixing furnace

- find out the temperature and the oxygen fugacity (be careful, melting point of fayalite = 1205 °C)
- high temperature is required to start the reaction, but the temperature must be below the melting point of fayalite → e.g., 1115 °C
- the oxygen fugacity should be slightly above the QFM buffer (Fig. 5); for 1100°C → $\log f_{O_2} = -9.0$
- look in the tabular value for the correct mixture of CO/CO₂
- the ratio is 2.5/97.5
- the minimum adjustable value of the flow-controllers is 5 cm³/s
- to keep the ratio, use an amount of 5 cm³/s CO and 195 cm³/s CO₂
- fix the platinum basket to platinum wire coming out of the thin ceramic tube with the metal lid
- fix it in a way that allows release by pulling at the platinum wire (but remember: platinum gets soft above 1000 °C)
- place the pill on the little platinum basket (Fig. 6)

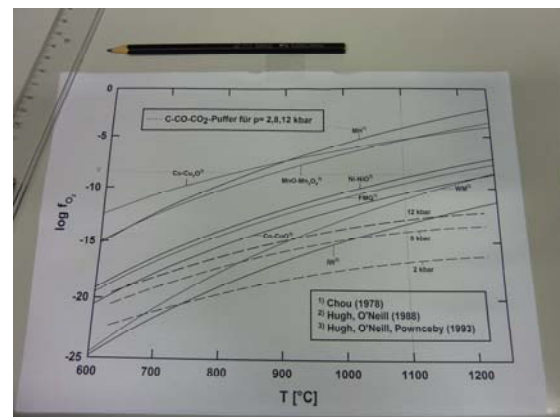


Figure 5: Finding out the right oxygen fugacity

- then adjust the height, measuring from the bottom edge of the metal lid
- mark the ceramic tube on the top of the lid
- then pull the wire out as far as possible (during heating or the gas-filling of the furnace the sample should be as far from the heating point as possible)
- remove the lid of the furnace (might be hot →gloves!)
- insert your sample, be careful not to touch the furnace wall
- fix the metal screw and insert the plastic tube into the extractor hood → it must not fall out (CO contamination!)
- set the furnace to the desired temperature (it has to be slightly above desired temperature, see table below the furnace display)
- max. ramp: 300 °C/h
- to set up the ramp, temperature and holding time, read the instructions of the furnace
- as soon as the desired temperature is reached, open the bottles in the gas cabinet
- open the gas conduits
- turn on the flow controllers (Fig. 7) and wait until the values on the display are stable
- set CO and CO₂ to the calculated values
- check, if the plastic tube of the lid is really in the extractor hood (and check that the extractor hood is running)
- wait 20 min until the furnace is completely filled with gas
- lower the sample down to the hottest position (be careful not to move the ceramic tube to much)

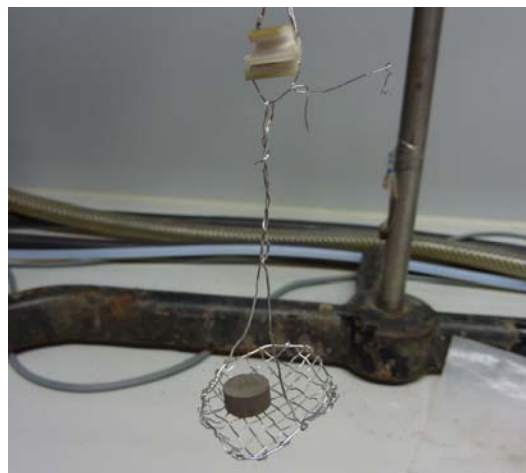


Figure 6: Pill on the platinum basket



Figure 7: The flow controller

4. Quenching

- leave the sample in the furnace for at least 2 hours
- before quenching the sample, fill the bottom of the furnace with water
- use a lab water bottle to fill water through the plastic tube (Fig. 8) into the plastic-cup (3-4cm)
- pull at the two platinum wire ends, coming out of the thin ceramic tube until the basket drops into the water quench



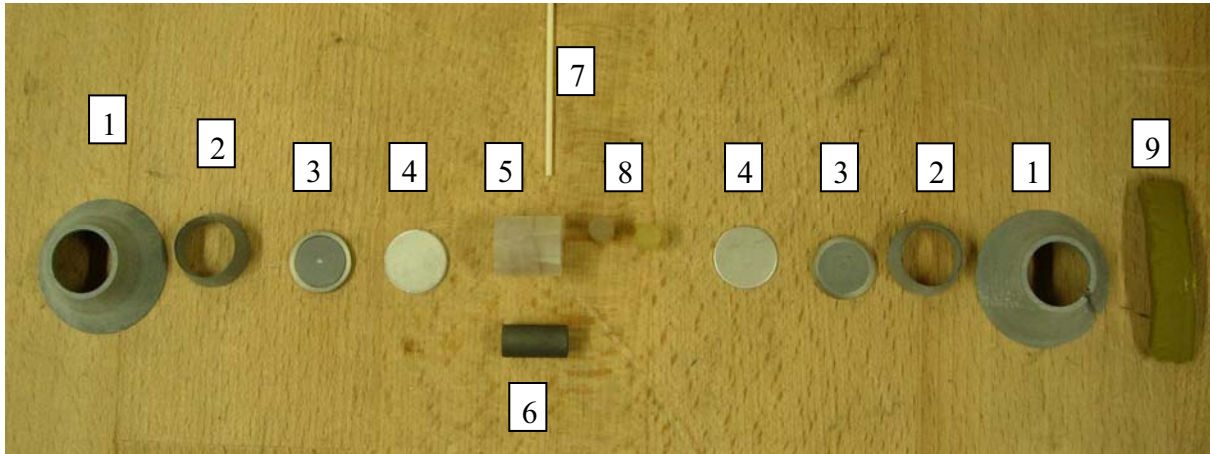
Figure 8: Lower part of the furnace

(or the pill drops down without the basket)

- turn off all the gas plugs and set the flowcontrollers to zero.
- open the furnace at the bottom (be careful, the remaining gas might burn)
- take the sample and the basket, throw away the water and close the furnace again
- remove the thin ceramic tube and put the lid without the tube on the furnace
- if the furnace is used in the next weeks set it to 700 °C, if not set it to 0 °C and then turn it off

Let the sample dry, then grind it carefully and repeat the whole process to achieve homogeneity.

Belt-Apparatus Manual



1. 2x pyrophyllite gaskets for the piston
2. 2x pyrophyllite gaskets
3. 2x steelrings + pyrophyllite insert
4. 2x steeldiscs (rhodium-coated)
5. 1x fluorite sleeve (FE15)
6. 1x graphite furnace
7. 1x 2-pin ceramic tube for the thermocouple
8. 2x fluorite cylinder for the capsule
9. putty to fix the gaskets

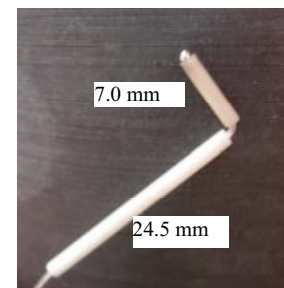
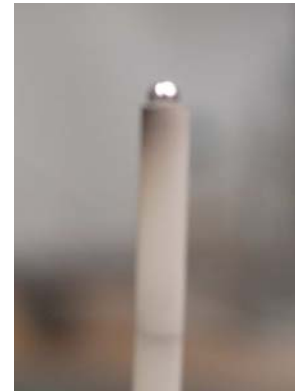
Additional: sample capsule, thermocouple wire, hematite powder, Al_2O_3 powder, tape, ethanol

Capsule-making:

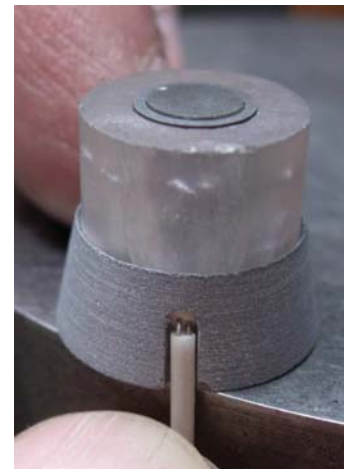
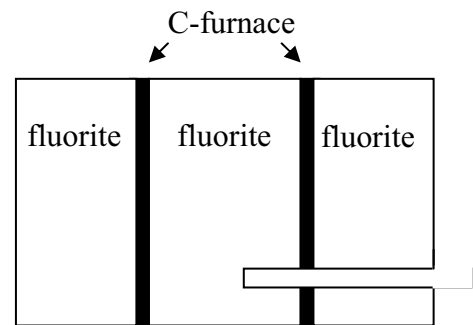
- material for intended purpose (gold, silver, platinum, rhenium)
- capsule height: ~ 4,6 mm capsule diameter: max. 4.4 mm
- fill the capsule
- weld/cold-weld the capsule (depending on purpose)
- drill a hole into one of the fluorite-plugs (depth: half of the length of the capsule) (4,5 mm capsule length → 2,25 mm deep) but not deeper than 2,4 mm. Be careful! Rim is very fragile
- drill the second fluorite plug, so that the capsule perfectly fits into both fluorite plugs
- use vacuum cleaner during drilling

Thermocouple:

- cut off a $7,0 \pm 0,005$ mm and a 24,5 – 25,0 mm long piece of the 2-pin ceramic tube
- feed the thermocouple (rolled up in a box) into both ceramic tubes (long one first), that both ends stick out a few mm
- turn welding apparatus to 90 and weld both thermocouple-ends to a small ball (with the diameter of the ceramic tube. Clamp it, that the wire touches the workbench (conduction). Turn off and discharge the apparatus after welding.
- bend the wires over at the point, where the ceramic tubes touch each other
- the wires must not intersect each other at the bending position
- put gasket, fluorite sleeve, furnace and fluorite cylinder together and put everything into drill gauge

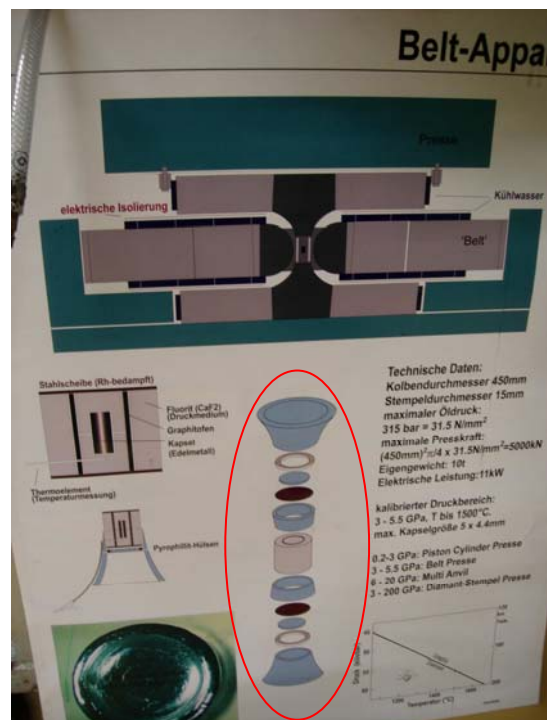


- drill a 1.6 mm (in diameter) hole (with a steel-drill)
- stop at the contact of drill with fluorite-sleeve
- remove gasket and put the remaining parts into the brass-form. The marked part (by the drill) must be exactly in the middle of the opening.
- attach the brass-form into the lathe and centre it
- drill a 8.3 mm deep hole (hint: diamond cover of the drill is ~ 8.3 mm long)(diameter of the sleeve + diameter of the furnace + diameter of the fluorite cylinder + half of the diameter of the welding beat) diameter of the hole = 1.6mm (either a perfect hole with the 1.6 mm drill or a little bit off with the 1.4 mm drill)
- put all parts over the pyrophyllite gasket (with tilted borehole) and assemble the thermocouple. Thermocouple wires must be parallel

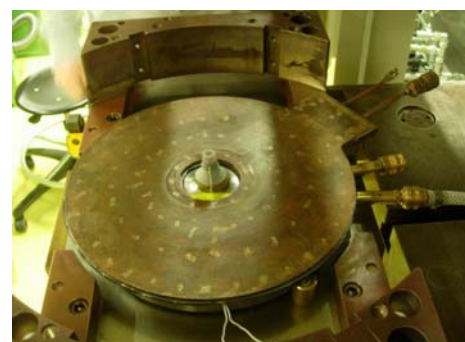
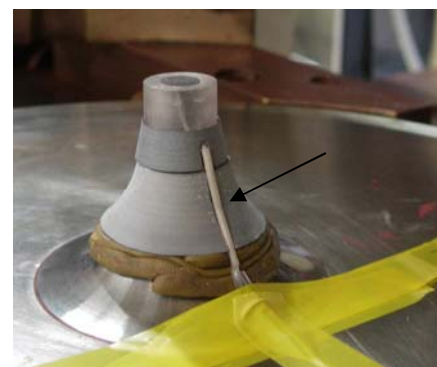
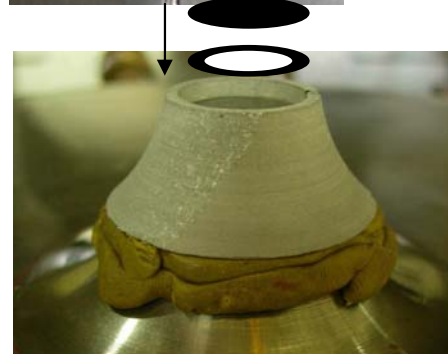


Assembly into the belt press

The assembly of every part into the press is described on a poster next to the press



- mix some hematite powder with ethanol and paint the lateral surface of the anvils (increases friction), but only where the gaskets cover the anvils
- leave the part open, where the thermocouple will be located
- the upper anvil don't need these open part
- put the big gasket on the lower anvil to have the line of the cut in the gasket in one line with the one in lower anvil
- attach a tape directly below the cut of the gasket and deep into the cut of the anvil.
- insert the metal plates in the correct order on the tip of the anvil (at the bottom: metal with pyrophyllite, then only metal)
- follow the instructions of the poster
- put the prepared parts on the discs
- attach the thermocouple
- break the longer ceramic tube (arrow) to have a close contact to the gasket
- move the isolation of the thermocouple close to the ceramic tubes
- fix and isolate the thermocouple wire with tape and press it deep into the cut
- attach the soldered cooling plate (be careful with its position; picture!)



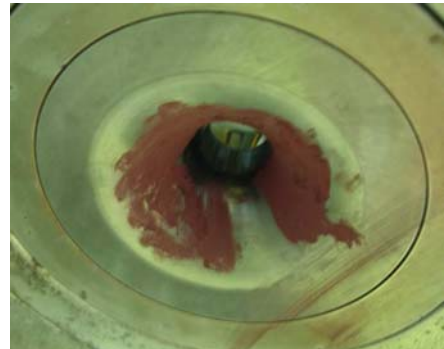
- mix Al_2O_3 powder with ethanol and fill the gaps at the thermocouple
- test thermocouple (see: „thermocouple control“)



- lift the belt with the crane and „paint“ the contact to the gasket with hematite, then do the same on the upper side



- leave a free space at the contact to the thermocouple

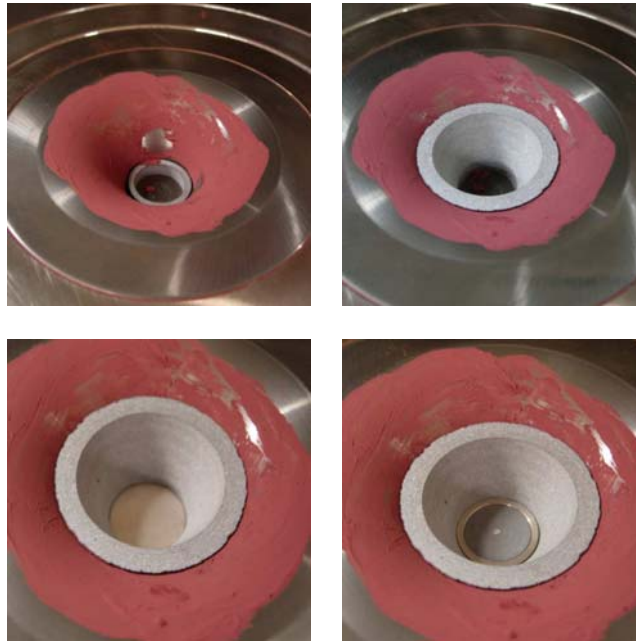


- clean the cooling plate and the lower side of the belt

- carefully lower the belt into the guiding block
- kneel the last cm in one go



- attach the remaining parts in the correct order: coated metal plate in contact to the furnace, then metal disc with pyrophyllite (no hematite between the different parts)

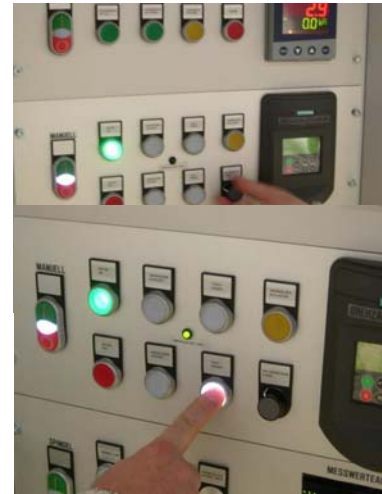


- clean the upper part of the belt and the cooling plate
- put upper cooling plate (single pipes) on the belt, be careful with the position of the plugs (picture)
- move the table below the upper anvil until the contact is touched (at the contact a green lamp flashes at the console)



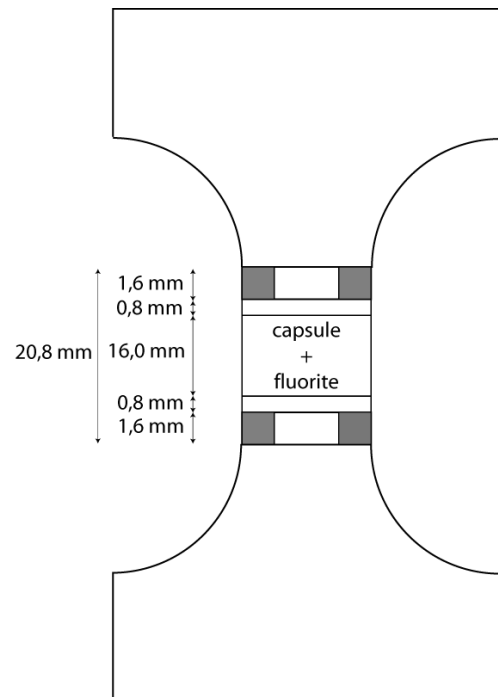
Pressure increase

- switch the console to „MANUELL“
- turn the engine on
- turn the engine on high speed
- press „TISCH SENKEN“, simultaneously press the table backwards and ensure that the green lamp is glowing. Stop as soon as the wheels of the table no longer touch the rail
- turn off „Manuell“
- bring spindle into starting position:



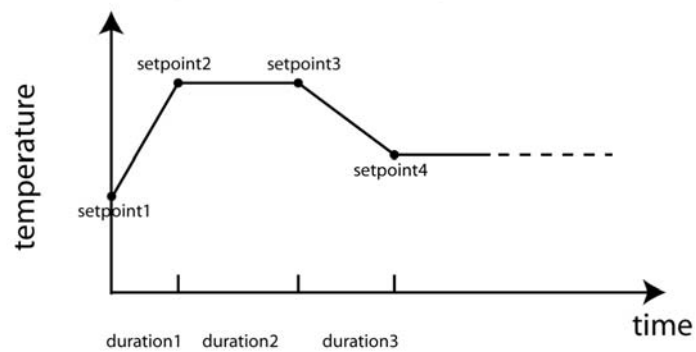
1. activate „SPINDEL“
2. „SPINDEL AB“ until it stops automatically at „Endschalter unten“
3. „SPINDEL AUF“ until program stops
4. turn off „SPINDEL“

- activate „MANUELL“
- turn on engine
- „OBERKOLBEN PRESSEN“ with max. speed
- as soon as the anvil distance reaches = 22,0 mm, reduce speed to ~ 2,5 hertz
- as soon as pressure increases (20,8 mm; see pressure display and anvil distance monitor if the spindle bulb moves downwards. If the pressure does not increase, slowly increase speed.
- increase pressure slowly to 10bar
- connect the plugs with the cooling plates and turn on the cooling system (first turn on the cooling water, then press the cooling water button 2-3 times until the water flow is constant



Pressure program

Es sind Sollwertprofile mit max. 8 Programmabschnitten möglich



- switch from „MANUELL“ to „DRUCK“
- „PGM“
- „▼“
- „PGM“
- „SP1“ has to be 0 (starting position)
- „▼“ + „PGM“
- „tP 1“ (= pitch off the ramp until the desired pressure is reached; recommended value: **1bar/min**)
- „▼“ + „PGM“
- „SP2“ = desired target value, a calibration scheme is on the left side of the press
- „▼“ + „PGM“
- „Zeit2“ = length of the duration time at the target value (always set to maximum (99:59))
- „▼“ + „PGM“
- „SP3“ must be the same value as „SP2“

If dwell time is longer than 4 days:

- „▼“ + „PGM“
- „Zeit3“ duration of second dwell time
- „▼“ + „PGM“
- „SP4“ target value

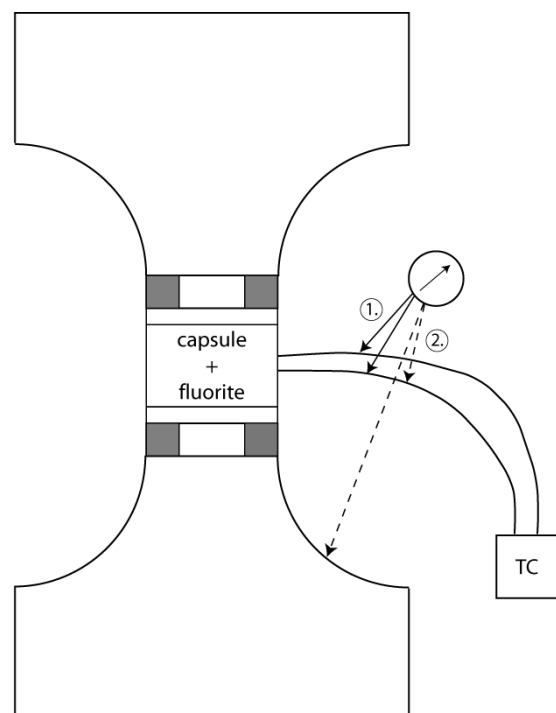
- 2x „EXIT“
- „▲“ = start
- „Druckregler mit Spindel“ must be pressed directly after that
-

Pressure monitoring

- turn on pressure monitoring as soon, as the desired pressure is reached (or shortly before). It avoids unregulated compression in case of failure e.g., breakage of gasket or anvil
- set upper, right turn-switch („Messen“ – „Min“ – „Max“) on „Min“
- remove the interlock at the lower turn-switch and adjust the minimum pressure (2 bar below target value)
- set maximum value (2 bar above target value)
- to start pressure monitoring press „Drucküberwachung“ (yellow button) but not until target pressure is reached

Thermocouple control

- **IMPORTANT:** control without inserted plug!
 1. measure thermocouple conductivity (multimeter) (should be 2 – 4 Ω)
 2. measure thermocouple contact to press (must be $\infty \Omega$)
- if everything is ok insert plug of black box into copper box
- close protection window



Alarms

The alarms help to regulate the heating power, the energy and the voltage, in case of failure (e.g., contamination or breakage of the thermocouple, breakage of the furnace, contact between cooling plate and anvil). A triggering of the alarms leads to an immediate switch-off of the heater.

Adjusting the alarms

- „P“ (press 3 sec)
 first take a value from the lab book + enough buffer (~20 %) e.g., 1200 ° – Exp. #1388
 $U = 3,13 \rightarrow 4,0 \text{ V}$
 $I = 313 \text{ A} \rightarrow 400 \text{ A}$
 $P = 990 \text{ W} \rightarrow 1200 \text{ W}$

- monitor the values during heating
- when target value is attained, reduce the alarm to measured value +10%
- values for 1200°: ~ 2,7 V; 250 A; 500 W

set Min/Max to zero: set all (3) values to zero (press „AUSBLASEN“ and „ALARM“ simultaneously)

Temperature

- **IMPORTANT: NEVER** bring copper box in contact to upper piston or produce a short circuit between upper and lower piston, respectively → danger of life! (several hundred ampere)
- „PGM“
- „▼“
- „PGM“
- „SP1“ must be zero (starting point)
- „▼“
- „Zeit 1“ (= pitch of the ramp until the desired temperature is reached; recommended value: **50 °C/min**)
- „▼“
- „SP2“ = desired target value, a calibration scheme is left to the press; Be careful: Scheme shows temperature difference between thermocouple and outer part of the capsule
- „▼“
- „Zeit2“ = length of the duration time at the target value (may be set longer)
- „▼“
- „SP3“ must bet the same value as „SP2“ (if > 4Tage see **pressure program**)
- 2x „EXIT“
- set control to manual drive → „Exit“ > 3s; „▼“ to 0; „Exit“ < 3s → if „1“ flashes, everything is ok
- „▲“ = start

- „HEIZUNG EIN“ simultaneously

Quenching

- „DRUCKREGLER MIT SPINDEL“ → off
- „DRUCKÜBERWACHUNG“ → off
- „HEIZUNG“ off
- few minutes after heater is turned off „KÜHLWASSER“ → off
- switch the water off
- „AUSBLASEN“

Pressure release

- „▲“ = stop
- „PGM“
- „▼“
- „PGM“
- „SP1“ maximum value: **141,2**
- „▼“
- „Zeit 1“ 2:21 hours or longer (pressure-, dependent of situation)
- „▼“
- „SP2“ = 0 (below 6 bar program and engine will be switched off)
- 2x EXIT
- „▲“ = start program
- „DRUCKREGLER MIT SPINDEL“ on
- if pressure is released (< 6bar):
- „DRUCK“ → off

Opening

- „MANUELL“ on
- „OBERKOLBEN ENTLASTEN“
- at ~ 3 bar „OBERKOLBEN RÜCKZUG“ at full speed
- once upper piston reaches arrester (sound changes) → stop
- „TISCH HEBEN“ until telltale turns off
- engine off
- „SPINDEL“ on
- „SPINDEL AB“ until light flashes
- „SPINDEL AUF“ turns off automatically in starting position
- „SPINDEL“ off
- pinch off both cooling plates
- pull out the table
- lift belt with crane ~2 cm
- transect thermocouple (with special tong)
- move belt on the table (use a paper underlay)
- remove metal discs (do not try to press them through the belt)
- hammer the remaining parts with drift bolt through the belt
- clean the belt
- wipe belt and both anvils and, if necessary grind them
- put the belt into the topmost drawer
- push back the table
- lower the table
- position the brass protection ring between both anvils
- put the tools back to the drawer

Multianvil apparatus manual

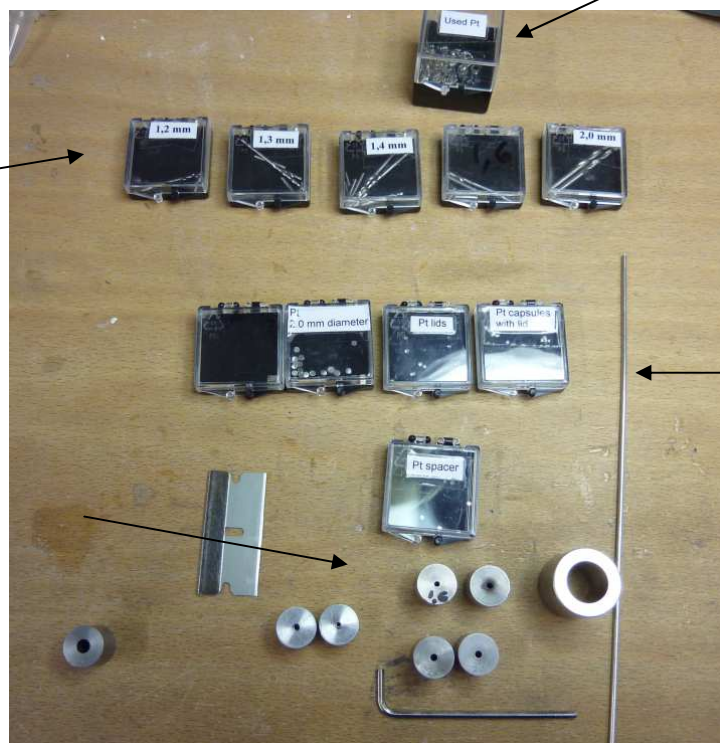
Capsule preparation

Materials for capsule-preparation (Pt)

„rubbish“ box for failed parts
(expensive material
e.g. Pt, Re, Au)

different drills (as
punching tool)

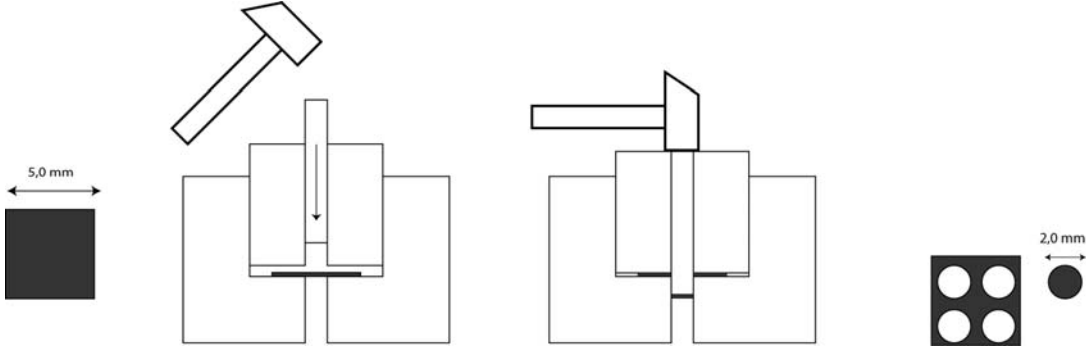
forms with
different
diameters



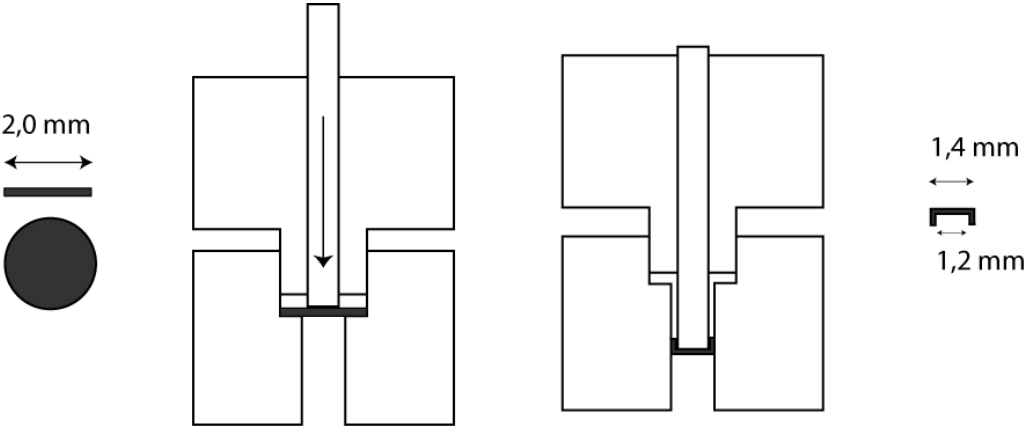
1. Lid

- 0,1 mm thick Pt sheet
- Cutting a ~ 5 x 5 mm piece
- blanking a 2 mm disc (hammering on the adequate drill)
- 2 discs if you use thinner sheet (0.05 mm)



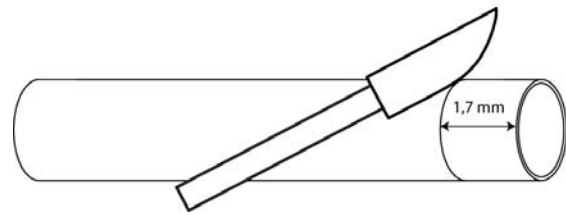


- bending over the rim of the Pt disc with the Al-form
- for one capsule two lids are needed
- don't hammer, use the press



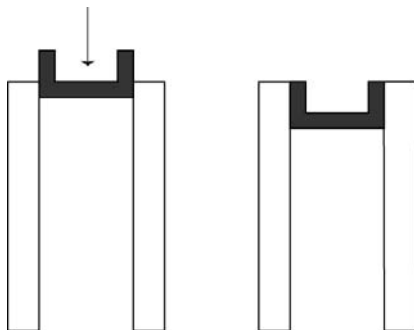
2. Capsule body

- cutting off a 1.7mm long piece with a scalpel of a platinum tube (outer diameter: 1.6mm; inner diameter 1.4mm)
- also possible with the lathe
- after cutting push the piece through the 1.6 mm form and push the 1.3mm drill through the tube

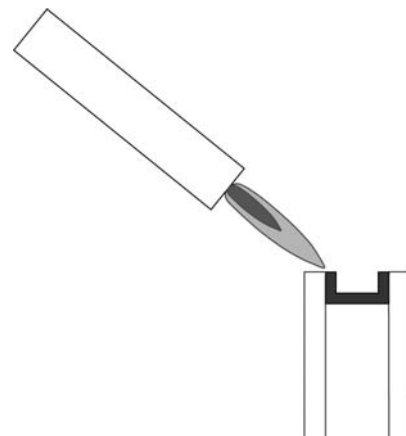


3. Putting the capsule together

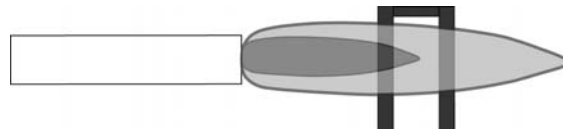
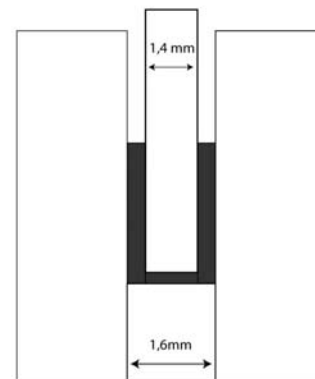
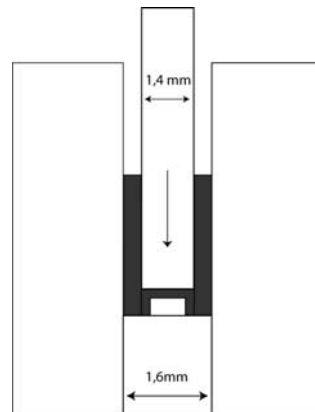
- put the lid on the platinum tube (photo)
- push the lid with a flat object (e.g., the grip of a scalpel) into the tube

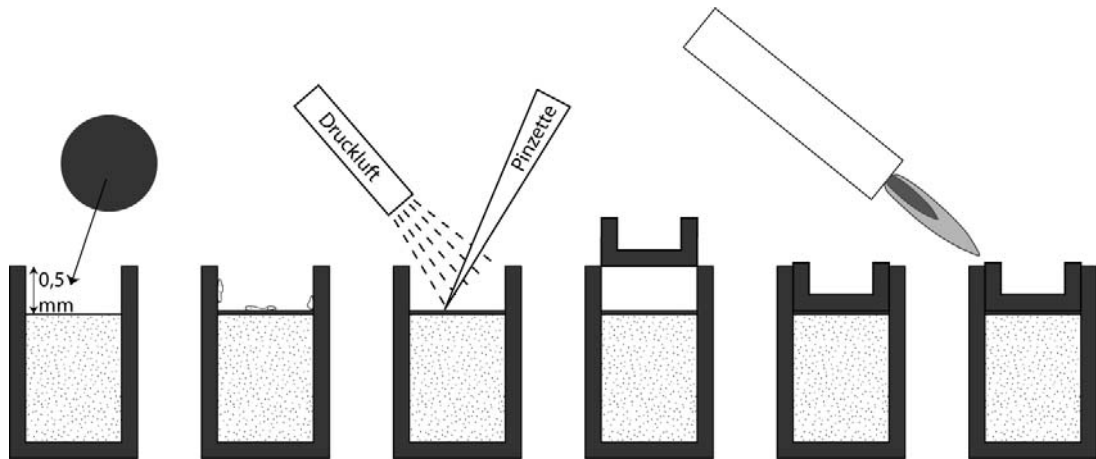


- next Step: welding the capsule
- stabilize capsule
- set the welding apparatus on **55**
- wear protection glasses!
- short, punctual contacts

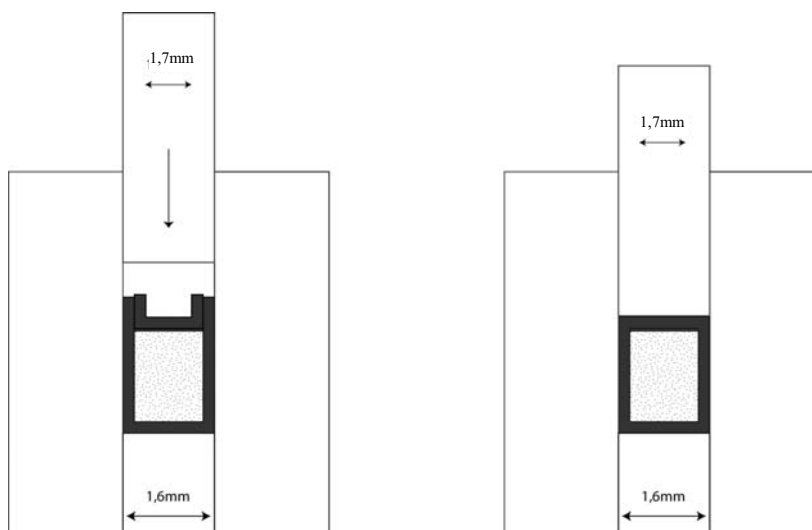


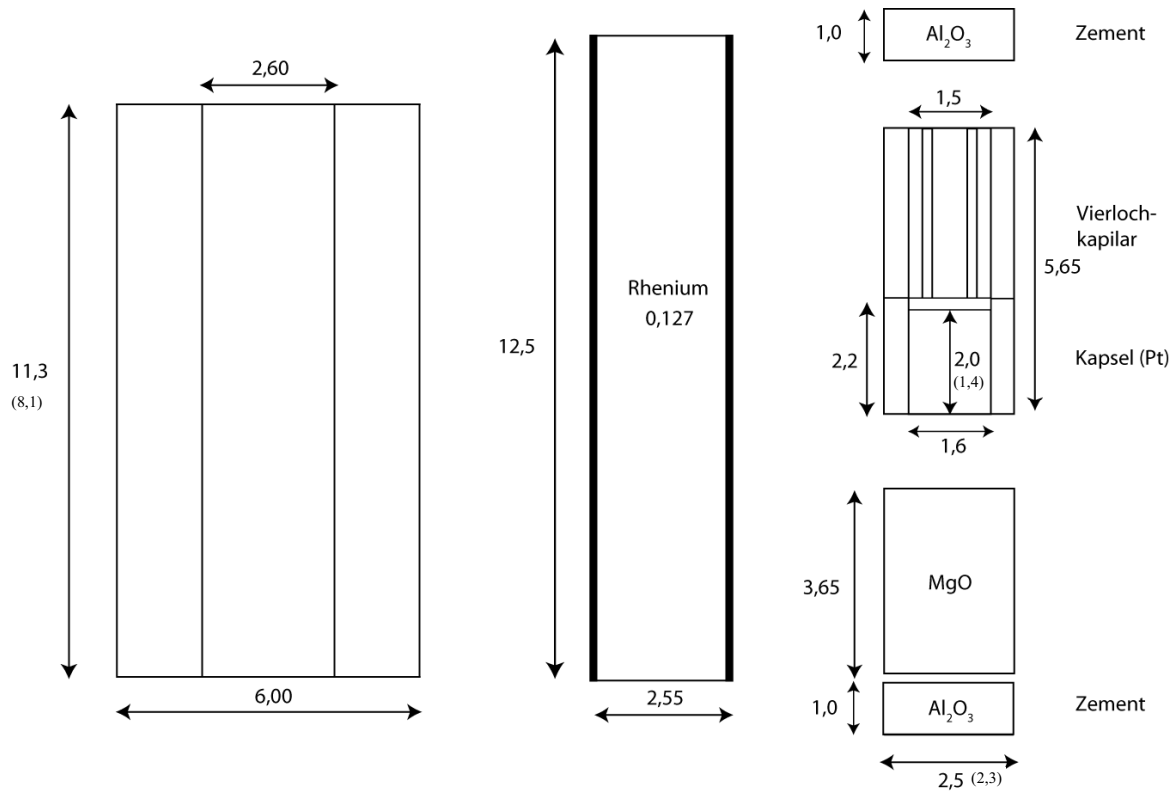
- put capsule with bulging rim into 1.6mm form (drawing)
- push 1.4 mm (1.3 is also possible) drill gently in capsule (drill must be vertical!)
- press with grey press, until needle nearly reaches zero
- to get drill out roll it with capsule on a smooth surface (be careful, capsule widens)
- grind flashes
- soak capsule with small gas jet thoroughly through (put it on small used thermocouplewire)
- fill capsule with sample
- leave 0,5 mm to the rim
- cut out thin 1.4 mm Pt disc
- put it on sample
- hold it with tweezers and remove any dirt with compressed air
- push 2. lid on capsule
- weld it





- same procedure as for the first lid
- mark one side (thermocouple should be in contact with the side with the extra lid)





4. Dimensions of the different octahedron parts

(primarily important parts on the right side of the picture)

Because the height of the capsule is variable, the other parts have to be adjusted to the capsule size. Maximum capsule length for 14m = 2 mm (10m = 1 mm)

Example for 14m:

- capsule length: 1,87 mm height of all parts: 9,3 mm

$\frac{9,3-1,9}{2} = 3,7$ because max. heat is not directly in the middle, capsule has to be shifted 0.2mm towards T.C.

→ upper space: $3,7 - 0,2 = 3,5$
 lower space: $3,7 - 0,2 = 3,9$

thermocouple: $3,5 - 0,2 = 3,3$
 capsule: $1,9 + 0,2 = 2,1$ (allows a 0.2 mm thick layer of cement on the top of the capsule)

lower space: **3,9**
 Σ 9,3

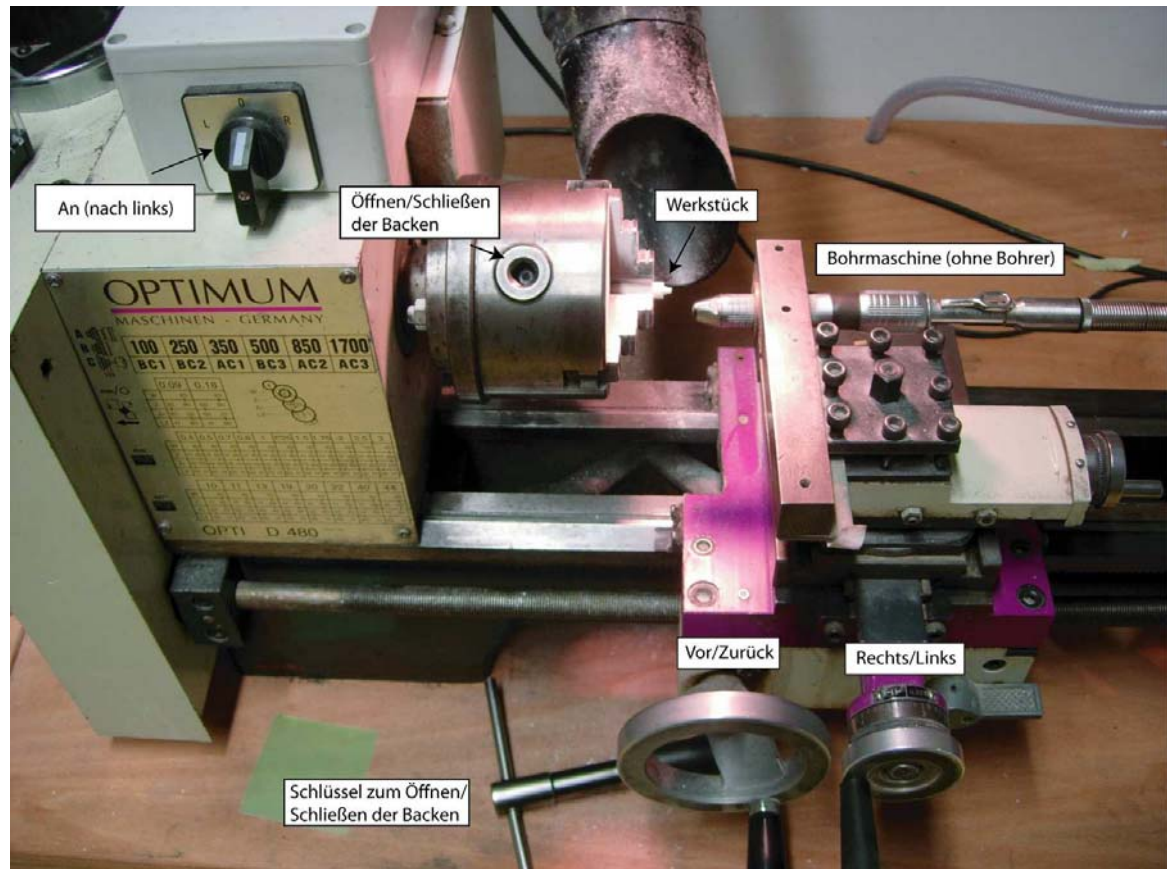
Example for 10m:

- capsule length: 1.00 mm height of all parts: 8.1 mm (always verify it) - 2x1 mm
= 6.1 mm

$$\frac{6.1 - 1.0}{2} = 2.55 \text{ because max. heat is not directly in the middle, capsule has to be shifted } 0.3(!) \text{ mm towards T.C.}$$

→ upper space: $2.55 - 0.3 = 2.25$
lower space: $2.55 + 0.3 = 2.85$

thermocouple: $2.25 - 0.20 = \mathbf{2.05}$
capsule: $1.00 + 0.20 = \mathbf{1.20}$ (0.2 mm thick layer of cement on the capsule)
lower space: $\mathbf{2.85}$
 $\Sigma \mathbf{6.10}$



5. Lathe

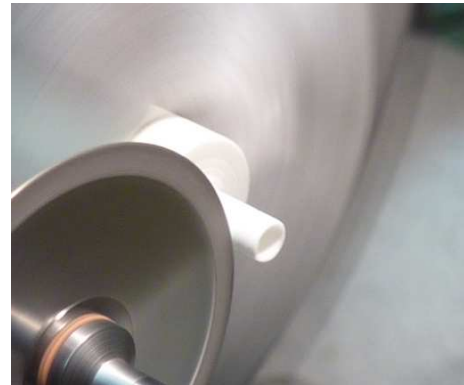
- next step is to produce the MgO cover for thermocouple and capsule. Starting material are 10cm long MgO bars (either in „Thermoelementschublade” or in Thomas locker.
- to machine the bars, 4 different diamond drills are used (also in Thomas’ locket)
- to attach the drills, pull down the cover of the drilling machine, unscrew it, put it in, screw it tight and let the cover jump back
- to attach the MgO bars, use the key at the flange of the lathe
- minimum length of the MgO bars: 1-2 cm
- turn on the vacuum cleaner (switch is next to the entrance door of the pressure lab)
- turn the switch of the lathe to the left, use the drilling machine with the pedal switch



- lathe and drilling machine must run simultaneously

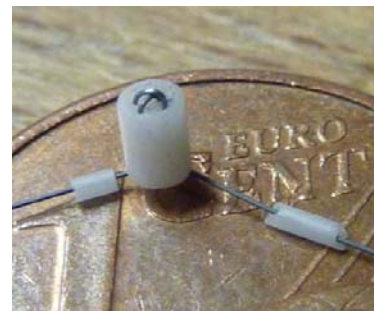
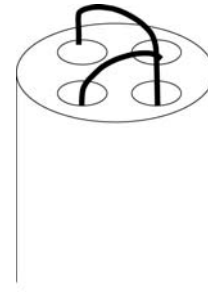
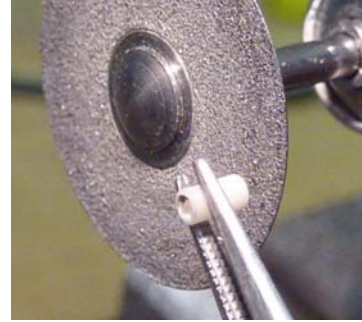
MgO-cover

- begin with the MgO placeholder (→ easiest)
- grind down clamped MgO bar with bevelled diamond drill in thin layers until you reached the wanted diameter
- test the diameter at the octahedron, MgO rod must not have too much play
- cut off the wanted length with the diamond saw blade
- if the rod is too long grasp it with the tongs and grind it down with the diamond saw blade (reduces tilted grinding)
- for the covers position the 1.2 mm drill exactly in the middle and drill a hole as deep as possible
- drill slowly or diamonds will burn!
- cut the cover off and grind it to the wanted length and perhaps widen the hole with a diamond drill) by hand
- fill the overlapping (0.2 mm) end of the cover with the capsule with ceramic cement



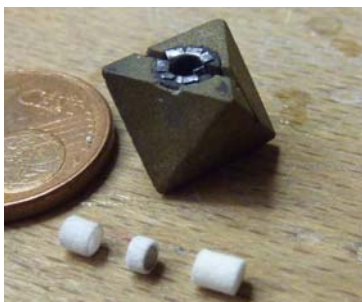
6. Thermocouple

- grind a 0.2 mm deep recess into the tip of a four-hole-capillary.
- cut it to the proper length
- thermocouple-wire in „Thermoelementschubblade“
- cut off 8.5cm of each
- bend over the end of the „blue“ wire
- fill the capillary with liquid cement; directly after that bend over both wires (~ 1 mm) and contrive the wires over cross into the capillary (see picture)
- keep contact between wires clean
- use a little bit drier cement to fill the 0.2 mm deep recess
- bead ca. 1.5 mm of thin ceramic capillary on both thermocouple



7. Assembly of the octahedron

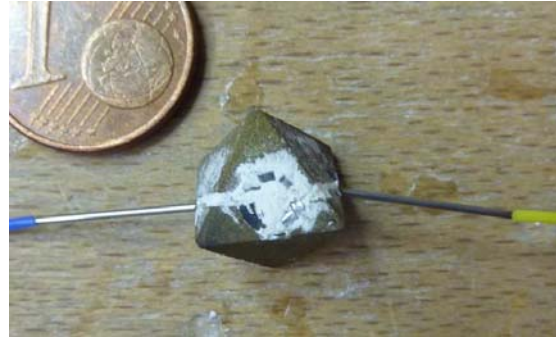
- fit single parts into the octahedron



- the last part is the thermocouple. Move the two ceramic-capillaries close to the four-hole-capillary to protect the wire from the furnace
- put ceramic cement on the thermocouple, on the back side and on the slits on both sides of the octahedron.

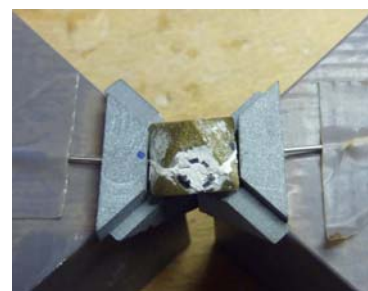
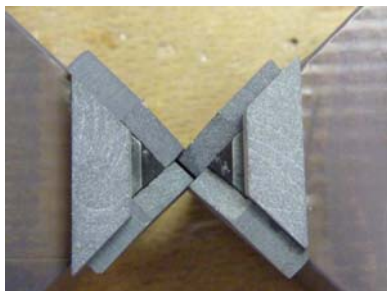
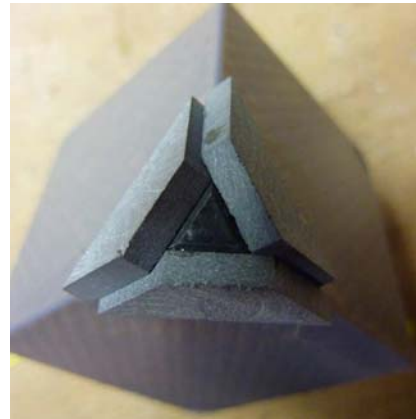


- do not let the wires push out of the ceramic (during cementing pull the wires to the back)
- wires must stick out of the octahedron at the equator line
- remove excess cement
- put the whole assembly into the drying furnace (do not forget to mark the wires)



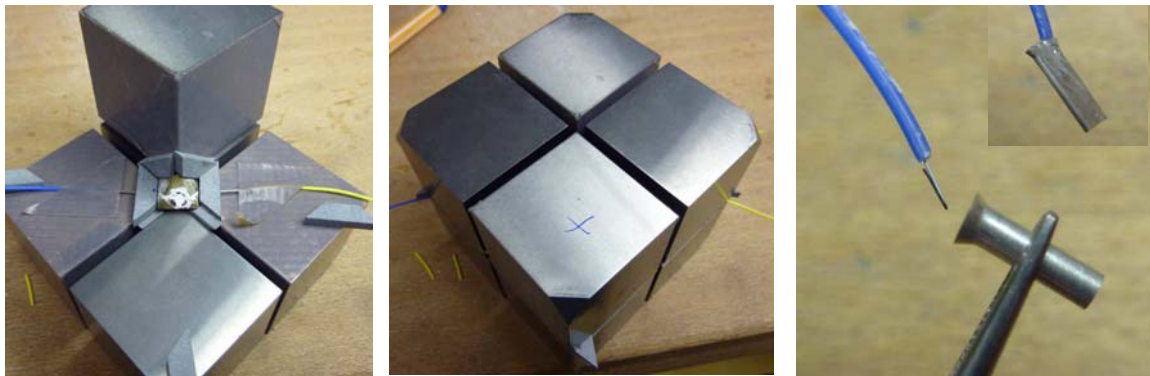
8. Preparation of the cubes

- material: WC-cubes, teflon-tape, 12 gaskets (for 14m 21 mm long; for 10m 17.5 mm), copper-tape, 6 glass-fibre plates
- fix three gaskets on each cube, so that they overlap each other to the half
- glue is in the can on the extension lead (add some acetone)
- distribute a thin layer of glue with a toothpick on backside of a gasket.
- drill a hole through to gasket for the thermocouple-wire (use the green drilling machine; diameter 2 mm)
- cover the surface of the cubes behind the gaskets with teflon-tape (electrical isolation → no metal should be visible)
- make a 2cm cut in 2 of the glass-fibre plates(2 cm far from an edge) widen the cuts and fit in a folded copper foil (for contact between cube and furnace)
- 4 of the glass-fibre-plates get a triangle cut in the middle of one side (to protect the thermocouple wire for cutting-off. Make two cuts on the opposing sides)



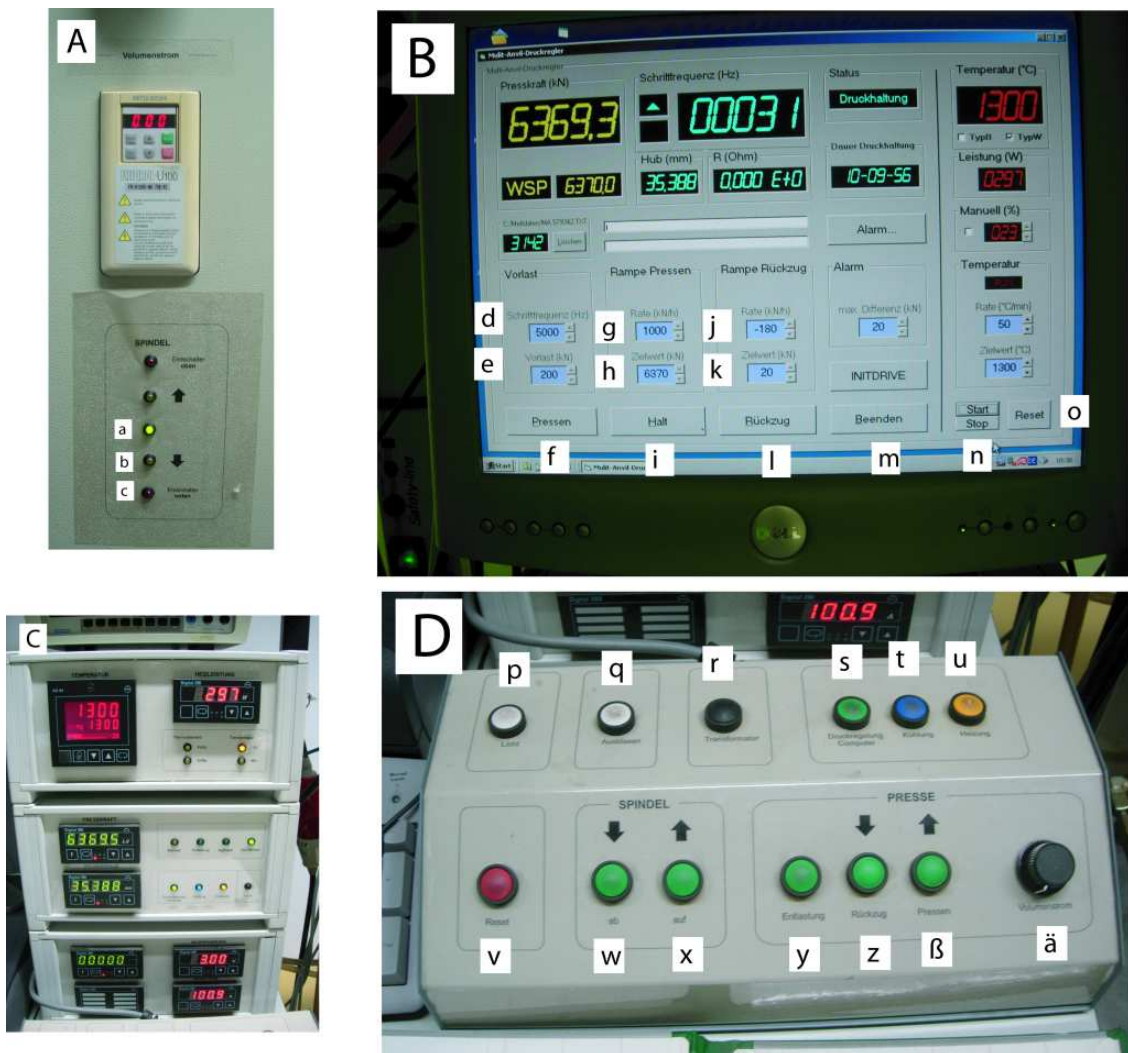
9. Emplacement of the octahedron

- take the octahedron from the furnace after two hours
- protect the wire coming out of the octahedron with a piece of surgery steel
- protect the thermocouple-wires with the proper isolation tube. The isolation tube should be 1 cm shorter than the wire
- bend over the end of the wire and fix a metal clamp on it
- fix the wires with teflon tape on the cubes
- mark the two cubes, that touch the opening of the octahedron. Glue the glass-fibre plate with the copper-foil on it (with the copper touching only the marked cube)
- put together all eight cubes (as placeholder you can use gaskets)
- glue the glass-fibre plates with four droplets of superglue on the cubes (be careful, that no glue is between the cube and the copper-foil)
- check the conductivity at the copper-foil (through the cube)



10. Emplacement of the cube into the press

- be careful to connect the right thermocouple-ends, while attaching the cube into the press. Fix the metal clamp in the lustre terminal (check).
- cover the luster terminals with isolation tape
- put the four upper shoes on the cube, be careful with the number on the shoes.
- put the lid on the shoes with the water-plugs facing to the wall.
- light patting, then trapping until it pushed up against the bedstop. During moving up the press, push it against the bedstop.



10. Pressure increase

- in general: if „alarm“ blinks; press „reset“ as well A as C (for C press Dv)
- to start pressing the spindle must be in home position (move the spindle completely down, then up until it stops automatically)
- spindle down (Dw) until red light (Ac) flashes (be careful, that “Zylinderhub” is below 8 mm, otherwise the spindle will not work)
- spindle up (Dx) – now Aa should flash
- press Dβ and Dä simultaneously. Turn Dä to the right until you reach 100% → press table lifts
- move until the gap got very small, the reduce „Volumenstrom“ to 1.6%
- close press until you reach 15 kN (C, middle part)

- increase „Volumenstrom“ to 2.1% until you reach 30 kN (at higher pressures 50 kN)
- push „Druckregelung Computer“ (Ds), now the computer controls the press
- write the rate for the „Drucksteigerung“ (Bg), at high pressure 1000 kN/h otherwise 1500 kN/h
- put in “Zielwert“ (Bh)
- set „Vorlast“ (Be) to 200
- push „Pressen“ (Bf), press should start with a clearly hearable sound, if not...

11. If press does not work...

- everything has been done as explained in 10. and after pushing „Pressen“ nothing happens, then:
 - a) stop program
 - b) start „Verknüpfung mit getcurrent“
 - c) „play“
 - d) „command“ (program is restarted)
 - e) „stop“
 - f) close
 - g) start again at c) and repeat procedure several times
 - h) click one time (!) up, until you hear the engine
 - i) close program and open again the press-program

12. Heating

- as soon as the wished pressure is reached:
- connect the plugs on the back side of the press (right tube to the right plug)
- press „Kühlung“ (Dt) (at least three times)

- control that the plugs are tight and if the water is permanently running (if not, press Dt again)
- insert target value
- press „Heizung“ (Du)
- press „Start“ (Bn)
- as soon as temperature is reached, write down the values (see lab book), write them down again during the heating and before quenching

13. Quenching and pressure release

- press „Druck halten“ (Bi)
- press „Heizung“ (Du)
- „Reset“
- „Kühlung“ (Dt)
- turn off the water
- „Ausblasen“ (Dq) for 2 – 4 minutes
- set „Alarm – max. Differenz“ to 200
- set „Rampe Rückzug“ to -180 (Bj) and 20 (Bk)
- „Temperatur Reset“ (Bo)
- press second time „Ausblasen“ (Dq) to stop it
- „Rückzug“ (Bl)

14. Finishing an experiment

- „Entlastung“ (Dy)
- „Druckregelung Computer“ (Ds)
- „Presse Rückzug“ (Dz) + simultaneously „Volumenstrom“ (Dä). First slowly then faster („Volumenstrom“ up to 100%); „Presskraft“ rises up to ~ 70-80 kN
- go below 6mm (even 0mm is possible)

- „Spindel ab“ (Dw) pressure increases; can take several minutes
- when alarm light flashes press „reset“ (Dv)
- „Spindel auf“ (Dx)
- „reset“ (Dv)
- press can be opened now
- take out the upper shoes with the long screws, clean them
- take out the cubes (be careful, they might fall apart), throw away the glass-fibre plates
- throw away the plastic foil
- take out the lower shoes, clean them, vacuum-clean the chamber
- cut two new plastic stripes (roll is in the MA-preparation lab)
- use the teflon-spray for one side each (use it outside)
- put it together with the sprayed sides facing to each other and let the stripes overlap a few cm
- put the plastic stripes and the lower shoes in the pressure chamber (be careful, that the numbers of the shoes are on the right position)

Acknowledgements

First of all I want to thank my supervisor Alan Woodland. He had always time to listen to my problems and waded through all my manuscripts, posters and abstracts. Thank you for your support and guidance during the last years!

Many thanks to Kevin Klimm for valuable discussions, important hints and proofreading,

Thomas Kautz, who explained the functions of the belt and the Multianvil with great patience and helped with all other technical problems,

Carolina Montoya Pino, for her help with English words and formulations and for the good time we spent together in our office,

Timo Luchs and Heidi Höfer, for helping me with the microprobe and the REM,

Franz Kneisel, who fabricated tools for the multianvil sample preparation,

Jan Heliosch for the preparation of the thin sections,

Margaret Hanrahan and Vadim Bulatov for introducing me to techniques of sample preparation and execution of multianvil experiments.

I would like to thank all people at the Bayerisches Geoinstitut, Bayreuth, who helped me accomplishing my thesis:

Dan Frost, for the introduction and support during the Multianvil experiments, for staying awake during long nights at the APS, for proofreading and always having a bed for me, when I came to Bayreuth,

Tiziana Boffa-Ballaran, for helping me with any question and problem I had with XRD and the analysis of the data,

Falko Langenhorst, for performing all TEM analysis,

Stefan Keyssner and Hans Keppler for enabling me always an enjoyable visit at the BGI without any problems,

Leonid Dubrovinsky and Konstantin Glacyrin for helpful suggestions and their support with the DAC experiments,

Hubert Schulze and Uwe Dittmann for their express sample preparation,

I would like to thank all the others apart from Frankfurt and Bayreuth:

Julia Regnery for careful proofreading,

Yanbin Wang for his assistance at the APS,

Ralf Engelmann for supporting me during the sample synthesis,

Ross Angel for important hints for data analysis with GSAS,

and everyone who helped to successfully finish my thesis.

Thank you Sonja, for being part of my life.

Curriculum Vitae

PERSONAL INFORMATION:

Name:	Klaus Schollenbruch
Date of birth:	15.09.1980
Place of birth:	Kaufbeuren
Address:	Heddernheimer Landstraße 86 60439 Frankfurt am Main, Germany



EDUCATIONAL DEVELOPMENT

04.2007 – current	Goethe University, Frankfurt PhD thesis: “Systematics of the post-spinel transition in Fe-bearing compositions” intended finish: summer 2010 Supervisor: Prof. Dr. Alan B. Woodland
03.2007	Diploma thesis with the title: „Spätmagmatische Eudialyt-führende Alkalifeldspat-Syenite innerhalb der Kakortokit-Sequenz der Ilímaussaq-Intrusion, Südgrönland“ Supervisors: Prof. Dr. Gregor Markl, Dr. Thomas Wenzel
10.2001 – 04.2007	Eberhard-Karls University, Tübingen Studies of Geoscience Degree: Dipl. Geol.
09.1991 – 06.2000	Allgäu-Gymnasium, Kempten Degree: Abitur

WORK EXPERIENCE

04.2007 – current	Wissenschaftlicher Mitarbeiter: Mineralogy, Goethe Universität Frankfurt Work: performing high pressure experiments (belt, multianvil, diamond anvil) analysis of samples by electron microprobe, SEM, Raman supervising the Raman lab teaching of students (laboratory methods, basic petrology)
10.2005 – 12.2005	Internship at the Alfred-Wegener-Institut, Bermerhaven

	Work: analysis of sediment samples via XRF, Atterberg facility, Leco CHNS-932
10.2003 – 11.2003	Crew member of the 257. “Walther Herwig III” journey around South Greenland
	Work: groundfish-survey, sampling of otolithes
12.2001 – 2004	drill assistant in the engineering company: Harress Pickel Consult
07.2000 – 09.2000	Internship at the “Schutzstation Wattenmeer e.V.”

CIVIL SERVICE

09.2000 – 08.2001	Civil service at the „Schutzstation Wattenmeer e.V“ on Pellworm
	Work: guided tours, public relations, nature conservation work

LANGUAGE SKILLS

German (mother language)
 English (business fluent)
 Latin (basic knowledge)

SOCIAL COMMITMENT

Member of the student representatives Geoscience (2002 – 2005)
 Member of the faculty council Geoscience (2002 – 2005)
 Member of the study commissions (2004 – 2005)
 Member of the diploma examination board (2004 – 2005)

FURTHER EDUCATION

Short course: “Exploration, occurrence and properties of diamonds” by Prof. h.c. Dr. Jeff Harris
 Exam: Best score (2010)

PEER REVIEWED PUBLICATIONS

- Schollenbruch, K., Woodland, A.B., Frost, D.J., and Langenhorst, F. (2009) Detecting the spinel – post-spinel transition in Fe_3O_4 by in situ electrical resistivity measurements. *High Pressure Research*, 29(4), 520-524.
- Schollenbruch, K., Woodland, A.B., and Frost, D.J. (2009) The stability of hercynite at high pressures and temperatures. *Physics and Chemistry of Minerals*, DOI 10.1007/s00269-009-0317-z.
- Schollenbruch, K., Woodland, A.B., Frost, D.J., Wang, Y., Sanheira, T., and Langenhorst, F. (2010) In situ determination of the spinel – post-spinel transition in Fe_3O_4 at high temperature and pressure by synchrotron X-ray diffraction. *American Mineralogist* (submitted)

ABSTRACTS

- Schollenbruch, K., Woodland, A.B., Frost, D.J. and Langenhorst, F. The post-spinel transition in $\text{Fe}_3\text{O}_4\text{-Fe}_2\text{SiO}_4$ and $\text{Fe}_3\text{O}_4\text{-FeCr}_2\text{O}_4$ solid solutions. EGU, Wien 2010 (Poster presentation)
- Schollenbruch, K., Woodland, A.B., Frost, D.J. and Langenhorst, F. Systematics of the post-spinel transition in Fe-bearing spinels. EHPGR, Paris 2009 (Poster presentation)
- Schollenbruch, K., Woodland, A.B., Frost, D.J., Langenhorst, F., Wang, Y. and Sanheira, T. Determination of the phase boundary $\text{Fe}_3\text{O}_4 - \text{h.Fe}_3\text{O}_4$ at high T and P using in situ synchrotron radiation. AGU, San Francisco 2009 (Poster presentation)
- Schollenbruch, K., Woodland, A.B., Frost, D.J. and Langenhorst, F. Systematics of the post-spinel transition in magnetite and hercynite. SPP1236 Meeting, Freiberg 2008 (Poster presentation)
- Schollenbruch, K., Woodland, A.B., Frost, D.J., Langenhorst, F. and Wang, Y. Determining the position of the spinel – post-spinel transition in Fe_3O_4 using X-ray diffraction and electrical resistivity measurements at high pressure and temperature. EMPG, Innsbruck 2008 (Oral presentation)
- Schollenbruch, K., Woodland, A.B., Frost, D.J. and Langenhorst, F. Determining the position of the spinel – post-spinel transition in Fe_3O_4 : First results. IGC, Oslo 2008 (Oral presentation)
- Klimm, K., Blundy, J.D., Schollenbruch, K., and Woodland, A.B. (2009) Linking geochemical signatures and sulphur contents of arc magmas: An experimental approach. *Geochimica Et Cosmochimica Acta*, 73(13), A668-A668.
- Schollenbruch, K., Woodland, A.B., Frost, D.J. and Langenhorst, F. (2007) Systematics of the post spinel transition in Fe-bearing compositions. SPP1236 Meeting, Hünfeld 2007 (Oral presentation)
- Pfaff, K., Krumrei, T., Rudolf, T., Schollenbruch, K., and Markl, G. (2007) Fractionation processes in the layered Ilímaussaq nepheline syenite. *Geochimica et Cosmochimica Acta*, 71(15), A783-A783.

OTHER PUBLICATIONS

- Woodland, A.B., Schollenbruch, K., Frost, D.J., and Wang, Y. (2008) In situ determination of the Fe_3O_4 – h- Fe_3O_4 transition at high pressures and temperatures using synchrotron-based XRD measurements. Bayerisches Forschungsinstitut für Experimentelle Geochemie und Geophysik, Universität Bayreuth, Jahresbericht 2008 pp.74-76.
- Schollenbruch, K., Woodland, A.B., and Frost, D.J (2007) High pressure behaviour of FeAl_2O_4 . Bayerisches Forschungsinstitut für Experimentelle Geochemie und Geophysik, Universität Bayreuth, Jahresbericht 2007 pp.88-89.
- Woodland, A.B., Schollenbruch, K., and Frost, D.J (2007) In situ determination of transitions in Fe_3O_4 at high pressures and temperatures using resistivity measurements. Bayerisches Forschungsinstitut für Experimentelle Geochemie und Geophysik, Universität Bayreuth, Jahresbericht 2007 pp.78-80.
- Schollenbruch, K. (2007) Hydrothermale Eudialytgesteine der Ilímaussaq Intrusion, Südgrönland. Dipl.-Arb., Universität Tübingen, 1-121.